TECHNISCHE UNIVERSITÄT MÜNCHEN
FAKULTÄT FÜR PHYSIK

Max-Planck-Institut für Plasmaphysik,
Garching, Germany

Studies of an inductively coupled negative hydrogen ion radio frequency source through simulations and experiments

Mainak Bandyopadhyay

Vollständiger Abdruck der von der Fakultät für Physik
der Technischen Universität München
zur Erlangung des akademischen Grades eines
Doktors der Naturwissenschaften (Dr. rer. nat.)
genehmigten Dissertation.

TECHNISCHE UNIVERSITÄT MÜNCHEN
FAKULTÄT FÜR PHYSIK

Max-Planck-Institut für Plasmaphysik,
Garching, Germany

Studies of an inductively coupled negative hydrogen ion radio frequency source through simulations and experiments

Mainak Bandyopadhyay

Vollständiger Abdruck der von der Fakultät für Physik
der Technischen Universität München
zur Erlangung des akademischen Grades eines
Doktors der Naturwissenschaften (Dr. rer. nat.)
genehmigten Dissertation.

Vorsitzender: Univ.- Prof. Dr. Peter Vogl

Prüfer der Dissertation: 1. Hon.- Prof. Dr. Rolf Wilhelm

2. Univ.- Prof. Dr. Rudolf Gross

Die Dissertation wurde am ***28.07.04.*** bei der
Technischen Universität München eingereicht und
durch die Fakultät für Physik am ***24.08.04*** angenommen

Dedicated to my wife, Pieu and my daughter, Maiolica

for their unconditional love, support and inspiration

Abstract

In the frame work of a development project for ITER neutral beam injection system a radio frequency (RF) driven negative hydrogen (H^-/D^-) ion source, (BATMAN ion source) is developed which is designed to produce several 10s of ampere of H^-/D^- beam current. This PhD work has been carried out to understand and optimize BATMAN ion source. The study has been done with the help of computer simulations, modeling and experiments. The complete three dimensional Monte-Carlo computer simulation codes have been developed under the scope of this PhD work. A comprehensive description about the volume production and the surface production of H^- ions is presented in the thesis along with the study results obtained from the simulations, modeling and the experiments. One of the simulations is based on the volume production of H^- ions, where it calculates the density profile of the vibrationally excited H_2 molecules, the density profile of H^- ions and the transport probability of those H^- ions along the source axis towards the grid. The other simulation studies the transport of those H^- ions which are produced on the surface of the plasma grid. It is expected that if there is a plasma flow in the source, the transport of plasma components (molecules and ions) would be influenced. Experimentally it is observed that there is a convective plasma flow exists in the ion source. A transverse magnetic filter field which is present near the grid inside the ion source reduces the flow velocity. Negative ions and electrons have the same sign of charge; therefore the electrons are co-extracted with the negative ions through the grid system, which is not desirable. It is observed that a magnetic field near the grid, magnetized the electrons and therefore reduce the co-extracted electron current. It is also observed experimentally that if the plasma grid is biased positively with respect to the source body, the electron density near the plasma grid is reduced and therefore the co-extracted electron current is also reduced. A double layer is formed near the positively biased plasma grid in the plasma, which would have an influence on the negative ion extraction mechanisms. In the process, two phase-sensitive diagnostic methods have been developed based on a new technique (modulation technique). One diagnostic is for measuring the H^- ion density and the other one is for measuring the electron temperature.

Zusammenfassung

Im Rahmen eines größeren Projekts wird am Institut für Plasmaphysik, Garching, eine HF-getriebene Plasmaquelle (BATMAN-Quelle) zur Erzeugung negativer Wasserstoffionen (H^- bzw. D^-) entwickelt, die im Endausbau mit H^- Stromstärken von mehreren 10 Ampère für die Neutralteilchen-Injektionsheizung am Fusionsexperiment ITER eingesetzt werden soll. Ziel der vorliegenden Arbeit war es, ein tieferes Verständnis der sehr komplexen physikalischen Vorgänge in einer solchen H^-Ionenquelle zu erzielen, um damit die Leistungsfähigkeit dieser Quelle entscheidend zu verbessern. Die Studie basiert auf Computersimulationen, Modell-Rechnungen und dem jeweiligen Vergleich mit den experimentellen Resultaten. Dabei wurden im Verlauf der Arbeit vollständige dreidimensionale Monte-Carlo Computercodes entwickelt, die eine detaillierte Beschreibung von Erzeugung und Transport der H^- Ionen liefern. Ein erster Code beschreibt die Erzeugung von H^-Ionen im Volumen (Volumenprozeß) und berechnet dazu das Dichteprofil der Vibrations-angeregten H_2-Moleküle, das daraus resultierende Dichteprofil der H^-Ionen und deren Transportwahrscheinlichkeit auf die Extraktionsfläche (Plasmagitter). Eine zweite Simulation untersucht den Transport von H^-Ionen, die unmittelbar an der Oberfläche eines (Cäsium-aktivierten) Gitters erzeugt werden (Oberflächenprozeß). Mit zu berücksichtigen war dabei der experimentell beobachtete konvektive Teilchenfluss, der offensichtlich neben positiven und negativen Ionen auch Neutrale (Atome, Moleküle) in Richtung Gitter mitführt. Da am Gitter selbst anstelle der gewünschten negativen Ionen in weit höherem Maße die leichten Elektronen extrahiert würden, sind hier geeignete Gegenmaßnahmen zu treffen. Diese bestehen aus einem schwachen Magnetfeld (zur Magnetisierung der Elektronen) und einer elektrischen Vorspannung des Plasmagitters. Dabei zeigt sich, dass die Elektronendichte bei positiven Werten der Gittervorspannung (gegen das Quellengehäuse) in Gitternähe stark abnimmt und der co-extrahierte Elektronenstrom damit deutlich unter den negativen Ionenstrom gedrückt werden kann. Zugleich bildet sich nahe dem Gitter eine Doppelschicht aus, die sich günstig auf die Extraktion der negativen Ionen auswirkt. Zur Detailanalyse wurden im Rahmen dieser Arbeit wurden zwei spezielle Diagnostikmethoden entwickelt, die auf ein neues, hoch-empfindliches Modulationsverfahren zurückgreifen. Hiermit lassen sich die Dichte der H^-Ionen und die lokale Elektronentemperatur erfassen.

Contents

1. Introduction 1 - 22

1.1 Introduction to plasma……1
1.2 Nuclear fusion……..3
1.3 Neutral beam heating……...5
1.4 Negative hydrogen ion sources……8
1.5 Major issues in negative hydrogen ion sources……..10
1.6 Negative ion and plasma diagnostics……15
1.7 Outline of the present work……18

2. Plasma chemical processes in a negative hydrogen ion source 23 - 35

2.1. Volume production of H^- ion.…….23
2.1.1. Creation of vibrationally excited $H_2^*(v'')$ states……...23
2.1.2. Destruction of vibrationally excited states…….……..25
2.1.3. Creation of H^- ions……...27
2.2. Surface production of H^- ion.…..28
2.2.1. Atomic process……28
2.2.2. Ionic process……30
2.3. Destruction of the H^- ions……..31

3. Description of the ion source 36 - 47

3.1. Introduction……....36
3.2. Description of the source……...…36
3.3. Description of diagnostic and other subsystems……41
3.3.1. Diagnostic system……....41
3.3.2. Other subsystems……42
3.4. Typical characteristics of the source……..43

4. Model and simulations for H^- ion production and transport 48 - 78

4.1. Introduction……...….48
4.2. Geometrical model of the source…….....50
4.3. Physical model……...50
4.4. Input and output structure of the computer code…….……...55
4.5. Neutral transport code for volume process…….……56
4.6. H^- ion production code for volume process…….……...……57
4.7. Volume produced H^- ion transport code……57
4.8. Particle balance model…….……...60
4.9. Results and discussion on simulation and model……...62
4.10. Transport of surface produced H^- ions……...68
4.11. Results and discussion on surface produced H^- ion transport……71
4.12. Conclusion……..77

5. Plasma flow measurements 79 - 97

5.1. Introduction……...…….79
5.2. Plasma flow measurements……80
5.3. Force balance…….…….84
5.4. Effect of plasma flow on the plasma sheath ...…….…….91
5.5. Influence of plasma flow on negative ion production …….…..93
5.6. Conclusion…….…….96

6. Grid bias experiments 98 - 103

6.1. Introduction…….……...98
6.2. Experimental setup…….……98
6.3. Results ……...…….……100
6.4. Conclusion……102

7. Ion source diagnostics by modulation technique 104 - 118

7.1. Negative ion density measurement……..…104
7.1.1. Introduction……104
7.1.2. Principle of the H^- ion diagnostic system……...105
7.1.3. Experimental setup……..…106
7.1.4. Results of the H^- ion diagnostic system……107
7.1.5. Discussion the H^- ion diagnostic system……109
7.2. Electron temperature measurement……..111
7.2.1. Introduction……111
7.2.2. Experimental setup……111
7.2.3. Principle and formulation of the electron temperature measurement system…..……..……...……113
7.2.4. Results and discussion……116
7.3. Conclusions of two different diagnostic systems…….117

8. Conclusions and outlook 119 - 125

8.1. Main results……..119
8.2. Conclusions…….……...……122
8.3. Possible future developments……...……124

Appendix 126 - 140

Appendix 1 Energy levels of Hydrogen molecules……....126
Appendix 2 Subsystems and diagnostic output of BATMAN ion source…….128
Appendix 3 Modelling of the source geometry……..133
Appendix 4 Magnetic field calculation…….……134
Appendix 5 Detailed flow chart diagrams…….....136
Appendix 6 Lock-in-amplifier…….……...……139

Acknowledgements 141

Chapter 1

Introduction

Summary: The present thesis work is a part of a project, intended to develop a negative hydrogen ion source for International Thermonuclear Experimental Reactor (ITER) neutral beam injection (NBI) system. The basic description of the plasma, nuclear fusion, NB heating, negative hydrogen ion source and its major issues, diagnostic and the outline of the present thesis work are discussed in this chapter.

1.1 Introduction to plasma

Plasma is the fourth state of matter, which is inherently quasi-neutral [1]. It is a collection of charged and neutral particles, which exhibits collective behavior. In nature and in the laboratory, the plasma exists in many forms, which are shown in fig.1.1.

In a laboratory plasma, for example: a gas discharge plasma most of the gas molecules are decomposed into neutral atoms and equal number of positive ions and negative electrons. The density of the charged particles should be large enough to ensure that the Coulomb forces between the charged particles, determine the statistical properties of the plasma.

Plasma has some basic properties. In unperturbed plasma, if a point positive charge, Q, is inserted, the charge will attract a cloud of electrons and repel local ions to such an extent that the point charge becomes shielded from the rest of the plasma. The electrostatic potential ϕ, due to the point charge Q can be calculated with the help of Boltzmann's equation and Poisson's equation. The electron distribution around the point charge, can be written as,

$$n_e \approx n_0 \exp\left(\frac{e\phi}{k_B T_e}\right) \tag{1.1}$$

where n_0 is the average plasma density when the plasma was unperturbed (i.e. Q is not inserted; $\phi \to 0$), T_e is the electron temperature, e is the electronic charge and k_B is the Boltzmann's constant. Since ions are heavy, it is assumed that the ionic density is not locally changed due to the presence of the point charge, $n_i \approx n_0$. Using Poisson's equation and neglecting higher order terms, it can be written as,

$$\nabla^2 \phi = \frac{n_0 e^2}{\varepsilon_0 k_B T_e}\phi = \frac{1}{\lambda^2{}_D}\phi \tag{1.2}$$

The solution of the Poisson's equation in 1D is,

$$\phi = \phi_0 \exp\left(-\frac{|x|}{\lambda_D}\right) \tag{1.3}$$

The quantity, λ_D is called as Debye length, which is the shielding distance from the point charge.

$$\lambda_D = \left(\frac{\varepsilon_0 k_B T_e}{n_0 e^2}\right)^{\frac{1}{2}} \tag{1.4}$$

It is to be noted that as the plasma density n_0 increases, λ_D decreases because in each layer of plasma more electrons are available for the shielding. The value of λ_D increases with the increasing of the electron temperature, T_e. Due to the electron temperature, the shielding is not complete and there is a leakage of potential due to the point charge. At a distance of λ_D the leakage potential is the 1/e value of ϕ_0. The number of charged particles within the sphere of radius λ_D, centered on the point charge Q is,

$$N_D = n_0 \frac{4\pi}{3} \lambda^3{}_D \tag{1.5}$$

The criteria for the effective shielding is $N_D >> 1$. Inside this sphere, charge neutrality is violated, but in outside charge neutrality is prevailed. This phenomenon is known as *Debye shielding* and the electron cloud sphere of radius λ_D around Q is known as *Debye sphere*.

For bounded plasma, the electrons in principle would escape more easily than ions and fall on the plasma chamber wall because the electrons have of less mass and therefore have higher mobility. Due to that unequal mobility, the plasma has positive potential with respect to (w.r.t) the wall which is usually electrically grounded. This potential is known as *plasma potential*. The potential drop from the plasma to the wall occurs within a distance, known as *sheath.* The dimension of the *sheath* is of the order of λ_D. Equating the electron flux and ion flux on the wall, the plasma potential w.r.t. the wall can be calculated as,

$$\phi_P = T_e \ln\left(\frac{M_i}{2\pi m_e}\right)^{\frac{1}{2}} \tag{1.6}$$

If the wall is floating with respect to the ground, the potential between the wall and the ground is known as *floating potential* ϕ_f at equilibrium. This potential is generated in the plasma to make the ion and electron flux equal towards the wall and produces a steady

state situation with net zero current on the floating wall. In the case of floating wall condition the equation (1.6) becomes,

$$\phi_P - \phi_f = T_e \ln\left(\frac{M_i}{2\pi m_e}\right)^{\frac{1}{2}} \tag{1.7}$$

If an electrostatic plasma distortion is created, the separation of positive ions and electrons would generate an electric field, **E**. This electric field would give rise a restoring force $\mathbf{F_r}$, which would try to make the separated charge particles close and bring the equilibrium. In collision-less regime, the force equation in 1D is,

$$\mathrm{F_r} = m_e \frac{d^2x}{dt^2} = -e\mathrm{E} = -\frac{n_0 e^2}{\varepsilon_0} x \tag{1.8}$$

Equation (1.8) is a simple harmonic equation, having a characteristic electronic oscillation with frequency,

$$\omega_{pe} = \left(\frac{n_0 e^2}{\varepsilon_0 m_e}\right)^{\frac{1}{2}} \tag{1.9}$$

This frequency is called as *plasma frequency* and it depends only on plasma density.

1.2 Nuclear Fusion

With time the human beings are becoming more and more technology oriented and due to that the demand of energy increases rapidly. The conventional way of energy production is the burning of fossil fuels, which were stored underground for millions of year, are at the verge of extinction. In addition, the burning of fossil fuels creates different toxic gases in the environment, which are responsible for green house effect and global warming. To cope with this increasing energy demand and to reduce the environmental pollution, the mankind requires a reliable alternative energy production mechanism, which can be utilized for unlimited time and having less pollution. Nuclear fusion is one of the most promising candidates. Nuclear fusion is the basic mechanism of the energy production in the sun or stars.

The raw materials required for nuclear fusion are the heavy isotopes of hydrogen. The fusion cross-sections of these isotopes are given in fig.1.2. The fusion reactors mainly rely on the following reaction between two isotopes of hydrogen [3], deuterium (D) and tritium (T). Deuterium is available plenty in the seawater.

$$\mathrm{D} + \mathrm{T} \rightarrow \mathrm{He}^4 + \mathrm{n} + 17.58\mathrm{MeV} \tag{1.10}$$

Tritium is not a stable isotope and therefore it is not obtained in large quantity in nature. Tritium is created inside the reactor when energetic neutrons (n) hit the Lithium blanket of the fusion device.

$$n + Li^6 \rightarrow He^4 + T + 4.8MeV \qquad (1.11)$$

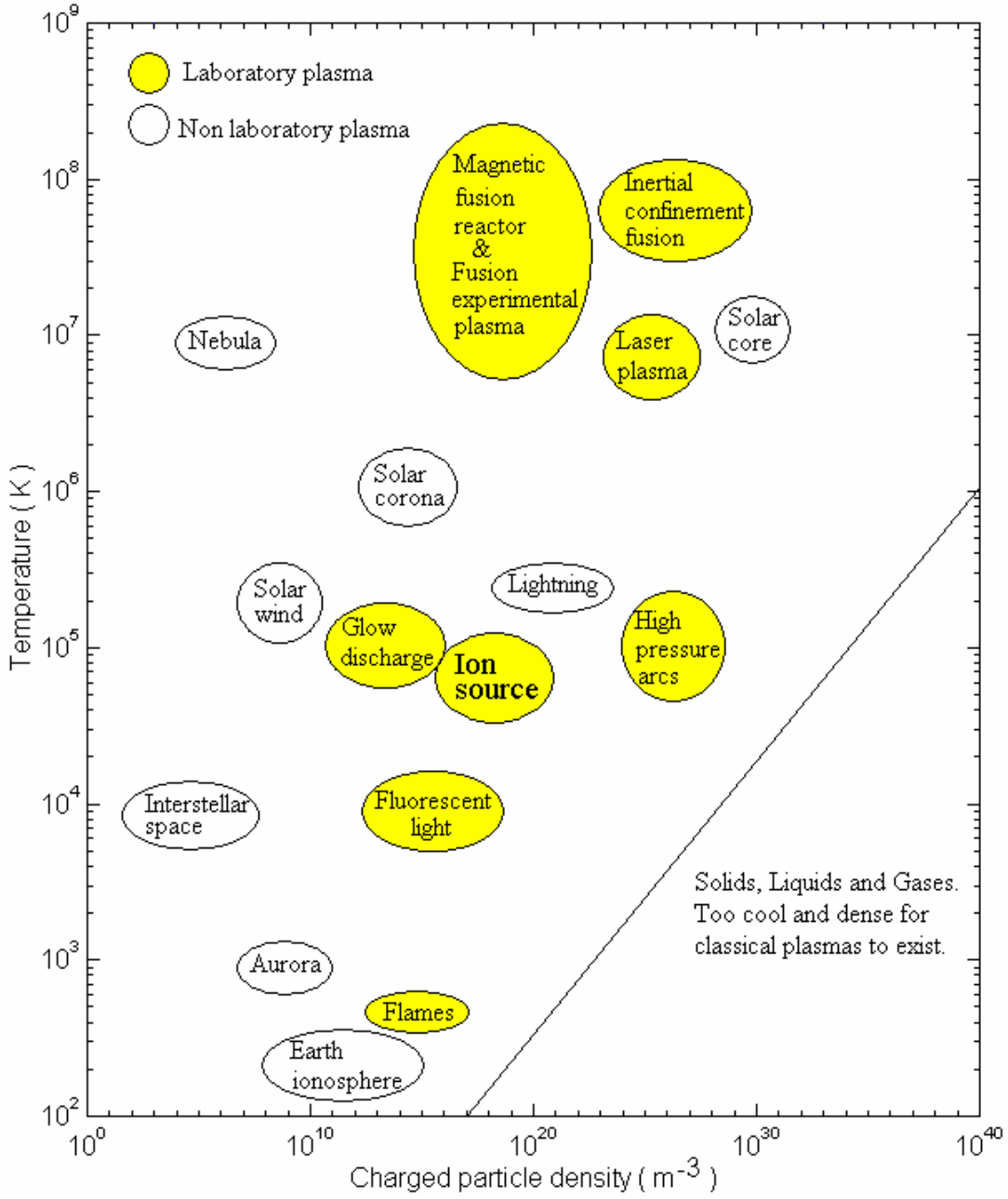

Fig.1.1. Graphical representation of different types of laboratory and non laboratory plasmas with relative density and temperature [2].

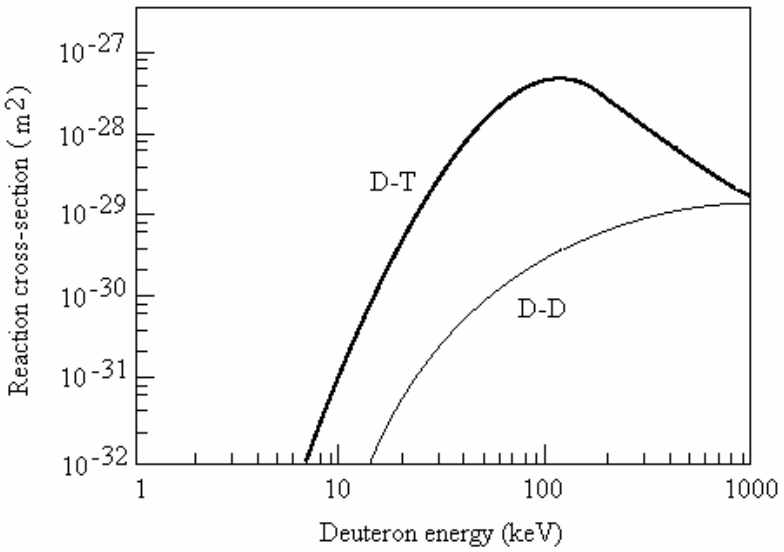

Fig.1.2. Cross-sections of various fusion reactions, as a function of Deuterium energy.

The fig.1.2 shows deuterium (D) and tritium (T) has the highest fusion cross-section near 100 keV. To realize the fusion Maxwellian plasma of D and T is created in the fusion devices, where only high-energy particles in the tail part of the velocity distribution will undergo fusion. If a continuous supply of power is provided to the plasma to compensate the power loss from the plasma, a steady state condition can be obtained. The criterion to obtain such steady state condition is known as *Lawson criterion* [4]. The continuous supply of power is not necessary if the fractional part of the energy released after each fusion collision is used as a feedback to replenish the power loss by the plasma. This is the basic concept of a steady state thermonuclear power plant. This criterion based upon the power balance is known as *ignition criterion* [3]. It imposes a condition on plasma density n_e and energy confinement time τ_E , as well as on the plasma temperature T, to produce more power by fusion than is required to heat the plasma and compensate the radiation losses. In terms of mathematical expression *ignition criterion* is [3],

$$n_e \tau_E > 1.5\times10^{20} \text{ (m}^{-3} \text{ s) with T around 20 keV} \qquad (1.12)$$

To heat the plasma up to the ignition temperature inside a fusion reactor, like a Tokamak or a Stellarator, different plasma heating mechanisms are utilized. These are ohmic heating, radio frequency heating and neutral beam injection (NBI) heating.

1.3 Neutral beam heating

The basis of NBI heating is the injection of high-energy neutral particles, particularly hydrogen (H) or deuterium (D) into the fusion plasma. The schematic diagram of a NBI system is shown in fig. 1.3.

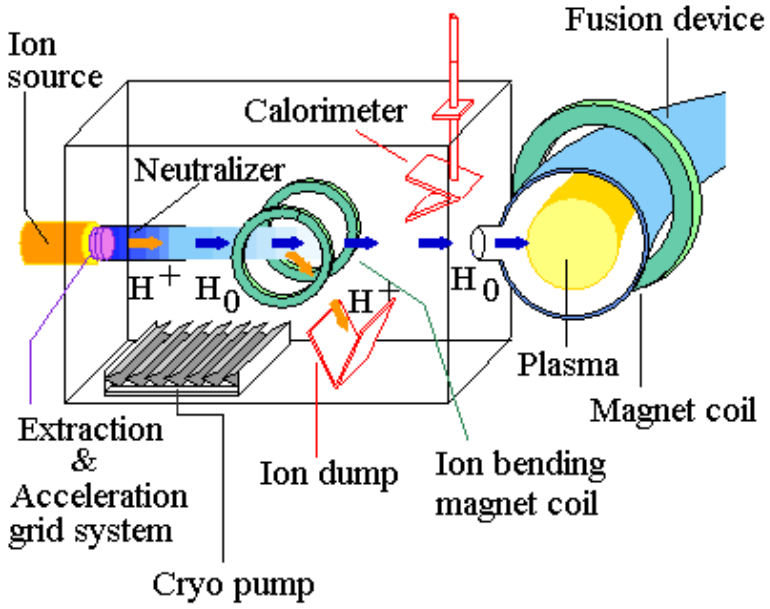

Fig.1.3. Schematic diagram of a neutral beam heating system with a positive ion source.

The high-energy neutrals in NBI systems are created by a series of steps. First, the volume of H or D gas is ionized in an *ion source* (positive or negative ion source). Second, these ionized particles are extracted and accelerated through an *extractor and accelerator system* using a large potential gradient. Third, accelerated ions are neutralized in a gas cell, known as *neutralizer*, through charge exchange (for the positive ions) and electron stripping (for the negative ions) collisions. The *ion bending magnet coil* filters out the ions which are not neutralized in the neutralizer. The filtered high-energy neutral particles are then injected into the fusion device. The neutral particles will suffer two types of collisions inside the fusion plasma.

(1) Charge exchange collisions with the background thermal ions H^+_{slow} convert those high-energy neutral particles H_{fast} into high-energy plasma ions H^+_{fast} and correspondingly the background plasma ions having low energy become neutrals H_{slow} having low energy. Further, H_{slow} can also be converted into background ions.

$$\begin{aligned} H_{fast} + H^+_{slow} &\rightarrow H^+_{fast} + H_{slow} \\ H_{slow} + e &\rightarrow H^+_{slow} + 2e \end{aligned} \tag{1.13}$$

(2) Ionization collisions with the plasma electrons and ions inside the fusion plasma make those fast neutrals coming from the NBI system into ions having high energy. So effectively the energy of the ions is increased inside the plasma.

$$H_{fast} + e \rightarrow H^+_{fast} + 2e \tag{1.14}$$

Since the neutral particles are unaffected by the magnetic confinement field of the fusion reactor, they can penetrate deep inside the fusion device before getting ionized and therefore can deposit their energy at the core of the plasma inside the reactor. The penetration depth, L of a neutral beam can be estimated as [5],

$$L = \frac{E/A}{18 n_e} \text{ meter} \tag{1.15}$$

where E is the neutral beam energy obtained when the ions from the ion source are accelerated in the accelerator system. E is denoted in keV unit, where V is the acceleration voltage in the accelerator system, n_e is the plasma density in 10^{19}m^{-3} unit and A is the atomic mass of the neutral particle in amu. The penetration depth is proportional to the beam energy/unit mass (acceleration voltage). In most of the NBI system, tangential injection geometry is adopted. Due to the tangential injection, the formation of banana orbits (local confined regions of ions and not desirable for fusion plasma) [3] would be less. The tangential injection geometry can also provide a current drive to the fusion plasma with having enough beam-plasma interaction length at low collisionality of the fusion plasma.

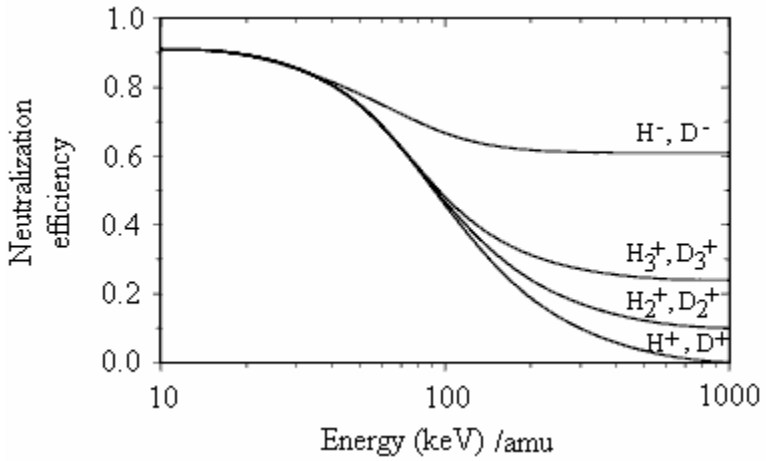

Fig.1.4. Neutralization efficiency of different Hydrogen/Deuterium ions. (Note: "amu" is atomic mass unit)

Most of the NBI systems used in fusion devices so far are based on generating positive H/D ion beams prior to neutralization [6, 7, 8, 9, 10]. The maximum energy of the positive ions in these NBI systems is below 100 keV/amu. The typical current density of the positive ion accelerator system is ~ 200 mA/cm^2. Therefore the injected power would be ~ few MW per beam line. The neutralization efficiency in the neutralizer for positive ions goes down drastically if the ion energy is above 100 keV/amu [11], as shown in fig.1.4. But the negative ion-based NBI systems, maintain a neutralization efficiency of about 60% above 100 keV/amu. To have enough neutral beam penetration inside ITER type bigger size plasma (minor radius ~ 2.8 m), ions from the ion source of the NBI system should be accelerated at least by 200 kV/amu potential difference in the accelerator system. In the case of tangential injection for efficient current drive, ~ 1MV

acceleration voltage is required and corresponding energy of the particles would be in MeV range. For this reason there has been much recent development of negative ion sources and negative ion beams. For the similar neutral beam power density in the plasma, the desired ion current density would be ~ 20 mA/cm^2 in a MV range accelerator system. The upper level of NBI delivered power is also determined by the power handling capability of the fusion device port, through which the neutral beam is injected. However, to produce even such lower current densities (20 mA/cm^2), the required H^-/D^- ion density in front of the plasma grid inside the ion source should be ~ 10^{12} cm^{-3} considering ~ 0.5eV H^- translational energy. It is very difficult to produce 10^{12} cm^{-3} H^-/D^- density in an ion source because the extra electron in a H^- ion is loosely bound (binding energy 0.75eV). Therefore, H^-/ D^- ion based NBI system has a merit that it can provide up to 60% neutral particles with energy more than 200keV/amu but the lower H^-/D^- ion production efficiency in the ion source is its demerit. The NBI systems used in LHD, JT 60-U fusion devices [12,13] are based on negative hydrogen ion sources.

1.4 Negative hydrogen ion sources

The H^-/D^- ion production mechanisms in an ion source are classified into two types. They are (1) **surface process** and (2) **volume process**.

(1) In the surface process, the negative ion production is realized on the electrodes, in contact with the gas discharge plasma. The energetic H atoms and H^+_n ions (n=1,2,3) would be converted into H^- ions on a low work function electrode, when they collide with the wall. For that reason the electrodes or special emitters with a very low work function (with cesium (Cs) work-function $\phi < 2$eV) are used for enhancement of negative ion production. The negative hydrogen ion source development for NBI system had been started through surface production route [14]. Since surface production rely on energetic H atoms and H^+_n ions, higher dissociation degree and higher ionization degree of the plasma is desirable.

(2) On the other hand, in the volume process, the H^- ions are formed directly in the plasma volume through two-step electron-neutral collisional processes [15].

$$\begin{aligned} &(1) \quad e_{hot} + H_2 \rightarrow H_2^{*}(\mathrm{v}''); \\ &(2) \quad H_2^{*}(\mathrm{v}'') + e_{slow} \rightarrow H^- \end{aligned} \tag{1.16}$$

Details of surface and volume production mechanisms are discussed in the next chapter. Since volume production rely on H_2 molecules, the plasma with low dissociation degree is preferable. In the volume source two opposite plasma conditions (electron temperature) are also required (see equation 1.16). For this reason, the volume sources are virtually divided into two parts with the help of a magnetic filter field. The schematic diagram of a volume source and the corresponding desired electron density and temperature are shown in figure 1.5.

For long pulse >1000 sec beam operation, volume source is more desirable than surface source, because with the operational time the performance of the surface source would deteriorate due to the surface degradation by the sputtering. Bacal and her colleagues [16] first demonstrate an intense volume source system. A significant improvement in the volume source performance has been observed by adding small amounts of cesium (Cs) into the discharge [17, 18]. It has been shown that with the addition of Cs [19], the processes of negative ion formation on the surfaces dominate in a volume source. This "Cs effect" gives a big boost to the volume sources, developed for the high-energy long-pulse neutral beam development programs.

The negative ion sources are developed mainly based on,

a. DC filament-driven discharge [20, 21, 22].
b. RF-driven inductive discharge [23, 24].
c. RF-hollow cathod discharge [25].
d. ECR-driven discharge [26].
e. Microwave discharge [27]

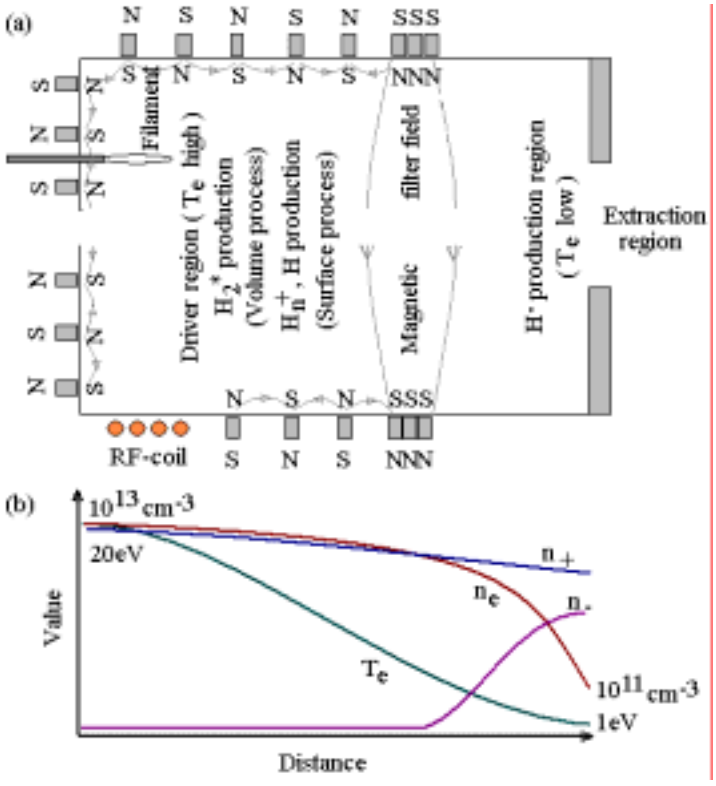

Fig. 1.5. (a) Schematic diagram of two different volume negative ion sources. Upper part is filament arc source and the lower part is RF source (our concept). (b) The desired profiles of plasma temperature (T_e), electron (n_e), positive ion (n_+) and negative ion (n_-) density inside a negative ion source along the axis.

The maximum H^- ion current density and total current from a big negative ion source developed for neutral beam system is achieved so far is from a cesiated (Cs is present in the plasma) DC-filament plasma source, made for LHD machine [28]. In LHD NBI system 20-25 A of H^- ion current with energy above 150 keV has been achieved. JT60-U NBI system is designed for 22 A D^- ion current at 500 kV acceleration voltage [29]. So far they have achieved 14.5 A D^- ion current at 400 keV energy. The conventional DC-filament source has an inherent drawback due to the lifetime of the filaments (2-4 months ~ few 100 hours operational time). It is a big disadvantage from the machine availability and maintenance point of views. In a radioactive environment like ITER, the replacement of the filaments from the NBI sources would be a difficult task. KAMABOKO, a filament source which is one-third size of the source required for ITER NBI, can deliver total extracted current ~ 2.1A, with current density 20mA/cm^2 (D^- ion) and 30 mA/cm^2 (H^- ion) at 0.3 Pa pressure and below 40 kV accelerating voltage [30]; but its performance would be limited due to the filament life time and therefore will not be useful in ITER. To overcome this problem, a major development work contract has been awarded to IPP, Garching to develop an inductively coupled RF based H^- ion source [31, 32]. IPP has vast experience on RF positive ion sources which are in operation in ASDEX NBI system since 1997. Furthermore it is to be also noted that the RF high voltage power supply is less complicated and more economical than that of filament power supply used for NBI systems.

The maximum current densities obtained so far in the negative hydrogen ion RF source, BATMAN (**BA**varian **T**est **MA**chine for **N**egative) ion source in IPP are 25 mA/cm^2 (H^-) and 17 mA/cm^2 (D^-) respectively. The present study is carried out in this inductively coupled RF source. The detailed description of this inductively coupled H^- ion source is discussed in chapter-3.

1.5 Major issues in negative hydrogen ion sources

a. Electron energy distribution and electron confinement

In a "volume" source, the formation of H^- ions relies on a two-step process. These two steps are vibrationally excitation of the H_2 molecules and then dissociative attachment (DA) of low-energy electrons (≤ 1eV) to those vibrationally excited H_2 molecules [33]. An efficient mechanism for exciting the uppermost portion of the vibrational spectrum of the electronically ground state H_2 molecules is via singlet excitation (E-V process) by fast electrons (≥20eV) [34]. The rate coefficients for E-V and DA processes need contradicting plasma temperature conditions. So the shape of the electron energy distribution function (EEDF) is an important parameter in determining the production and destruction rates for vibrationally excited H_2 molecules and negative ions. The E-V process needs better primary electrons (having high energy) confinement but DA process does not require better confinement of the electrons having high energy [35].

b. Collisional reactions

Due to the presence of non-uniform plasma density, background pressure, electron temperature, plasma potential, magnetic field topology and several inter-linked collisional reactions, the complete H^- ion production and destruction processes are highly nonlinear. Therefore it is very difficult to identify the conditions inside the source to make some reactions dominant or to subdue for optimization and to get the best performance from the source. Different source configuration has different characteristic [36, 37]. To optimize a source, contributions from different reactions and their dependency on plasma parameters are important to know. The best method to tackle this problem is by particle simulation through computer codes, considering proper source configuration as inputs [38].

c. Magnetic filter

H^- ion production in "volume" source needs contradicting plasma temperature conditions. Due to this fact the magnetic filter field is a very crucial parameter. Its transverse magnetic field mainly divides the ion source volume into two parts, the hot zone (driver) and the cold zone (extraction) [39, 40]. This type of source configuration is known as *tandem* source configuration [41]. The diffusion of the low energy electrons through the transverse magnetic field is either due to the elastic collision with the neutrals or the e-e coulomb collision [42] or some turbulence created by **E×B** force [43] or combined. The magnetic filter helps to reduce the electron temperature near the grid to facilitate the H^- ion formation and reduce the H^- ion destruction. But the transverse magnetic field reduces also the electron density near the extraction region [44]. The electron density reduction near extraction is not desirable as far as H^- ion production is concerned. In the case of "surface" sources, the surface process relies on the flux of the H atoms and positive ions, which suggests more plasma density near the plasma grid is better for H^- ion production. The presence of transverse magnetic field reduces the plasma flow towards the grid and effectively reduces the flux of the H atoms and positive ions. Due to these merits and demerits of the transverse magnetic filter, understanding of the physics behind the magnetic filter and the optimization of its topology is very important.

d. Temporal filter

In DC-filament discharge, it is observed that the H^- ion production is increased by a considerable amount in the plasma volume during the after glow of the plasma shot (when the filament power supply is switched off suddenly) [45]. In the after glow, the presence of primary electrons reduces drastically and only slow electrons are there in the plasma. This situation helps to reduce the H^- ion destruction reactions. This method is known as *temporal filtering* [46]. This technique is even used in bigger-size negative ion sources [47]. Temporal filter is an alternative approach of magnetic filter, but it would result into a time-varying beam which is not acceptable for continuous neutral beam heating.

e. Plasma flow in the source

In many ion sources, especially those, which are developed for NBI systems in fusion devices, considerable gradients of plasma density and pressure are present along the axis [48]. In a fluid dynamic description of such ion sources, these gradients need to be balanced by the spatial distribution of electric field and by the changes in plasma momentum [49, 50]. During the plasma shot, the flow of the plasma must have a great implication on pressure, plasma density and vibrationally excited molecules distribution profile inside the ion source. The present thesis describes the experimental measurements of the plasma flow in an ion source made for NBI system. There is no report obtained so far on such measurements in any other ion sources made for NBI system.

f. Extraction physics

For the negative ion extraction system, the standard models [51] which are used for positive ions cannot be used. The reasons are as following. (1) Since plasma potential is generally positive with respect to the wall or plasma grid, the negative ions are trapped electrostatically within the plasma volume. (2) Usually in a negative ion source magnetic filter fields are present just before the extraction hole, so the electron temperature is low and therefore ionization is absent there. (3) Since negative ions and electrons have the same sign of charge, both are extracted by the extraction system and accelerated too. To filter out the electrons from the negative ion beam, a separate magnetic field arrangement is provided by installing permanent magnets inside the individual grids [52]. Whealton and his group [53] attempted to resolve some of the extraction issues like: (a) the electric field from the extraction grids system and its penetration into the plasma, (b) the role of transverse magnetic field on the beam emittance and extractability. They also put some light on space charge compensation issue for negative ion extraction [54]. The effect of negative ion stripping and various atomic collisions are taken into account in a computer code developed by C.Michaut [55]. The positive ions formed due to stripping inside the extraction system, are accelerated towards the ion source plasma and change the sheath near the extraction hole. Due to such stripping reactions and complicated magnetic field topology inside the extraction system, a complete self-consistent model for a negative ion beam extraction system is still far away.

g. Grid bias and its effect on the extraction

The extracted negative ion current and electron current appeared to be sensitive to the bias potential applied to the electrode of the extraction system in contact with the plasma (called plasma grid, PG) [56, 57.] It is observed that there is an optimal bias voltage for a particular source and this optimal bias potential is close to the plasma potential of that source. When the bias voltage (positive polarity) of the PG is increased up to the plasma potential, negative ion current increases and the electron current and the electron density decreases. But above that optimal bias voltage, both the currents and density decrease with different rate. In fact with proper biasing,

complete suppression of the co-extracted electron current is possible [58], without much reduction in the negative ion currents. To explain these observations, different groups suggested different reasons. K. N. Leung et.al [56] suggested that it is an **E×B** drift effect on negative charged particles due to the magnetic field **B** near the grid (~100 gauss) and the electric field **E** due to positive grid bias. M. Bacal et.al [57] suggested that due to the positive bias the plasma grid depletes the electron population near by and to compensate that depletion of electrons and to maintain the charge neutrality, negative ions from the volume plasma try to come there and increase the negative ion density. A. A. Ivanov et. al. [59] observed in their photo detachment experiment that when the plasma grid is biased positively, the negative ions used to gain a directed velocity towards the grid, which helps to improve the beam current.

h. Plasma drift in front of the grid

Due to the presence of a strong transverse magnetic filter field near the extraction grid, there will be an **E×B** drift as well as a **j×B** drift in the plasma. The electric field **E** is generated in the source along the axis due to the plasma potential gradient and also as a consequence of grid bias voltage. The gradient of plasma potential is developed because of the ambipolar diffusion. If the plasma near the grid has a drift, the beam optics will not be uniform through out the extraction area. For ITER type bigger size negative ion source whose extraction area is (1.54 x 0.58) m^2 [60], the plasma uniformity over that whole extraction area is a serious challenge. Plasma uniformity has a direct impact on the beam optics and as a result on the beam divergence. The acceptable limit of the plasma uniformity for ITER is ~ ±10%.

i. Cs effects

The effect of cesium (Cs) seeding in negative hydrogen ion source is observed long back [61]. The performance of a source is improved by several factors as far as negative ion current density and negative ion density are concerned, if Cs is added into the source. But the reasons behind this enhancement of negative ion density and current are still ambiguous. The most probable reason is the enhancement of surface production yield of the negative ions, because Cs coverage on a metallic surface reduces the work-function of the surface and low work-function surface produces more negative ions [62, 63]. Another possible reason is addition of Cs in the plasma reduces the electron temperature, which helps to reduce H^- destruction. Some people have argued over its volume effect because of electron cooling which is suitable for dissociative attachment with vibrationally excited hydrogen molecules to make H^- ions [64, 65]. In the same experiment they have also observed a considerable reduction of electron density n_e, plasma potential V_p, and co-extracted electron current and increase of H^- ion current. But in other experiments [66, 67] these volume effects are not observed. The cross-sections of the excitation and ionization collisions of Cs atoms with the electrons are large. This may be the cause for electron cooling in the discharge region after introduction of Cs vapor.

Further explanation of Cs effect is based on the space charge limited current budget point of view (plasma neutrality, $n_- + n_e = n_+$ near the grid) [68]. Due to the reduction of the electron density, the remaining part of the negative component of the space charge limited current has to come from negative ion only. The transverse space charge limited current can be increased absolutely, without changing the geometry of the electrodes by addition of more positive space charge near the extraction sheath. This can be achieved by adding more Cs^+ ions for example. The Cs^+ ions are created in the pre-sheath region after coming out from the grid wall due to the H^+ ion bombardment. The Cs^+ ions, generated in the discharge due to the electron collision are also arrived near the extraction grid by simple diffusion. But this hypothesis is yet to be validated.

j. Grid temperature

If the plasma grid temperature is increased from the room temperature H^- current density is also increased. This effect is observed when the source contains some amount of Cesium [66 (already referred)]. The maximum H^- ion current is obtained during the plasma grid temperature lies between 170^0C - 200^0C. At that temperature the Cs coverage on the surface of the plasma grid is nearly one monolayer (60% coverage), which corresponds to a minimum work function ~ 1.7eV.

k. Argon effects

In many H^- ion volume sources, addition of some noble gases, particularly argon, increases the H^- ion density [69, 70, 71] and extracted H^- ion current density [72]. N. P. Curran et. al presented a hypothesis [69] to explain the effect of argon (Ar) on H^- production. According to them it is a resonant energy exchange between excited Ar atoms and H_2 molecules, which is responsible to increase the vibrational levels of H_2 molecules. But observations by M. Bacal [71] and T. Mosbach et. al [73, 74] are against it. In Mosbach's experimental results, it is clearly observed that vibrational level of H_2 molecules goes down with addition of Ar and Xe in H_2 discharge. According to M. Bacal, the noble gas effect improves the volume processes because; their addition increases the electron density. In BATMAN also it is observed [72] that not only Ar but also with krypton (Kr) and xenon (Xe) addition improves the H^- ion current density, which effectively cancel the hypothesis presented by P. Curran [69]. To explain this result obtained in BATMAN [72] R. Wilhelm [75] tries to explain the noble gas effect with the help of RF pondermotive pinch. Due to the presence of the heavier noble gas ions in the discharge, RF power coupling to plasma is better compare to that of pure H_2 discharge. Argon can be ionized easily; therefore addition of Ar increases the electron density inside the discharge. If the total pressure inside the source is kept constant, addition of Ar dilutes the hydrogen plasma. Another negative effect of Ar addition is the sputtering of the surface due to the heavier Ar^+ ions.

l. Stripping losses

The electron which is attached with the hydrogen atom to make the H^- ion, is very loosely bound (~0.7eV) [76]. Collisions with the background gas molecules or electrons can easily destroy the H^- ions by stripping that loosely bound electron. Stripping loss is a serious problem inside the extraction system where the geometry of the grids restricts the conductance and correspondingly pressure is high there. The stripped electron inside the extraction system may land in undesired location and may damage the grid. Since H^- ions become H atom after the stripping, it can not be accelerated to the full energy and therefore the deliverable power of the NBI would be reduced. If the pressure inside the extraction system is high, double stripping is also possible and a positive ion can be formed from a negative ion. After double stripping, the positive ion would accelerated towards the ion source (source is at ~ kV negative potential with respect to the ground and 3rd grid) and would damage the back plate of the ion source. To avoid the stripping loss, H^- ion sources for neutral beam injectors are usually operated in low pressure (~ 0.5 Pa or less) [77].

1.6 Negative ion and plasma diagnostics

The following parameters are the most important to optimize a negative ion source. These are: (1) Negative ion density (n_-), (2) Negative ion temperature (T_-) by measuring the negative ion velocity (v_-), (3) Electron density (n_e) at the driver region and at the extractor region, (4) Electron temperature (T_e), (5) Electron Energy Distribution Function (EEDF) and (6) Excited H_2 density (n_{H2}) at the driver region. In case of positive ion source, probes, mass spectroscopy, emission spectroscopy and laser-induced-fluorescence are the usual methods to measure the plasma parameters to investigate a positive ion source. But in case of negative ion source, special diagnostics are required to measure the above mentioned parameters due to its several features.

(i) Since electrons and negative ions are having same charge state, straight forward electrostatic probe cannot be used.

(ii) Since plasma are having positive potential due to high mobility of the electrons, negative ions are confined in the plasma and high fields are necessary to extract them for the use in mass spectrometry.

(iii) Few negative ions, particularly H^- ions have no single electron excited state below the detachment limit. So, no light is emitted when those H^- ions exhibit electron or heavy particle collision and for the same cause laser induced fluorescence does not apply directly.

The most popular diagnostic technique for measuring the negative ion density (n_-) and its temperature (T_-) is *Laser induced photo-detachment* technique

a. Negative ion density (n_-) and negative ion temperature (T_-) measurement

In Laser induced photo-detachment method, the H^- ions are pumped from the ground state to the continuum state by the laser pulse. After that the attached electron was detached according to equation (1.17).

$$H^- + h\gamma \Rightarrow H + e \qquad (1.17)$$

This reaction tells that due to the photo-detachment, there is an increase of electron density without an immediate increase of positive ion density. The outcome of the reaction consists of two particles - an electron and a hydrogen atom. By measuring the increase of electron density or H atom density, the corresponding negative ion density (n_-) either can be found. Most of the works reported so far are based on electron detection [78, 79, 80, 81, 82] method. There are few techniques are used to measure the electron density, which are,

(i) Variation of saturation current of positively biased Langmuir probe [83, 84, 85].
(ii) Shift of resonance frequency of a microwave cavity [86].
(iii) Variation of the standing wave pattern in a microwave interferometer [87, 88, 89].
(iv) Laser Thomson scattering [90].

In a *Laser detachment* diagnostic technique, choice of the laser is an important issue. The laser wavelength should have highest cross-section for photo-detachment for the specific negative ions. Nd-Yag laser pulse are most suitable [91] for H^- ions, since the corresponding photon energy (1.2 eV) is sufficient to detach the electron (affinity ~ 0.75eV) from the H^- ion but it is too low to interact with the back ground plasma by other single photon processes, such as photo-ionization. In this energy range, photo-detachment cross-section is the maximum ($4X10^{-17}cm^2$). Schematic diagram of the experimental setup is given in fig-1.6. The details of this experimental technique and the data analysis can be found in many scientific papers [78, 79, 80, 81, 82, 83, 84, 85, 91, 92].

There is another powerful diagnostic method exist to measure the negative ion density. It was found long back [93] that with the increase of negative ion density in the plasma, the damping term of the fast mode of an ion-acoustic wave decreases and the phase velocity of that mode increases. The phase velocity and the damping of that fast mode of an ion-acoustic wave is a direct measurement of negative ion density [94, 95]. This method is used so far to measure the density of highly electronegative ions like SF_6^-, O^- etc.

The negative ion temperature is derived from the negative ion velocity measurement. The velocity information is present in the time evolution of the laser photo detachment signal [76, 80].

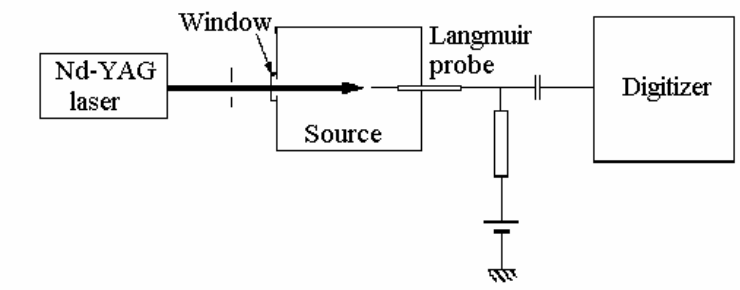

Fig.1.6. Schematic diagram of laser photo-detachment experimental technique.

b. Density measurement of vibrationally excited H_2 molecules

There are several attempts had been made to measure the population of H_2 molecules at different vibrational state in H_2 discharge plasma. G. C. Stutzin [96] has used (VUV) absorption measurement technique. D. Wagner et. al.[97] also have used the same (VUV) absorption spectroscopic method to measure the different vibrational population of H_2 molecules. P. J. Eenshistra et.al [98] have used Resonance Enhanced Multi-Photon Excitation (REMPI) method to observe high vibrational excitation of H_2 molecules. Tomash Mosbach and his group [99] have used Laser-Induced Fluorescence (LIF) technique with Vacuum Ultra Violet (VUV) radiation to detect electronic-ground state hydrogen molecules. They have measured absolute level population and decay times up to v"=13 in situ.

c. Plasma density (n_e), electron temperature (T_e), electron energy distribution function (EEDF) measurement

Langmuir probes are used to measure some basic plasma parameters like plasma density (n_e), electron temperature (T_e), floating potential (ϕ_f), plasma potential (ϕ_p) [100]. Double probe characteristic can also give the same information with less accuracy. Double probe measurements has an advantage, it is less noise prone in RF environment than that of Langmuir probe. The spectroscopic measurement can also provide the same information by studying the emission or absorption of some specific wavelengths in the plasma. Double derivative of electrostatic probe data (probe current I_p vs. probe bias voltage ϕ_b) gives the EEDF.

d. Plasma flow measurement

Mach probe (also known as *Janus probe*) is commonly used to measure the plasma flow [101, 102]. It measures the plasma velocity normalized to ion-acoustic velocity. The plasma flow has a considerable influence as far as the excited molecules transport, different ions transport and the negative ion production on the plasma grid surface [103,104]. This is the first time the plasma flow is measured in an ion source made for NBI system.

1.7 Outline of the present work

The main objective of the present work is to investigate different characteristics of an inductively coupled H^- ion source named BATMAN (**BA**varian **T**est **MA**chine for **N**egative) ion source, which is being developed for ITER NBI system. The performance of the BATMAN ion source is measured in terms of negative ion current density falling on to the calorimeter. The value of the current density varies from 2 mA/cm^2 to $25mA/cm^2$ (maximum obtained so far with proper optimization) depending upon various parameters like, the source pressure, the RF power, the extraction and acceleration voltage combination, the magnetic filter, the plasma confining field, the source depth, the cesium coverage on the plasma grid and its work function, the quantity of cesium present in the plasma, the grid temperature etc. Many of these parameters are interlinked to each other. For a given time frame and a given effort it is difficult to optimize all these parameters. Therefore the source modeling and simulation is required which can give a direction for optimization. There is no complete theory present, which can describe all the features of a negative ion source. Therefore, experiments are required to find out the characteristics of the source.

In this thesis some of the issues related to negative ion sources, which are already mentioned, are addressed and corresponding results along with the conclusion are presented. The first problem which is attempted for BATMAN 6-1 type source is to quantify its ability as a pure volume source. Three different Monte-Carlo simulation codes are developed independently by me for that purpose. The plasma transport and its relation with the pressure profile inside the source are important to understand the negative ion transport to the extraction grid. The performance of the ion source is continuously being improved by optimization of these parameters using the output of the source modeling and simulation. Measurement with Mach probe (Janus probe) identifies a clear convective plasma flow in the source. Positive grid bias helps to reduce the co-extracted electron current with the negative ions. To understand the effect of positive grid bias a series of experiments with the Langmuir probe and with the Mach probe are carried out. These measurements are very important to understand the negative ion transport, extraction physics and to design an efficient negative ion extraction system. To quantify the H^- ion density present near the grid for different source and plasma condition a novel diagnostic method based on modulation technique is developed and used. In a negative ion source, electron temperature is a crucial parameter and its determination should be precise. In high power RF source due to the presence of higher harmonics of the driving frequency creates noise to the Langmuir probe signal and produce uncertainty to the measurements. To cope with this noise, based on ion-acoustic phase detection technique an electron temperature measurement method has been established.

The presentation of the complete work is organized in the following way in this thesis. In chapter –2 main reaction processes, which are important to produce H^- ions are discussed in details. The importance of different plasma conditions and surface conditions like surface work function, surface temperature etc are highlighted on the basis of requirements of different reactions. The description of BATMAN ion source of type 6-1 is depicted in chapter –3. In chapter –4 the Monte-Carlo simulation codes which are

developed independently as a part of this PhD are described. Using a combination of three Monte-Carlo codes the present simulation job has been done. These Monte-Carlo codes are written based on the reactions discussed in the chapter-2. A zero-order estimation of H^- ion density and how it depends on different plasma parameters are also presented in this chapter through the solution of a particle balance equation. A comparison between the results obtained by the code calculation and balance equation solution are also presented here. In the same chapter the transport probability of the surface produce negative ions are also calculated by another Monte-Carlo code, which is also developed in the same process. The chapter –5 contains the experimental results of the plasma flow measurement by a Mach probe. The influence of Grid bias is described in chapter-6. Results of H^- ion density measurement by ion- acoustic wave modulation technique is presented in chapter-7. In the same chapter the electron temperature measurement by ion-acoustic wave detection method is also described. Finally the general conclusions and the outlook of the present work are presented in chapter –8.

References

[1] F. F. Chen, *Introduction to Plasma Physics*, Plenum Press, New York, 1974.
[2] J. D. Huba, NRL Plasma Formulary, Naval Research Lab., Washington DC, 2000.
[3] J. Wesson, Tokamaks, Clarendon Press, Oxford, 1987.
[4] J. D. Lawson, *Some criteria for a power producing thermonuclear reactor*, Proc. Phys. Soc., **B70**, 6, 1957.
[5] D.R.Sweetman, Nucl. Fusion, **13**, 157, (1973).
[6] H. Altman, Proc. of 13th Symp. on Fusion Technology (SOFT), Varese, Italy, 579, (1984).
[7] O. Vollmer et.al. Proc. of 15th IEEE/NPSS Symp. Fusion Eng. (SOFE), MA, (1993).
[8] W. Ott, D. Hartmann, F. P. Penningsfeld, E. Speth, Proc. 27th EPS Conf. Control. Fusion Plasma Phys., Budapest (2000).
[9] T. Stevenson et. al. Proc. of 16th IEEE/NPSS Symp. Fusion Eng. (SOFE), 537, (1995).
[10] R.W.Callis et.al. , Proc. of 15th Symp. on Fusion Technology (SOFT), Utrecht, Netherlands, 662, (1988).
[11] K.H. Berkner, R.V. Pyle, J.W. Stearns, Nucl. Fusion, **15**, 249, (1975).
[12] Y. Takeiri et.al., Rev. Sci. Instrum, **71**, 1225, (2000).
[13] M. Kawai et.al., Rev.Sci.Instrum, **71**, 755, (2000).
[14] Y. Belchenko, G. Dimov, V. Dudinikov, Nucl. Fusion, **14**, 113, (1974).
[15] M. Allen, S. Wong, Phys. Rev. Lett., **41**, 1791, (1978).
[16] M. Bacal, E. Nicolopoulou, H. Douset, Proc. Int. Symp. Production & Neutralization of Negative ions and beams, 26, BNL, New York, (1977).
[17] S. R. Waltner, K. N. Leung, W. B. Kunkel, J. Appl. Phys., **64**, 3424, (1988).
[18] Y. Okumura, M. Hanada, T. Inone, Proc. 5th Int. Symp. Production & Neutralization of Negative ions and beams, 169, Brookhaven, (1989).
[19] K. N. Leung, S. Waltner, W. B. Kunkel, Phys. Rev. Lett., **62**, 764, (1989).
[20] T. Kosaka et. al., Rev. Sci. Instrum., **73**, 961, (2002).
[21] T. Kuo et. al., Rev. Sci. Instrum., **73**, 986, (2002).
[22] K. N. Leung et. al., Rev. Sci. Instrum., **61**, 1110, (1990).
[23] J. Peters, Rev.Sci.Instrum, **69**, 992, (1998).
[24] K. N. Leung, et.al., Rev.Sci.Instrum, **62**, 100, (1991).
[25] Y. I. Belchenko, A. S. Kupriyanov, Rev.Sci.Instrum, **69**, 929, (1998).
[26] V. D. Dougar Jabon et.al., Rev.Sci.Instrum, **69**, 950, (1998).
[27] M. Mozjectchkov et. al., Rev.Sci.Instrum, **69**, 971, (1998).
[28] Y. Oka et.al., Rev.Sci.Instrum, **69**, 920, (1998).
[29] T. Ohga et. al., Rev. Sci. Instrum., **73**, 1058, (2002).
[30] Y. Okumura, et.al., Rev.Sci.Instrum, **71**, 1219, (2000).
[31] W. Kraus et.al., Rev.Sci.Instrum, **69**, 956, (1998).
[32] O. Vollmer et. al., Rev.Sci.Instrum, **71**, 939, (2000).
[33] M.Bacal et. al., Comments At. Mol. Phys., 23, 283, (1990).
[34] J. R. Hisks et. al. J. Appl. Phys., **58**, 1759, (1985).
[35] M.Bacal et. al. , J. Appl. Phys., **55**, 15, (1984).
[36] P. Berlemont, D.A. Skinner, M. Bacal, Rev.Sci.Instrum, **64**, 2721, (1993).

[37] T. S. Green, Plasma Phys. Control. Fusion, 30, 1505, (1988).
[38] R. N. Franklin, J. Phys. D: Appl. Phys., **35**, 536, (2002).
[39] O. Fukumasa et. al., J. Appl. Phys., **74**, 848, (1993).
[40] A. J. T. Holmes, Rev.Sci.Instrum, **53**, 1523, (1982).
[41] A. T. Young et.al., Rev.Sci.Instrum, **63**, 2744, (1992).
[42] A. J. T. Holmes, Rev.Sci.Instrum, 6**5**, 1153, (1994).
[43] T. A. Sathosh kumar et. Al. Phys. Plasmas, **9**, 2946, (2000).
[44] A. J. T. Holmes, Rev.Sci.Instrum, **53**, 1517, (1982).
[45] M. B. Hopkins et. al. Phys. Rev. Lett., **67**, 449, (1991).
[46] M. B. Hopkins et. al., J. Appl. Phys. **70**, 2009, (1991).
[47] T. C. Christensen et.al., IEEE Trans. Nuclear Sc., **NS-28**, 2666, (1981).
[48] P. McNeely, B. Heineman, W. Kraus, R. Riedl, E. Speth, O. Vollmer, Fusion Engineering and Design **56-57**, 493, (2001).
[49] Helen H, H. Wong, M. J. Kushner, Plasma Sources Sci. Technol, **3**, 190, (1994).
[50] F.A.Hass, L.M.Lee and A.J.T.Holmes, J.Phys.D: Appl.Phys.,**24**, 1541 (1991).
[51] A. Septier, "*Focussing of charged particles*", Academic Press, (1967).
[52] B. Heinemann, J. Bucalossi, P., Frank, R. Riedl, A.Simonin, E. Speth, R. Trainham, O. Vollmer, Proc. 20th Symp. Fusion Technol., Marseille (1998).
[53] J. H. Whealton et.al., J. Appl. Phys., **64**, 6210, (1988).
[54] J. H. Whealton et.al., Rev. Sci. Instrum., **71**, 872, (2000).
[55] C. Michaut, Phys. Rev. E, **49**, 5688, (1994).
[56] K. N. Leung et.al., Rev. Sci. Instrum., **54**, 56, (1983).
[57] M. Bacal et.al., Rev. Sci. Instrum., **56**, 649, (1985).
[58] O. Vollmer, B. Heineman, W. Kraus, P. McNeely, R. Riedl, E. Speth, R. Trainham, R. Wilhelm, Fusion Engineering and Design **56-57**, 465, (2001).
[59] A.A. Ivanov, et. al., Phys. Rev. E, **55**, 959, (1997).
[60] H. D. Falter, CCNB Meeting, Padua, Italy, (2003).
[61] Y. Belchenko, G. Dimov, V. Dudinikov, Doklady AN SSSR **213**, 1283, (1973).
[62] K. Shinto et. al., Jpn. J. Appl. Phys., **35**, 1894, (1996).
[63] J. D. Isenberg, H. J. Kwon, M. Seidl, Proc. 6th Int. Symp. Production & Neutralization of Negative ions, (1992).
[64] M. Bacal et. al., Rev. Sci. Instrum., **69**, 932, (1998).
[65] F. G. Baksht et. al., Plasma Phys. Reports, **29**, 231, (2003).
[66] T. Morishita et. al., Jpn. J. Appl. Phys., **40**, 4709, (2001).
[67] Y.Oka et.al. Research Report NIFS-**620**, Dec., (1992).
[68] J. H. Whealton et.al., Rev. Sci. Instrum., **69**, 1103, (1998).
[69] N. P. Curran et. al. Plasma Sources Sci. Technol., **9**, 169, (2000).
[70] M. Tanaka, K. Amemiya, Rev. Sci. Instrum., **71**, 1125, (2000).
[71] M. Bacal et. al., Rev. Sci. Instrum., **73**, 903, (2002).
[72] W. Kraus, P. McNeely, E. Speth, B. Heinemann, O. Vollmer, R. Wilhelm, **73**, 1096, (2002).
[73] T. Mosbach, PhD Thesis, **ISBN 3-89873-487-0**, Cuvillier Verlag Göttingen, (2002).
[74] T. Mosbach et. al., Contrib. Plasma Phys., **42**, 650, (2002).
[75] R. Wilhelm, Phys. Plasma, **10**, 513, (2003).
[76] M. Bacal, Rev. sci. Instrum., **71**, 3981, (2000).

[77] Y. Oka, et. al. Rev. Sci. Instrum, **73**, 1054, (2002).
[78] M. Bacal et. al. Phys. Rev. Lett., **42**, 1538, (1979).
[79] E. J. Eenshuistra et. al., J. Appl. Phys., **67**, 85, (1990).
[80] P. Devynck et. al., Rev. Sci. Instrum., **60**, 2873, (1989).
[81] M. Hamabe et. al., Rev. Sci. Instrum., **69**, 1298, (1998).
[82] S. Kajita et. al., Proc. 5th Int. Wokshop on Elec. Probes in Mag. Plasmas, Greifswald, Germany, (2003).
[83] F. M. Dias et. al., Rev. Sci. Instrum., **72**, 1680, (2001).
[84] M. Nishiura et. al., J. Appl. Phys., **83**, 2944, (1998).
[85] A. G. Nikitin et. al., Plasma Sources Sci. Technol., **5**, 37, (1996).
[86] W. W. Stoffels et. al., Proc. ESCAMPIG XI, St. Petersburg, Russia, 248, (1992).
[87] K. E. Greenberg et. al., Appl. Phys. Lett., **44**, 299, (1984).
[88] G. A. Hebner, J. Vac. Sci. Technol. A, **14**, 2158, (1996).
[89] C. B. Fleddamann et. al., , J. Vac. Sci. Technol. A, **15**, 1955, (1997).
[90] M. Noguchi et. al., Plasma Sources Sci. Technol., **11**, 57, (2002).
[91] M. Bacal, Plasma Sources Sci. Technol., **2**, 190, (1993).
[92] H. M. Katsch, C. Manthey, H. F. Döbele, Plasma Sources Sci. Technol., **2**, 190, (1993).
[93] N.D'angelo, S.V.Goeler, T.Ohe, Phys.Fluids, **9**, 1605, (1966).
[94] Y.Nakamura, T.Odagiri, I.Tsukabayashi, Plasma Phys. Control. Fusion, **39**, 105, (1997).
[95] A.Y.Wong, D.L.Mamas, D.Arnush, Phys.Fluids ,**18**, 1489, (1975).
[96] G. C. stutzin et. al., Rev. Sci. Instrum., **61**, 619, (1990).
[97] D. Wagner et. al., Plasma Sources Sci. Technol., **7**, 462, (1998).
[98] P. J. Eenshuistra et. al., Phys. Rev. Lett., **60**, 341, (1988).
[99] T. Mosbach et. al., Phys. Rev. Lett., **85**, 3420, (2000).
[100] M. B. Hopkins et. al., Rev. Sci. Instrum., **57**, 2210, (1986).
[101] P. C. Stangby, Phys. Fluids, **27**, 2699 (1984).
[102] I. H. Hutchinson, Phys. Fluids, **30**, 3777, (1988).
[103] A. Tanga, M. Bandyopadhyay, P. McNeely, Appl. Phys. Lett., **84**, 182, (2004).
[104] M. Bandyopadhyay, et.al., to be published in Oct. issue in J. Appl. Phys. (2004).

Chapter 2

Plasma chemical processes in a negative hydrogen ion source

Summary: It is evident that the an optimized negative ion source relies on the combination of several factors, involving the basic ion source chemistry as well the plasma parameters of the source itself. In this chapter ion source chemistry will be reviewed in a critical fashion in order to highlight the role of different reactions. It is already mentioned that, the H^- ion sources are mainly classified into two separate branches based on their H^- ion production processes, which are volume process and surface process. It is to be realized that optimizing one option often requires sacrifices on the other options and hence a source that optimize the surface production, cannot at the same time optimize the volume production.

2.1 Volume production of H^- ion

Volume H^- ion production mechanism is a two-step process [1-3]. These steps are,

a. Creation of high concentration of vibrationally and rotationally excited $H_2^*(v")$ molecular state. Here (v") denotes the vibrational state.
b. $H_2^*(v")$ molecules dissosiatively attached (DA) with low energy electrons ~ 1eV and make H^- ions.

$$H_2 \rightarrow H_2^*(v") \rightarrow H^- \qquad (2.1)$$

These two steps are described in details in the following sections. The energy level diagram and the nomenclature of the different electronic levels of a hydrogen molecules are described in [4-6] and in Appendix-1.

2.1.1 Creation of vibrationally excited $H_2^*(v")$ states

a. Low energy electron excitation (e-V)♣

The low energy electrons (< 5 eV) in the plasma collide with the ground electronic state $X^1\Sigma_g^+$ of the H_2 molecules and excite them to the higher vibrational states within the same electronic state [7].

$$e + H_2(X^1\Sigma_g^+, v") \rightarrow e + H_2^* (X^1\Sigma_g^+, v"+\Delta v") \qquad (2.2)$$

♣ All the nomenclatures of the reactions are taken from the reference [10].

The most probable change in v" is $\Delta v"=\pm 1$, so a high collision rate would be required to populate significantly the $H_2(v")$ spectrum. The e-V excitation is responsible for vibrational excitation of Hydrogen molecules up to v"=4 only. The cross-sectional data are available in data books [8, 9]. Reaction rate for this reaction is $\langle \sigma v \rangle_{eV} \approx 2\times10^{-15}$ m^3s^{-1} for v"= 0 to1 [10]. The reaction rates for every higher v" are reduced nearly one order [8].

b. High energy electron excitation (E-V)

The high energy electron excitation **(**E-V) reaction process is the main reaction which populates the higher (v" > 4) vibrationally excited H_2 molecules. The H_2 molecules with v" > 4 are most important for H^- ion formation through volume production mechanism. The E-V reaction is a two step process. This reaction is efficient only if high energy electrons *e* (>20eV) collide with ground electronic state of hydrogen molecules $X^1\Sigma_g^+$ and excite it to its upper electronic states including $B^1\Sigma_u^+$, $C^1\Pi_u^+$,...singlet states. Through radiative decay, these singlet states eventually repopulate the ground state $X^1\Sigma_g^+$ but in higher vibrational levels.

$$e + H_2(X^1\Sigma_g^+, v"=0) \rightarrow e + H_2^*(B^1\Sigma_u^+, C^1\Pi_u^+, ...) \rightarrow e + H_2^* (X^1\Sigma_g^+, v") + h\nu \qquad (2.3)$$

For radiative transition, triplet states are not considered because $X^1\Sigma_g^+$ state is singlet and radiative decay towards singlet state from triplet state is not allowed. For details of the energy level diagram please refer appendix-1. The reaction cross-sections for each vibrational levels can be estimated using corresponding Frank-Condon factor and $X^1\Sigma_g^+$ to $B^1\Sigma_u^+$, $C^1\Pi_u^+$ excitation cross-section, $\sigma(X\rightarrow B)$ and $\sigma(X\rightarrow C)$ [11] as,

$$\sigma(v">0, v') = 1.25\sigma((X \rightarrow B, C)[F(B, v", v') + F(C, v", v')] \qquad (2.4)$$

Here excitation cross-section, $\sigma(X\rightarrow B)$ and $\sigma(X\rightarrow C)$ are considered equal, because there values are very close [9,11]. F(*B*,v",v') and F(*C*,v",v') are the Franck-Condon factors, whose values are available in ref. [11]. The notation v" is the final vibrational level and v' is the initial vibrational level. The reaction rate for this reaction is, $\langle \sigma v \rangle_{EV} = 5\times10^{-17}$ m^3s^{-1}, for v"=7 [10]. The average cross-section for this excitation reaction in presence of 25 eV electrons lies in between 10^{-21} to 10^{-22} m^2, considering different vibrational levels [12]**.** Vibrational levels, from v"=5 to 12 and higher are created in this process.

c. Surface assisted excitation process (s-V)

The surface assisted vibrational excitation process creates all possible vibrationally excited H_2 molecules [13], from v"=0 to 14. This process had been proposed by Hiskes and Karo [14] and it relies on the Auger neutralization of molecular hydrogen ions H_2^+ and H_3^+ on the wall. These ions are accelerated due to the plasma potential in the sheath and hit the wall with higher velocity.

$$H_2^+ + \text{Wall} \rightarrow H_2^*(v") + \text{Wall} \qquad (2.5)$$

$$H_3^+ + \text{ Wall} \rightarrow H_2^*(v'') + H + \text{ Wall} \quad (2.6)$$

In a discharge, where H_2^+ and H_3^+ concentration is more, particularly in low pressure (~10^{-4} torr) RF discharge plasma, s-V process is more pronounced than E-V process [15]. The reaction rate is proportional to the H_2^+, H_3^+ velocity u_{ion} towards the wall. It can be written as $\langle\sigma v\rangle \propto u_{ion}.A_{eff}$. If the wall is floating, u_{ion} is expressed as Bhom velocity and A_{eff} is the effective surface area of the wall [16].

d. Surface recombination process

H atoms from the volume combine with the adsorbed H atoms on the surface of the discharge chamber and form H_2 molecules. It is recently found [17] that the molecules desorbing from the surfaces as a result of atomic recombination could also be vibrationally excited.

$$H_{volume} + H_{surface} \rightarrow H_2^*(v'') \quad (2.7)$$

The H_2 molecules, created by the surface recombination process lie mostly in the lower vibrational levels, i.e. v"=0 to 2 and populates the higher v" levels through E-V reaction [18]. This surface recombination is the only process, which can reduce the H atom concentration in the discharge. As far as volume production is concerned, the H atoms have detrimental effect on H^- formation scheme [7]. The surface recombination coefficient of a surface depends upon many parameters like, surface material, surface temperature, surface condition and texture etc. [19].

2.1.2 Destruction of vibrationally excited states

The vibrationally excited $H_2^*(v'')$ molecules are destroyed or relaxed to lower vibrational levels by many processes.

a. Excited molecule – excited molecule relaxation (V-T)

Collisions between excited H_2 molecules determine the population at the uppermost part of the spectrum. The V-T relaxation is the principle source of relaxation for v">10 [20] and populates lower v" levels.

$$H_2^*(X^1\Sigma_g^+, v'') + H_2(X^1\Sigma_g^+, v') \rightarrow H_2^*(X^1\Sigma_g^+, v''-1) + H_2(X^1\Sigma_g^+, v'+1) \quad (2.8)$$

The reaction rate is $\langle\sigma v\rangle_{VT} \sim 10^{-17}$ m^3s^{-1} for v">7 [10] and 10^{-15} m^3s^{-1} for v"=14 [20].

b. Excited molecule – ground state molecule relaxation (V-V)

It is a type of V-T reaction, where the ground state molecules collide with vibrationally excited molecules.

$$H_2^*(X^1\Sigma_g^+,v'') + H_2(X^1\Sigma_g^+,v'=0) \rightarrow H_2^*(X^1\Sigma_g^+,v''-1) + H_2(X^1\Sigma_g^+,v'=0) \qquad (2.9)$$

The reaction rate for each vibrational level is obtained from ref. [20]. The maximum reaction rate is $\langle\sigma v\rangle_{VV} \sim 1.5\times10^{-16}$ m^3s^{-1} for v'=5.

c. Excited molecule – atom relaxation (V-t)

This relaxation process takes place when vibrationally excited molecules collide with nascent hydrogen atoms, which are created in the discharge.

$$H_2^*(X^1\Sigma_g^+,v'') + H \rightarrow H_2(X^1\Sigma_g^+,v'),\ v'< v'' \qquad (2.10)$$

It is an important loss mechanism for vibrationally excited states. The reaction rate $\langle\sigma v\rangle_{Vt}$ lies between 10^{-16} m^3s^{-1} and 10^{-15} m^3s^{-1} for v"=0 to 14 [21].

d. Ionization reaction

The electrons collide with the H_2 molecules and ionize them. At higher energies and higher electron densities, above 10^{17} to 10^{18} m^{-3}, ionization becomes progressively more pronounced.

$$e + H_2^* (X^1\Sigma_g^+,v'') \rightarrow H_2^+ + 2e \qquad (2.11)$$

The ionization cross-sections are available in ref. [22]. The threshold energy for the electron impact ionization reaction decreases and corresponding reaction cross-section values increases for higher vibrational H_2 molecules [23].

e. Dissociation reaction

Electron impact excitation of the ground electronic state $X^1\Sigma_g^+$ of H_2 molecule to its first excited electronic repulsive state $b^3\Sigma_u^+$, leads to dissociation into H atoms.

$$e + H_2^* (X^1\Sigma_g^+,v'') \rightarrow H_2 (b^3\Sigma_u^+) \rightarrow 2H + e \qquad (2.12)$$

The threshold energy for this reaction is ~ 8eV [24]. For higher vibrational level, threshold energy decreases and cross-sectional value for this reaction increases [25].

f. Wall relaxation

The wall relaxation is the most dominant loss mechanism for ion sources having smaller size, which are used for plasma processing (dimensions are below 20-30 cm). After colliding with the wall, the molecules with higher vibrational states relaxed to very low vibrational states, close to the ground states.

$$H_2^*(v'') + \text{wall} \rightarrow H_2(v'),\ v' < v'' \tag{2.13}$$

Decay of $H_2(v'')$ molecules due to the wall relaxation can be approximated by [26],

$$n(v') = n(v'')\exp\left[-\frac{c}{b(v'')}\right] \tag{2.14}$$

where *c* is the number of wall collision, v'' is the ground vibrational level = 0,1,2…; and b(v'') is the decay constant. Its value varies from 1 to 2.5 for different vibrational level v''[27]. Due to wall collision, the vibrational energy would be redistributed among rotational and translational energies. The density of molecules having lower vibration levels is denoted by $n(v')$ and that of higher vibrational level by $n(v'')$.

g. Dissociative attachment (DA)

Dissociative attachment reaction is the most desirable reaction in the extraction region because in a volume H^- ion source, approximately 90% of the negative ions are generated from the $H_2^*(14 \geq v'' \geq 5)$ molecules through this process.. But this reaction is not desirable in the driver region where vibrationally excited molecules are produced.

$$H_2^*(X^1\Sigma_g^+, v'') + e \rightarrow H + H^- \tag{2.15}$$

The excited H_2 molecules are dissociated into H atom and H^- ion when it collides with low energy electrons. The dissociative attachment rate increases rapidly with increase of v'' and rotational level *J* through endothermic reaction [28,29]. The average reaction rate is $\langle \sigma v \rangle_{DA} = 5\times10^{-15}$ cm^3s^{-1} [28].

2.1.3 Creation of H^- ions

a. Dissociative attachment (DA)

The DA reaction is a loss mechanism for vibrationally excited hydrogen molecules in the driver / discharge region in a negative hydrogen ion-source, but in the extraction region it is the main mechanism to produce H^- ions through volume process. The low energy electrons combine dissociatively with vibrationally excited hydrogen molecules and form H^- ions. Some details are already presented in the previous section.

b. High Rydberg (HR) states

The Rydberg (HR) states is very close to the ground electronic state $^2\Sigma_g^+$ of H_2^+ ions, lying between $^2\Sigma_u^+$ and $^1\Sigma_u^+$ (see fig. A.1 in appendix-1) [30]. The life time of these states are ~ 100μsec [31]. The reaction rate $<\sigma v>$ to make H^- ions from these states is in between 5×10^{-5} cm^3 sec^{-1} and 1×10^{-6} cm^3 sec^{-1} [32,33]. The different possible roots to produce H- ions through this HR states are,

$$H_2^+ + e \rightarrow H_2^{**}(SES) \rightarrow H_2^*(HR) \rightarrow H^- + H^+ \quad (2.16)$$

$$H_2^+ + e \rightarrow H_2^{**}(SES) \rightarrow H_2^*(HR) + e \rightarrow H^- + H \quad (2.17)$$

The creation of HR states is indirect, via Super Excited States (SES) of H_2^+ ion. The HR states are populated through decay of SES (life time ~ 10^{-14} to 10^{-15} sec) at the potential curve crossing at the inter-nuclear distance beyond the stability point [30]. This is near the intersection region of the potential curves for SES with that for the ground electronic state $^2\Sigma_g^+$ of H_2^+ ion [34]. The Rydberg states are highly polarized in nature and dissociate to form H^- ions [35, 36]. The required electron temperature of the plasma to produce sufficient Rydberg molecules is above 50 eV [36].

2.2 Surface production of H^- ion

The H^- ions are produced on a surface in two ways,

1. Energetic hydrogen atoms (H) hit the wall having low work-function and are bounced back as H^- ions [37]. This process is defined here as, atomic process.
2. The hydrogenic ions (H^+, H_2^+, H_3^+) are also re-emitted as H^- ions from a surface with low work-function (Cs covered surface) when it hit that wall with higher velocities [38]. This process is defined as, ionic process.

2.2.1 Atomic processes

The production mechanism of an H^- ion by an energetic H atom can also be classified in to two categories.

a. By interaction with wall, the high-energy (super-thermal) H atom can bounce back as an H^- ion.

b. The low energy (thermal) H can be adsorbed on the wall surface and capture one electron from the surface and after that it can be evaporated as an H^- ion from the wall and goes back to the plasma. This mechanism is known as “surface ionization” [39].

In the first process, the energy of the H atom must be above the work function of the surface. The yield of the reaction depends upon the energy of the impinging atom and the

nature of the surface. Here the word "yield" is defined as the ratio of number of H^- ions coming out from the surface to that of the impinging H atoms. The yield goes through a maximum of value ~ 2×10^{-2} when an H atom having energy 30 eV hits the pure Tungsten (W) wall. The maximum yield value obtained so far is ~ 0.6 when an H atom having energy 2 eV collides a Cesium (Cs) covered W surface [40]. It is to be noted that the yield depends on the Cs coverage of the surfaces.

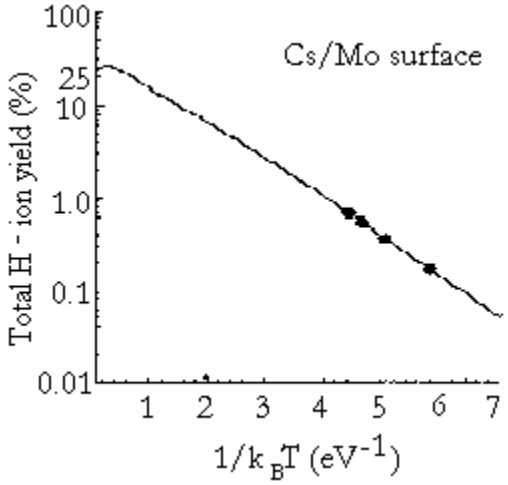

Fig.2.1. Total H^- ion yield as a function H atom energy [41]. The • marks are experimental values on Cs/Mo surface of work function 1.7eV.

The second mechanism, surface ionization is possible only if the electron affinity of the surface is smaller than that of H atom, which is 2.1 eV [42]. In such case, this process is energetically convenient to generate an H^- ion, even in the case of zero kinetic energy of the H atom. Surface ionization method has been used to create large amounts of I^-, Cl^-, Br^- ions [43]. The surface ionization efficiency can be expressed as [44],

$$\beta = \left[1 + \frac{g_0}{g_-}\exp\left(\frac{\phi - E_A}{k_B T_S}\right)\right]^{-1} \tag{2.18}$$

This is famous Saha-Langmuir equation. Here β is the surface ionization efficiency, g_0 and g_- are statistical weight of the atom and negative ion, ϕ is the surface work function, E_A is the electron affinity of the gas atom, k_B is the Boltzmann constant and T_S is the surface temperature.

The work function (electron affinity of the surface material) of Cs = 2.14 eV and LaB_6 = 2.3 – 2.7 eV which is very close to the electron affinity of H atom. The surface work function ~ 1.5 eV is observed with partial coverage of Cs on metal surface [45]. Hence one would expect a contribution of H^- ion by surface ionization if one could go sufficiently down in work function and increase target temperature.

The energy distribution of the H atom

The energy distribution of the H atoms is a critical parameter for the surface H^- formation. According to energy level diagram (see fig. A.1. in appendix-1) an average energy ~ 4.5eV is available per H atom pair during dissociation of the H_2 molecule. The dissociative attachment (DA) process also produces an H atom with energy > 1 eV. The wall interaction of the H atom is quasi elastic for a large number of targets and energies [46], see fig.2.2. At energy below 1eV, the reflection coefficient starts to go down very fast because the H atom starts sticking to the surface. It would be expected that with the "Hot" walls, the H would be able to make more bounces. It is likely that the produced H atom cross the source chamber several times in a quasi-elastic mode before been adsorbed on the wall surface. The H atom evaporated from the surface will be thermal or sub-thermal. The density of the H atom at energies of 2eV will be simply the volume rate of H_2 dissociation multiplied by the time it takes to bounce ~ 10 times on the wall [47]. The energy distribution function of H will be made of a thermal part due to re-evaporated atoms and a super-thermal part centered on 1eV made of the native H atoms. It can be reckoned that for the values of electron density, neutral gas density mentioned before and corresponding dissociation rate gives the super-thermal tail is of the order of ~3% of the background molecular gas density. In a typical small ion source, at low pressure ~ 0.5 Pa and having plasma conditions like n_e~10^{18} m^{-3}, T_e~500 K, the mean free path λ of the H atom is ~ 100 cm. The atoms are mainly colliding with the wall before colliding with the background gas molecules.

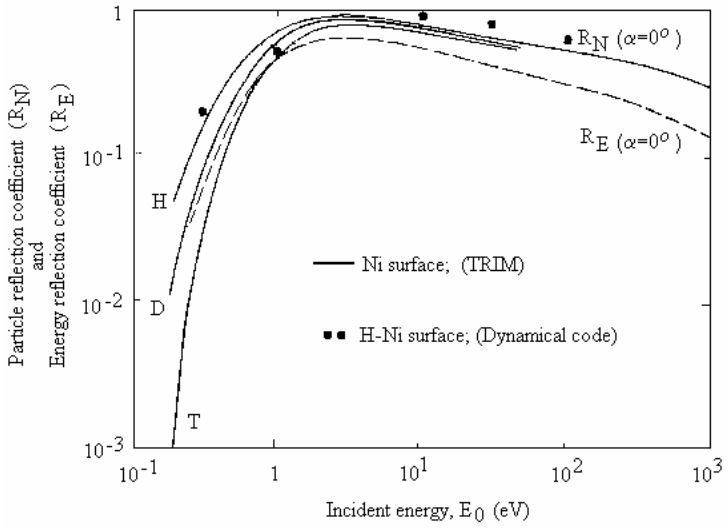

Fig.2.2. Particle and energy reflection coefficients R_N, R_E for the H atom having different energy [46].

2.2.2 Ionic processes

The H^- ions are produced on a surface by the energetic positive ions (H^+, H_2^+, H_3^+), when they collide with a surface having low work function. The positive ions are accelerated in the sheath near the wall by the sheath potential. If the energy of those accelerated ions is of the order of ~20 eV, the H^- ion yield is near the maximum in the yield curve, see

fig.2.3 (a) [48]. The above data was obtained for a Cs/Mo surface having work function 1.7 eV. In the ref. [48], the minimum value of work function achieved experimentally was 1.35 eV ± 0.5 eV. In figure.2.3 (b), the surface produced H^- ions have energy ~ eV.

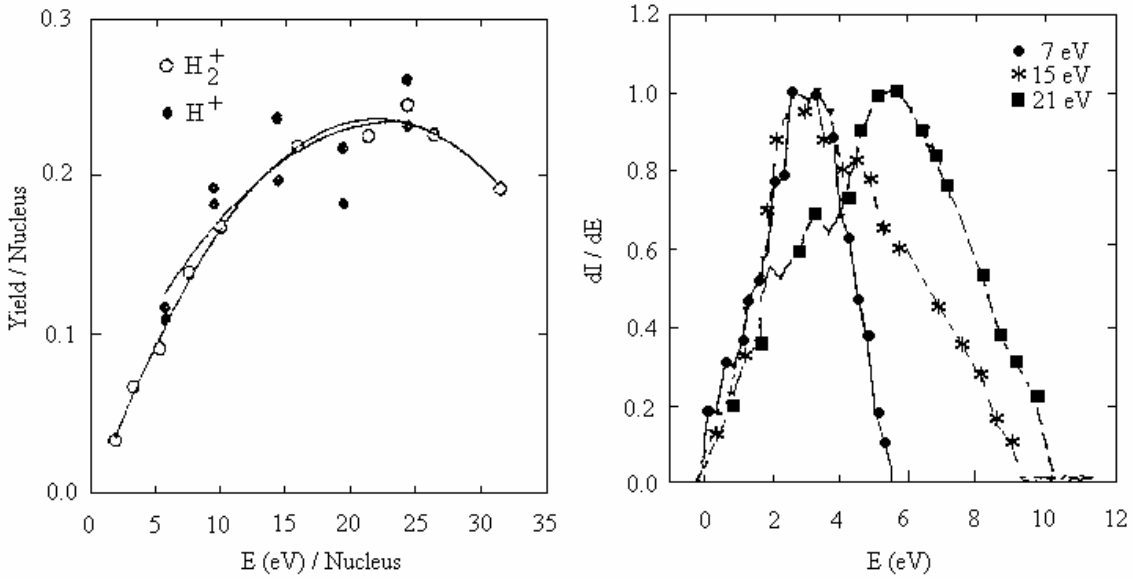

Fig.2.3. (a) Optimum H^- ion yield per nucleon for H^+ and H_2^+ ions on Cs/Mo surface.
(b) Energy distribution of H^- ions for H_2^+ incident on Cs/Mo @ 1.7 eV work-function [48].

2.3 Destruction of H^- ions

a. Electronic detachment (ED)

The binding energy for the loosely bound electron in an H^- ion is ~ 0.75 eV [49]. If an electron having energy above 0.75 eV collides with an H^- ion, it will destroy the H^- ion by stripping that loosely bound electron.

$$H^- + e \rightarrow H + 2e \qquad (2.19)$$

The reaction rate of the ED reaction increases with electron temperature and it is, $\langle\sigma v\rangle \sim 2\times10^{-14}$ m^3s^{-1} for energy ~ 1.5eV and $\langle\sigma v\rangle_{ED} \sim 1.3\times10^{-12}$ cm^3s^{-1} for energy ~ 30eV. To minimize the ED process near the extraction grid, the electron temperature near that region should be below 1eV in an H^- ion source. The reaction rates and cross-sectional values of the ED reaction for different electron temperature are available in ref. [50].

b. Mutual neutralization (MN)

The neutralization reactions are the most dominant H^- ion loss process. The cross-sectional data are available in ref. [51].

$$\boldsymbol{H^- + H^+ \rightarrow 2H} \qquad \textbf{(2.20)}$$

$$\boldsymbol{H^- + H_2^+ \rightarrow H_2 + H} \qquad \textbf{(2.21)}$$

$$H^- + H_3^+ \rightarrow 2H_2 \qquad (2.22)$$

The reaction rate of these reactions are $\langle\sigma v\rangle_{MN} \sim 1\times10^{-13}$ cm^3s^{-1} [52]. In spite of this loss mechanism, the space charge compensation principle requires positive ions in the extraction region to extract negative charged particles.

c. Associative detachment (AD)

AD reaction and ED are inter-linked and create a cascade effect [53]. To avoid this destruction process, the pressure, the atomic density and the electron temperature in the extraction region should be kept low. The reaction rate is $\langle\sigma v\rangle_{AD} \sim 10^{-15}$ m^3s^{-1} [52].

$$\boldsymbol{H^- + H \rightarrow H_2 + e} \qquad \textbf{(2.23)}$$

$$H^- + H_2 \rightarrow H + H_2 + e \quad \text{(stripping loss)} \qquad (2.24)$$

As a summary of this chapter the complete reaction branches are depicted in fig. 2.4.

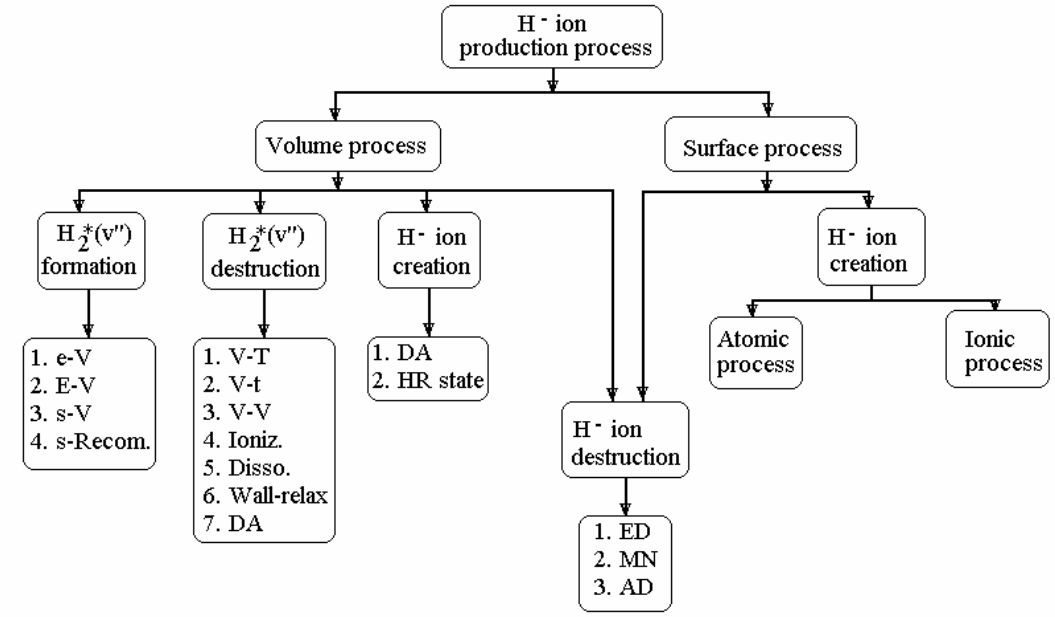

Fig. 2.4. Reaction branches of H^- ion production process. The nomenclatures of the reactions are also given in ref. [10].

References

[1] M. Bacal et. al., Rev. Sci. Instrum., **67**, 1138, (1996).
[2] A. I. Livshits et. al., Plasma Sources Sci. Technol., **3**, 465, (1994).
[3] O. Fukumasa, M. Shinoda, Rev. Sci. Instrum., **69**, 938, (1998).
[4] G. Herzberg, *Molecular Spectra & Molecular Structure*, VNR, (1966).
[5] P. M. Morse, Phys. Rev., 34, 57, (1929).
[6] T. E. Sharp, Atomic Data **2**, 119, (1971).
[7] M.Bacal et. al., Comments At. Mol. Phys., 23, 283, (1990).
[8] C. F. Barnet et.al. *Atomic Data for Controlled Fusion Research*, ORNL, C.2.17, (1977).
[9] H. Tawara et. al., Atomic data Involving Hydrogen relevant to Edge Plasma, IPPJ-AM-46, (1986).
[10] P. Berlemont, D.A. Skinner, M. Bacal, Rev.Sci.Instrum, **64**, 2721, (1993).
[11] J. R. Hiskes, J. Appl. Phys., **70**, 3409, (1991).
[12] J. R. Hiskes, Comments At. Mol. Phys., **19**, 59, (1987).
[13] J. R. Hiskes et. al., J. Appl. Phys., **67**, 6221, (1990).
[14] J. R. Hiskes et. al., J. Vac. Sci. Technol. **A 3**, 1229, (1985).
[15] J. R. Hiskes, Appl. Phys. Lett. 57, **231**, (1990).
[16] M. A. Liebermann, A. J. Lichtenberg, *Principles of Plasma Discharges and Materials Processing*, John Wiely & Sons, NY, (1994).
[17] R. J. Hall et. al., Phys. Rev. Lett., **60**, 337, (1988).
[18] M. Bacal et. al., AIP Conf. Proc. **639**, 13, (2002).
[19] H. J. Wise, B. J. Wood, J. Phys. Chem, **67**, 1462, (1963); *Errata*: J. Phys. Chem, **68**, 3911, (1964).
[20] J. Loureiro, C. M. Ferreira, J. Phys. D: Appl. Phys., **22**, 1680, (1989).
[21] J. R. Hiskes, A. M. Karo, J. Appl. Phys., **56**, 1927, (1984).
[22] D. Rapp, P. Englander-Golden, J. Chem. Phys., **43**, 1464, (1965).
[23] M. Cacciatore et. al., J. Phys. D: Appl. Phys., **13**, 575, (1980).
[24] M. A. Khakoo et. al., J. Phys. B: At. Mol. Opt. Phys., **27**, 2355, (1994).
[25] D. T. Stibbe et. al., New J. Phys., **1**, 2.1-2.9, (1998).
[26] A. M. Karo et. al., J. vac. Sci. Technol. A, **3**, 1222, (1985).
[27] J. R. Hiskes et. al., Appl. Phys. Lett., **54**, 508, (1989).
[28] A. P. Hickmann, Phys. Rev. A, **43**, 3495, (1991).
[29] J. M. Wadehra, Phys. Rev. A, **29**, 106, (1984).
[30] J. F. Schneider et. al. J. Phys B, **24**, L289, (1994).
[31] S. M. Tarr et. al. J. Chem. Phys., **74**, 2869, (1981).
[32] P. G. Datskos et. al., Phys. Rev. A, **55**, 4131, (1997).
[33] A. Garscadden et. al., Plasma Sources Sci. Technol., **4**, 268, (1995).
[34] L. A. Pinnaduwage et. al., Phys. Rev. Lett., **70**, 754, (1993).
[35] L. A. Pinnaduwage et. al. J. Appl. Phys., **85**, 7064, (1999).
[36] V. D. Dougar-Jabon, Physica Scripta, **63**, 322, (2001).
[37] Y. Belchenko, Rev. Sci. Instrum., **64**, 1385, (1993).
[38] M. Ogasawara et. al., Proc. IAEA TCM Neg. Ion based NBI, Ibaraki-ken, Japan, 99, (1991).
[39] A. Piotrowski et. al. Nucl. Instrum. Meth. Phys. Research B, **129**, 410, (1997).

[40] H. L. Cui, J. Vac. Sci. Technol. A, **9**, 1823, (1991).
[41] B. S. Lee, M. Seidle, Appl. Phys. Lett., **61**, 2857, (1992).
[42] http://web.mit.edu/3.091/www/pt/pert8.html.
[43] M. Shmid et. al., Nucl. Instrum. Meth., **186**, 349, (1981).
[44] J. Pelletier et. al., J. Appl. Phys., **50**, 4517, (1979).
[45] M. Seidle et. al., Proc. 6th Int. Symp. Prod. & Neutralization of Neg. Ion, AIP, 25, (1992).
[46] D. E. Post, R. Behisch, Physics of Plasma-Wall Interactions in Controlled Fusion, NATO ASI series B, **131**, 423, (1986).
[47] J. Geddes et. al. Plasma Sources Sci. Technol., **2**, 93, (1993).
[48] J. D. Isenberg et. al., Proc. 6th Int. Symp. Prod. & Neutralization of Neg. Ion, AIP, 38, (1992).
[49] B. M. Smirnov, Phys. Uspekhi, **44**, 221, (2001).
[50] D. S. Walton et. al., J. Phys. B: At. Mol. Phys., **4**, 1343, (1971).
[51] M. J. J. Eerden et. al., Phys. Rev. A, **51**, 3362, (1995).
[52] A. A. Matveyev et. al., Plasma Sources Sci. Technol, **4**, 606, (1995).
[53] M. S. Huq et. al., Phys. Rev. A, **27**, 2831, (1983).

Chapter 3

Description of the ion source

Summary: This chapter describes the different parts of the BATMAN type 6-1 ion source and its utility in the sense of negative ion production. The typical behavior and characteristics of the ion source in terms of different current densities for different filling pressures, input power levels etc. are also presented.

3.1 Introduction

The conventional filament based ion sources are used mostly for the existing neutral beam (NB) systems [1,2]. The operational life of these ion sources are limited by the life time of the filaments (~ few 100 operational hours). Therefore for the ion sources designed for long pulse and for long operational time NBI systems, ion sources having filaments are not desirable because its need more maintenance for the filament replacement. In a fusion reactor, like ITER, radio-active environment will make this maintenance job difficult. Generally, the ion sources driven by radio-frequency (RF) have no filament inside and therefore maintenance will be much less. Moreover, RF power supply is simple and economical compare to that of filament source. Due to these advantages, the RF sources are more attractive than the conventional filament arc sources for long pulse operation.

BATMAN ion source is an inductively coupled (IC) negative hydrogen ion radio frequency (RF) source. It is under a development project for ITER Neutral Beam (NB) system and its performance is continuously being improved by optimization of different operational parameters and geometrical shape. Therefore it is obvious that its shape and components are likely to be different in the future than what it has now.

3.2 Description of the source

The BATMAN 6-1 type source can be divided into three parts: *driver*, *expansion* region and *extraction* system.

Driver

The *driver* is the region where the plasma is created. It is a ceramic Alumina (Al_2O_3) cylinder of diameter ϕ = 24.5cm, length l = 15cm and wall thickness 8mm sitting backside of the ion source. A water cooled RF coil (6.5 turns, 14.5 μH inductance) is wrapped externally around that ceramic cylinder (see fig.3.1). The ceramic cylinder acts

as a vacuum encloser and help to couple RF power between the coil and the plasma. The coil is connected to a 1 MHz RF generator which can deliver up to 170kW. A photograph of the *driver* during the plasma shot is shown in fig.3.2.

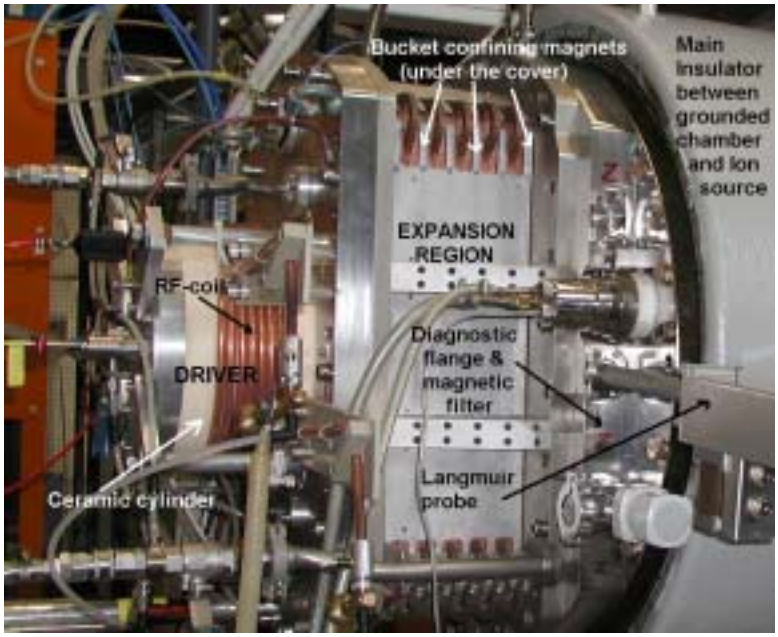

Fig.3.1. Photograph of BATMAN 6-1 type ion source, fitted with the test bed.

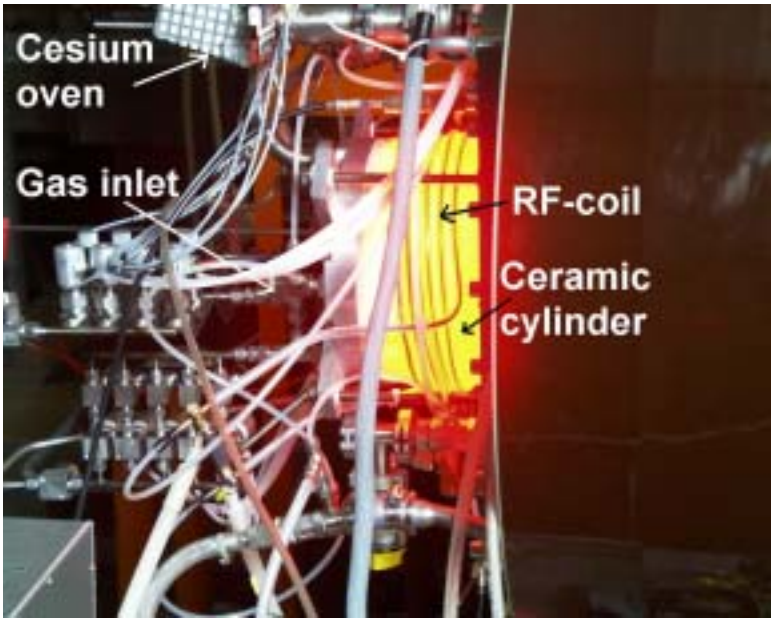

Fig.3.2. Hot *driver* during a plasma shot. The present plasma discharge is done without FS.

To protect the ceramic cylinder from thermal load and plasma sputtering and erosion, a water cooled tungsten coated *Faraday screen* (FS) is used inside the cylinder (see fig.3.3). Due to the presence of the FS, the capacitive coupling between the RF coil and the plasma is avoided, which helps to reduce the sputtering of the ceramic by the bombardment of the ions. It is measured by water calorimetry that around 20% of the RF power is deposited on the FS. The temperature of the hottest point of the *driver* goes ~ 70^{o}C, measured by an infra-red (IR) camera at 100kW input power for 15 seconds of continuous operation.

Fig. 3.3. Tungsten coated faraday screen is sitting inside the driver, attached with the expansion region.

Expansion region

The *driver* is attached to the *Expansion* region (a rectangular box of volume ~ 30×58×19 cm^3) with the help of a *transition* flange of thickness ~ 4cm. The *expansion* region is a "bucket" [3] source chamber (standard Joint European Torus (JET) type), made of copper with permanent magnets are situated outside the chamber (see fig. 3.1). Permanent magnets are Sm-Co (Somarium-Cobalt) type, having field strength ~ 1 Tesla on the surface of the magnet. These permanent magnets are arranged in a line cusp configuration [4]. The cusp magnetic field helps to confine the electron in the plasma, because the electron diffusion across a perpendicular magnetic field is reduced by several orders. The *transition* flange and the *back plate* of the *driver* are also equipped with the confining magnets to avoid the loss of plasma. The chamber is water cooled.

At the end of the *expansion* chamber, a special adapter flange of thickness 5cm and having the same opening area as *expansion* chamber is attached. There are few ports are available in that flange for the diagnostic purpose near the grid; therefore we called it *diagnostic flange*. The *diagnostic flange* is also the housing of the filter magnets (see fig.

3.1). Magnetic filter is an essential component of a negative ion source, because it helps to reduce the electron diffusion from the driver towards the grid and therefore reduce the co-extracted electron current. It also helps to reduce the electron temperature T_e near the grid and therefore reduce the destruction of negative ions. Next to the *diagnostic* flange, the extraction system for negative ions is placed.

Extraction system

BATMAN ion source has three-grid extraction system. The first grid which is facing the plasma is called *plasma grid* (PG), the second grid is called *extraction grid* (EG) and the third grid is called *acceleration grid* (AG). During our negative ion extraction experiments, the potential of the ion source and the PG are typically 20 kV negative with respect to (w.r.t) the AG. The AG is grounded and has the same potential with the rest of the test bed body. This potential arrangement makes the EG and AG positive w.r.t. the source and PG and therefore negative ions are extracted and accelerated. The EG is 3 – 6 kV positive w.r.t . the PG (17 – 14 kV negative w.r.t. the ground and AG). The potential on the EG is not a free parameter. It is linked with the maximum extractable current density, based on Child's law [5].

Child's formulation is derived for electrons, as shown in the equation (3.1), which estimates the space charge limited electron current density, the maximum electron current density an extraction hole can deliver.

$$j_e = \left[\left(\frac{4 \in_0}{9} \right) \left(\frac{2e}{m_e} \right)^{1/2} \left(\frac{\phi^{3/2}_{EG}}{d_{eff}^{\ 2}} \right) \right] \tag{3.1}$$

where $\in_0$ is the free space permittivity e and m_e are the electronic charge and mass respectively, d_{eff} is the effective distance of the electron emission surface from the EG plane, ϕ_{EG} is the extraction voltage applied on the EG w.r.t. the ion source (w.r.t. PG) and j_e is the electron current density through the PG hole which can be calculated as ($n_e e v_e/4$). The electron temperature (T_e) near the PG determines velocity of the electrons v_e. The Child's law is applicable to other charges also where e and m_e have to be replaced according to the charge and mass of the ion to be extracted. The quantity,

$$P = \frac{j_e \pi a^2}{\phi^{3/2}_{EG}} \tag{3.2}$$

is known as *perveance*. It depends only on the geometry of the extraction hole (radius = a) and the charge type. At properly matched condition (*perveance* matched condition [5]) between the extracted current density and the extraction voltage, the beam has minimum divergence.

The AG is 17 – 14 kV positive w.r.t. the EG. This potential is the pre-acceleration voltage (before1 MV acceleration). Two different sets of grid structure are used for the H^- ion beam extraction: CEA (obtained from CEA, Cadarache, France) and large area grid

(LAG) which is designed and fabricated in-house. The comparative dimensions of these two grid systems are shown in fig.3.4. The actual photographs are shown in fig3.5 and fig. 3.6. Due to the positive potential of EG, both electrons and negative ions are extracted through the PG. Magnetic field inside the EG helps to filter out the co-extracted electrons from the negative ion beam. The orientation of the electron suppression magnets in the EG are such that, the magnetic field can penetrate deep into the plasma and help to reduce the electron density near the PG holes. The reduction of electrons reduces the co-extracted electron current. In BATMAN source PG can be biased separately w.r.t. the ion source body.

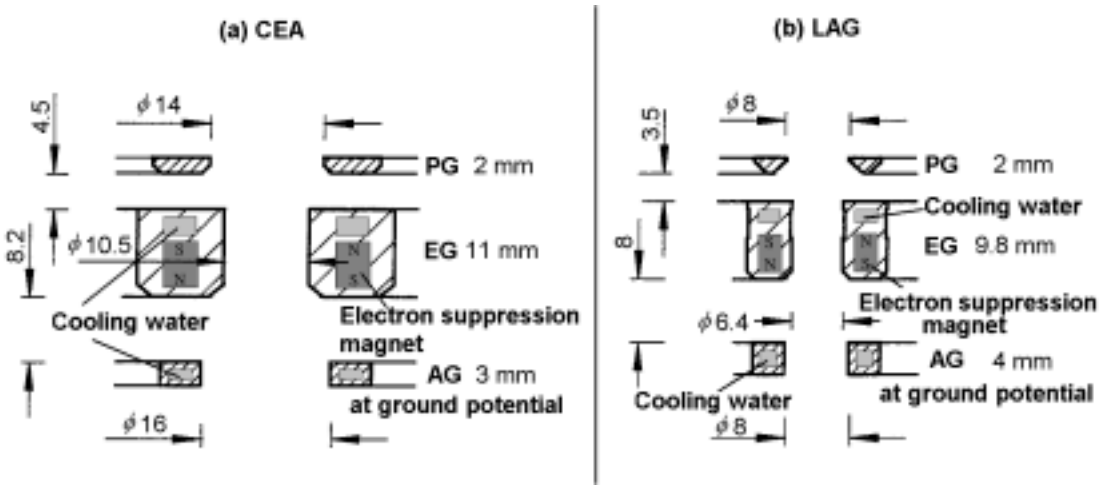

Fig.3.4. Comparative schematic representation of (a) CEA and (b) LAG grid system, with dimensions. In both the system PG is made of Molybdenum and EG and AG is made of copper.

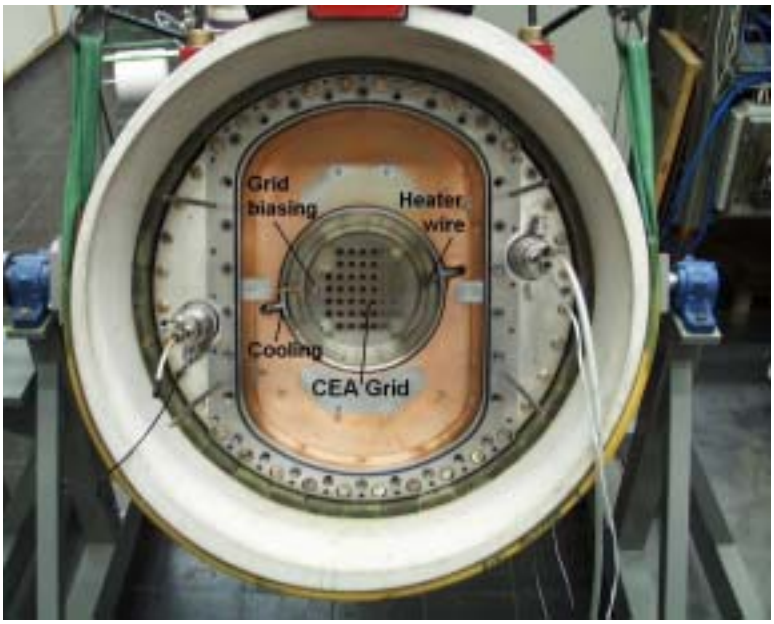

Fig. 3.5a. Photograph of CEA grid system, housed inside the main insulator. CEA grid has 44 holes and having ~ 67 cm^2 extraction area.

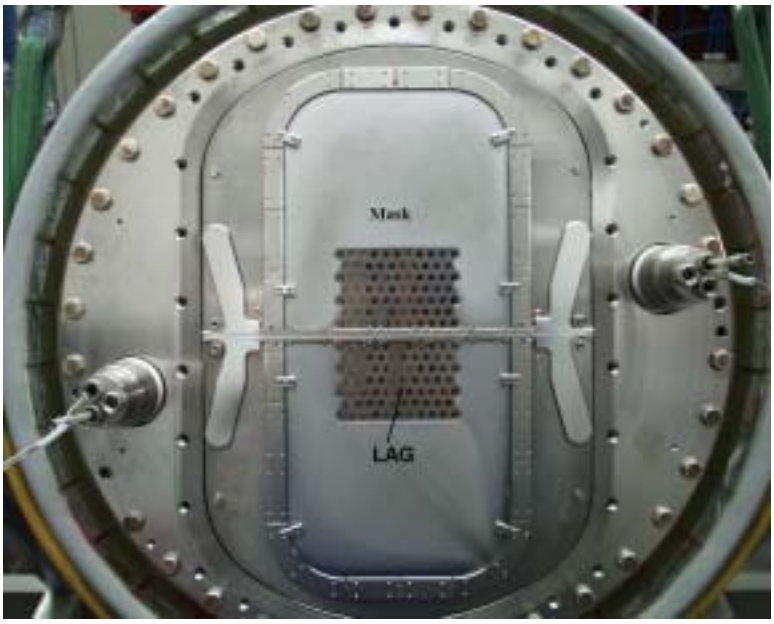

Fig. 3.5b. Photograph of masked LAG system. LAG has total 383×2 (sections) holes but only 148 holes are exposed to plasma for extraction (~74 cm^2 extraction area). The masking is done to compare its results with CEA grid system.

3.3 Description of the diagnostic and other subsystems

3.3.1 Diagnostic system

BATMAN ion source is being optimized by measuring the H^- ion current density on the calorimeter. The H- ion current density depends on the gas pressure, gas temperature, densities of different ions and molecules, the plasma parameters like n_e, T_e, the plasma potential, the floating potential etc. It also depends on the extraction and acceleration voltage combination, Cesium coverage on the plasma grid and therefore the work function of the plasma grid surface and so on. The measurements of these parameters are essential for the optimization purpose. The diagnostic system comprised of electrical probes (Langmuir probe, Mach probe, double probe), spectroscopy, calorimeter etc. A list of the diagnostic systems is given in table-3.1.

Table 3.1 Different diagnostic systems

Parameter	Diagnostic technique
1. Plasma density n_e.	1. a. Langmuir probe, b. Doble probe, c. Optical emission spectroscopy.
2. Plasma temperature T_e and Electron energy distribution function (EEDF).	2. a. Langmuir probe, b. Double probe, c. Optical emission spectroscopy and d. Ion-acoustic modulation technique.
3. Plasma potential and Floating potential.	3. Langmuir probe.
4. Density of H, H_2 and H_2^*.	4. Optical emission spectroscopy.
5. Density of Cs atom and Cs^+ ion.	5. Optical emission spectroscopy.
6. Density of H^- ion n..	6. Modulation technique and laser photo-detachment (in preparation).
7. H^- ion beam profile, beam divergence and beam power.	7. a. Thermocouples embedded into the calorimeter plate. b. Infra red camera.
8. H^- ion total current and current density.	8. a. Water calorimeter, b. Evaluating from the beam profile on the calorimeter, c. Electrical measurement (by shunt) in the grid system.
9. Gas temperature.	9. Optical emission spectroscopy.
10. Plasma flow.	10. Mach probe.
11. RF power.	11. a. Voltage and current measurement, b. Magnetic loop. c. Water calorimetry in the FS.
12. Temperature of the source body and plasma grid.	12. Thermocouple.
13. Stripping loss	13. a. Faraday cup in the beam line (in preparation). b. Doppler shift spectroscopy (in preparation).
14. Work function measurement of the plasma grid surface.	14. Probe based on photoelectric effect (in preparation).

3.3.2 Other subsystems

The other subsystems are electrical system, internal vacuum system, external vacuum system, gas feed system, data acquisition and control system.

The electrical system contains HV power supply for the RF generator, HV power supply for the extraction and acceleration grids with proper voltage divider and shunt resistances for the electrical measurements of the currents and voltages. The measurements of the

total extracted plasma current through the PG (*I-drain*), electron currents through the EG (*I-electron*) and negative ion current through the AG (*I-G3*) are done. The complete electrical circuit is depicted in appendix-2 in fig. A.2.1.

The internal vacuum system is comprised of Titanium sublimation pump having pumping speed ~ few times 10^5 liters/sec. for hydrogen gas (H_2/D_2) gas only. The base pressure in the test bed tank is ~ 10^{-7} mbar, measured by ionization pressure gauge. The pressure inside the driver is measured by (Baratron) a capacitance type membrane manometer.

The external vacuum system comprises of a combination of turbo pumps and rotary pumps. The total pumping speed of the external vacuum system is ~ 2650 liters/sec. The layout of the external vacuum system is shown in appendix-2, fig.A.2.2. The layout of the gas feed system is shown in appendix-2 in fig.A.2.3. The working gas is H_2 or D_2. There are provisions to mix other gas as well, particularly the noble gases because it is observed that small admixture of argon (Ar) helps to increase the negative ion density and current [6,7,8].

A CAMAC based system is used for a data acquisition and control (DAC) in BATMAN ion source test bed. Typical outputs of the (DAC) system are shown in appendix-2, fig.A.2.4 and fig.A.2.5.

3.4 Typical characteristics of the source

The performance of the BATMAN ion source is measured in terms of negative ion current density falling on to the calorimeter. The value of current density varies from 2 mA/cm^2 to 25mA/cm^2 (maximum obtained so far with proper optimization) depending upon various parameters like, the source pressure, the RF power, the extraction and acceleration voltage combination for a given extraction grid system (perveance), the magnetic filter, the plasma confining field, the source depth, the cesium coverage on the plasma grid and its work function, the quantity of cesium present in the plasma, the grid temperature etc. Many of these parameters are interlinked to each other. For a given time frame and a given effort it is difficult to optimize all these parameters. Therefore the source modeling and simulation is required which can give a direction for optimization. The performance of the ion source is continuously being improved by optimization of these parameters using the output of the source modeling and simulation. There is no complete theory present, which can describe all the features of a negative ion source. Therefore, experiments are required to find out the characteristics of the source. Some typical characteristic results are shown in fig. 3.6, 3.7 and 3.8.

BATMAN ion source is operated both in surface production process mode (with Cs) and in volume production mode (without Cs). From the fig.3.6 it is observed that with Cs, the extracted H^- ion current density is nearly independent on the H_2 gas filling pressure, which is a pure signature of surface process. Without Cs, the current density increases linearly with the pressure, as expected in a pure volume process. The estimated current

density with the help of simulation, based on volume production (chapter-4) is 1-2 mA/cm^2 with 0.5 Pa pressure in the driver.

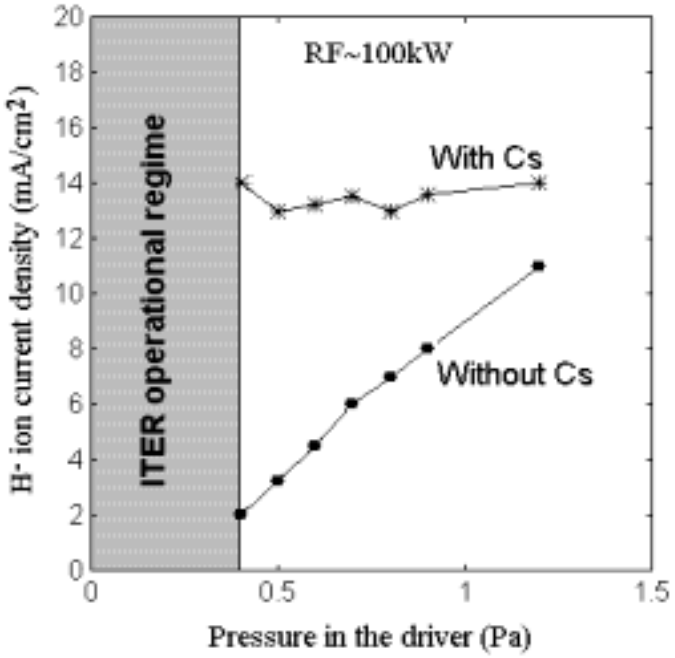

Fig.3.6. The typical extracted H^- ion current density using LAG grid for different pressure inside the source during the pulse. Below 0.3 Pa pressure is the ITER requirement.

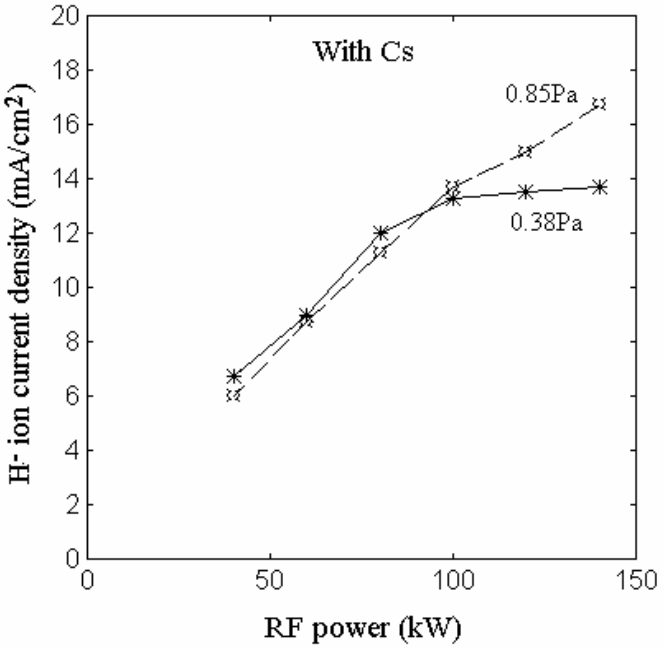

Fig.3.7. The typical extracted H^- ion current density using LAG grid for different RF power.

At low pressure, below 0.5 Pa the source can deliver 4 - 5 times more H^- ion current density, if it is operated with Cs. ITER operational regime is below 0.3 Pa filling pressure and the target is 28 mA/cm^2. Since Cs injection helps to get higher current density even at lower pressure (below 0.5 Pa), it is necessary to operate the source with Cs. But operation with Cs has few problems which are under investigation. These are: (1) the H^- ion current density is strongly depends on the surface coverage with Cs, the source wall temperature, the sputtering and impurity deposition on the wall, gas mixture, amount of Cs in the plasma etc. Due to that the H^- ion current density with Cs, is unstable and difficult to control. (2) Cs is also deposited inside the grid structure which leads to often breakdown between the grids. Therefore with time the holding capability of the required voltage level between the two grids becomes low.

The fig.3.7 shows that the H^- ion current density increases linearly with input RF power. At lower source pressure, saturation with RF power is also observed. The extraction voltage applied in to the EG has a considerable influence on the extracted current density as discussed with equation (3.1) and shown in fig.3.8. The experimentally observed relationship between the negative ion current density and the extraction voltage is also observed qualitatively in the simulation result (chapter-4, fig. 4.22).

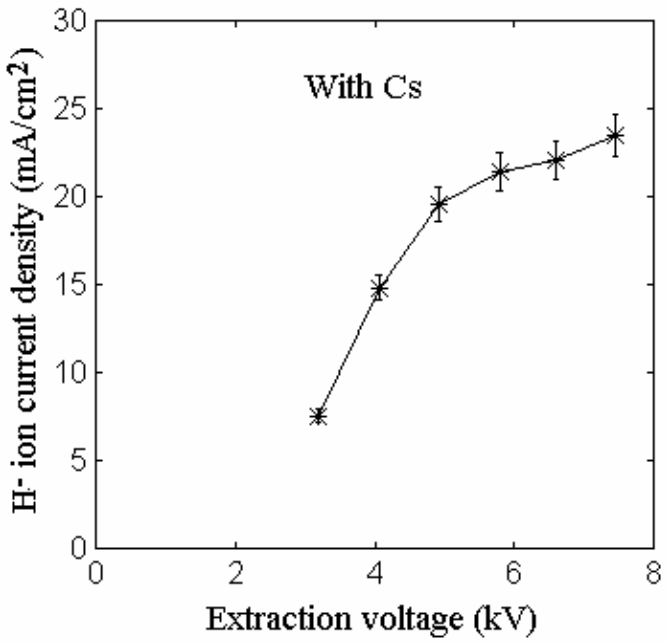

Fig. 3.8. The extracted H^- ion current density using LAG grid for different extraction voltages. The source is operated with Cs.

The addition of argon (Ar) increases the H^- ion current density in BATMAN source [9] only when CEA grid was used for the extraction. The diameter of the extraction holes, drilled on the CEA plasma grid (PG) is 1.4cm. The argon effect is not observed when

LAG grid, having 0.8cm PG hole diameter is used. It is expected from the principle of optics, that if a lens has a bigger diameter, it is susceptible to the aberrations and makes the optics bad. The same principle is applicable here also, because by applying different voltages on different grid systems, electrostatic lenses are formed in front of the grid holes which extract and guide the ions in a defined path. When Ar is added into the hydrogen plasma, the electron density increases and the positive heavier ions (Ar^{+}) are also present in the plasma which may change the plasma meniscus in front of the plasma grid holes and alter the ion optics. It is experimentally observed in BATMAN that when Ar is added in the source having CEA grid, the beam get narrower (beam profile on the calorimeter) and almost all the beams falls on the calorimeter and correspondingly the calculated current density from the calorimeter data is also increased. When Ar is not used in the same source configuration (with CEA grid), fraction of the beam falls outside the calorimeter and lost. The LAG grid has smaller grid holes and therefore has better optics. No further improvement of optics in LAG is observed when Ar is applied [10].

References

[1] O. Vollmer, et. al., Proc. of the 15th IEEE / NPSS Symposium on Fusion Eng. (SOFE), MA, USA, 579, (1993).

[2] Y. Takeiri, et. al., Rev. sci. Instrum., **71**, 1225, (2000).

[3] H. Altmann, Proc. of the 13th Symposium on Fusion Technology (SOFT), Varese, Italy, 579, (1984).

[4] K. N. Leung and K. W. Ehlers, Rev. Sci. Instrum., **55**, 342, (1984).

[5] S. Humphries, Jr., *Charged Partcle Beams*, Wiley, New York, page-199, (1990).

[6] N. P. Curran et. al. Plasma Sources Sci. Technol., **9**, 169, (2000).

[7] M. Tanaka, K. Amemiya, Rev. Sci. Instrum., **71**, 1125, (2000).

[8] M. Bacal et. al., Rev. Sci. Instrum., **73**, 903, (2002).

[9] W. Kraus, P. McNeely, E. Speth, B. Heinemann, O. Vollmer, R. Wilhelm, **73**, 1096, (2002).

[10] W. Kraus, M.Bandyopadhyay, H.D. Falter, P. McNeely, E. Speth, B. Heinemann, O. Vollmer, R. Wilhelm, presented Rev. Sci. Instrum., **75**, 1832, 2004)

Chapter 4

Model and simulations for H^- ion production and transport

Summary: Negative hydrogen ion production by volume process and its transport in a negative hydrogen ion source has been simulated by a combination of three 3-D Monte-Carlo codes which are developed. These are (1) neutral transport code, (2) negative hydrogen ion production code and (3) negative hydrogen ion transport code. The first code has been used to calculate the spatially resolved density spectrum n_v of the vibrationally excited H_2 molecules. With the second code, the production and the distribution of H^- ion density n_- in the discharge volume has been calculated. And with the third code, the calculation of the survival probability of H^- ions up to the extraction grid has been carried out. In all cases, the experimentally observed plasma parameters as well as background gas density and temperature profiles are inputs during trajectory calculation. It has been found that the negative ion density is almost uniform from the ion production zone (driver) to the grid. However H^- ions, which are produced within a few centimeters from the grid, are only able to reach the extraction hole. To compare the code calculation, a 0-D particle balance rate equation is also solved. In the case of volume production mechanism, both the code calculation and particle balance equation solution show that n_- near the grid strongly depends on the local n_v only and n_- is increased if electron temperature T_e is reduced. The H^- ion density near the grid increases with the local electron density n_e until n_e becomes equal to n_v. Beyond that point, n_e dependency decreases slowly.

Another code is developed to simulate the transport of negative ions, which are produced on the plasma grid surface. It is observed from the code result that 35% of the H^- ions which are produced on the plasma grid surface are able to pass through the extraction hole in the plasma grid. The initial directions of these H^- ions are towards the plasma and not towards the grid hole. Due to the presence of strong magnetic field coming from the electron suppression magnets, situated inside the extraction grid, the direction of motion of H^- ions are changed.

4.1 Introduction

Computer simulations of plasmas with Monte Carlo particle codes play important roles in research where a large number of parameters are involved, for example the transport phenomenon, the heating processes and the production processes through collisions and so on. In such situations analytical solutions are not possible to obtain. This chapter describes a 3-D code called MOCASINIS (**MO**nte **CA**rlo **SI**mulation for **N**egative **I**on **S**ource), which is developed by me [1] to simulate negative Hydrogen ion (H^-) production and transport due to volume process [2] in BATMAN (**BA**varian **T**est **MA**chine for **N**egative ion) source [3]. The code MOCASINIS is a combination of three independent 3-D Monte Carlo codes. These are (1) neutral transport code, (2) negative hydrogen ion production code and (3) negative hydrogen ion transport code. Three independent codes are written instead of a single code for the sake of technical simplicity. The first code has been used to estimate the spatially resolved density of the vibrationally excited H_2

molecules, n_v and the spectrum of those excited H_2 molecules. With the second code, the production and the distribution of H^- ion density n_- has been calculated in the discharge volume. And with the third code, the calculation of the survival probability of H^- ions up to the extraction grid has been carried out. In all the individual codes, the experimentally observed plasma parameters as well as background gas density and temperature profiles are considered as inputs during the trajectory calculation. The basic structure of the code is shown in fig. 4.1. The code results are also compared with a 0-D particle balance model.

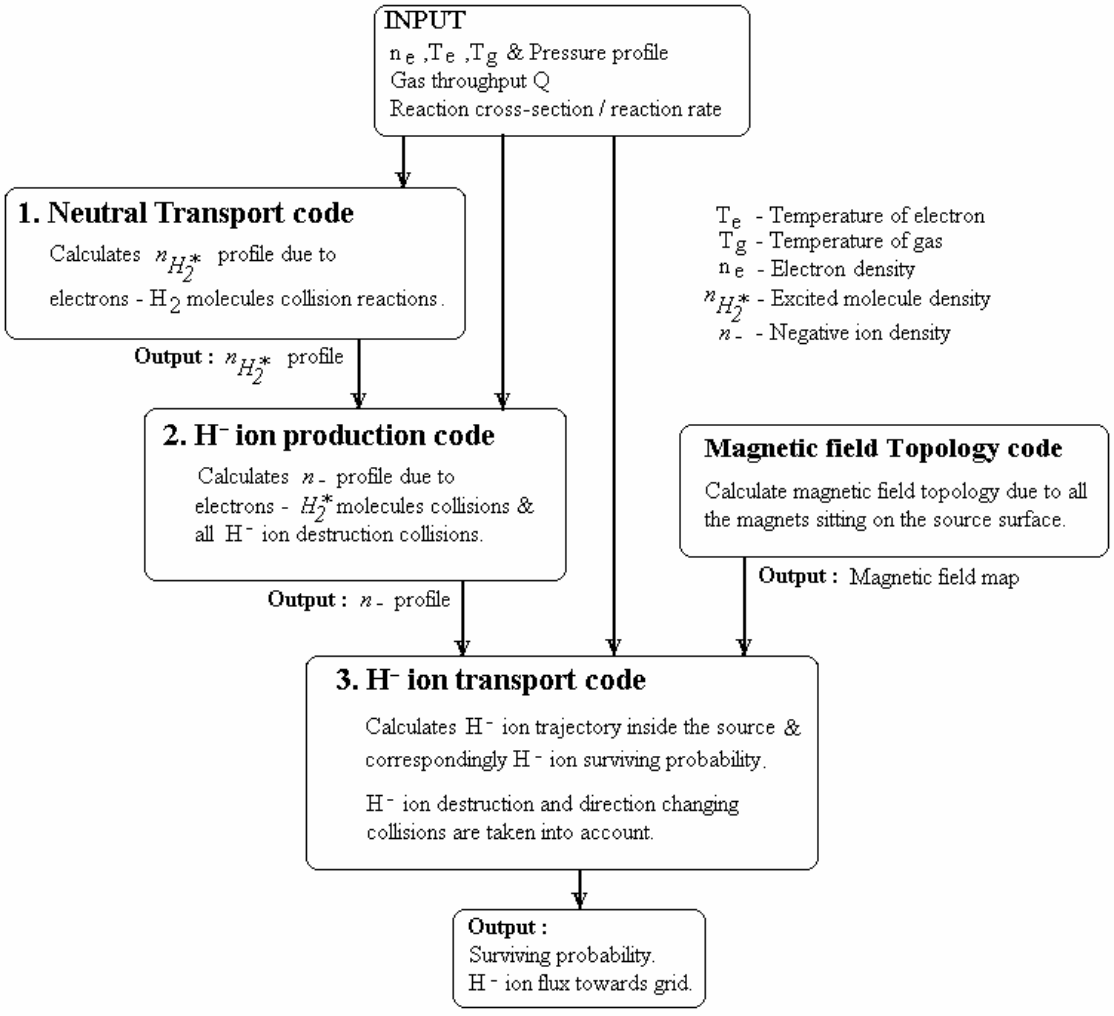

Fig. 4.1 Basic structure of MOCASINIS code.

To simulate the transport of the H^- ions produced on the plasma grid surface a separate Monte-Carlo code is developed. Those H^- ions are accelerated towards the plasma by the plasma potential which is positive with respect to the plasma grid potential and therefore those negative ions would go away from that grid surface. The H^- ions produced on the plasma grid surface could be extracted only if its direction is changed. Due to the presence of strong magnetic field coming from the electron suppression magnets, situated inside the extraction grid, the direction of H^- ions is changed. Their direction of motion

would also be changed due to the charge exchange and elastic collisions with the neutral atoms and molecules respectively. The effect of magnetic field and the collisions are investigated in this chapter.

4.2 Geometrical model of the source

BATMAN ion source and its equivalent model are schematically represented in fig. 4.2. The detail description is described in the chapter 3. The driver is approximated as a cylinder and the expansion part of the BATMAN source is modeled as a rectangular box having volume (30×60×30) cm^3. The surface of each face of that box is denoted by a unique parametric form, $U_i x+V_i y+W_i z=T_i$ with the help of three orthogonal corner points of each rectangular surface plane. The mathematical description of the expansion volume geometry is discussed in appendix-3.

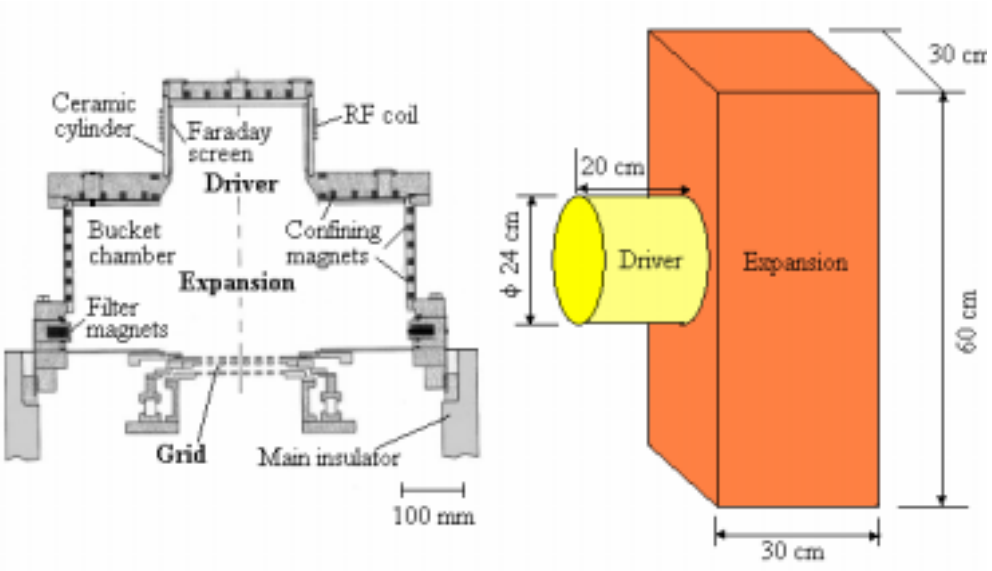

Fig. 4.2. Schematic representation of BATMAN 6-1 type source. Different sections of the source are identified.

4.3 Physical Model

a. Plasma and neutral gas density profile

In the driver

The plasma density, temperature and velocity components of the particles are specified individually for each location co-ordinate during trajectory calculation. The radial plasma density profile in the driver is,

$$n_e(\mathrm{r}) = n_{e_0} \exp\left(-\frac{\mathrm{r}^2}{\lambda_{\mathrm{n}}^{\,2}}\right) \tag{4.1}$$

During calculation it is assumed that at the center of the driver, r = 0, $n_e(r) = n_{e0} = 1\times10^{19}$ m^{-3} and near the diver wall, r = R =12 cm, $n_e(r) = 1\times10^{18}$ m^{-3} respectively. In a similar way the radial electron temperature profile is,

$$T_e(r) = T_{e_R}\exp\left(-\frac{(R - r)}{\lambda_T}\right) \tag{4.2}$$

The assumed boundary conditions are, near the wall T_e(r=R=12cm) =T_{eR} = 20 eV and at the center of the driver T_e(r=0) = 5 eV respectively. The above boundary conditions are derived from the experimental observations obtained by spectroscopic measurements [4]. It is assumed that axial n_e and T_e profiles are constant inside the driver.

The background neutral gas density is uniform through out the cylinder, because below 0.5 Pa pressure and 1200 K gas temperature (measured separately by spectroscopic method), the mean free path ~ 10 cm [5], which is approximately the same as the cylinder dimension. But the present code can also incorporate a neutral density profile.

In the expansion region
It is assumed that in the expansion region plasma density n_e and electron temperature T_e follow

$$n_e(y) = n_{e0}\exp\left(\frac{y}{\alpha}\right) \tag{4.3}$$

and

$$T_e(y) = T_{e0}\exp\left(\frac{y}{\beta}\right) \tag{4.4}$$

where α and β are fitting constant. Typical values are -0.13 and -0.23 respectively when y is in meter. The source axis is assumed as y-axis in a right-handed co-ordinate system. The neutral gas pressure and the corresponding gas density are linearly increasing from the driver to the grid as it is observed during plasma shot in BATMAN [6]. The pressure at any location on the source axis is calculated as,

$$P(y) = P_0 + \left(\frac{P_L - P_0}{L}\right)y \tag{4.5}$$

In the above three equations 0 denotes the value near the driver and L = 0.3m is the distance between the driver and the grid.

b. Mean free path calculation

The mean free path λ for a collision between an electron and a gas molecule is calculated as,

$$\lambda = \frac{v_g}{n_e \sigma v_e} \text{ or } \frac{v_g}{n_e \langle \sigma v_e \rangle} \tag{4.6}$$

where v_g and v_e are the velocity of the molecule and the electron respectively, σ is the collision cross-section. When a collision occurs between two particles, the reaction cross-section and the reaction rate $<\sigma v>$ depends on their energies. An individual polynomial is fitted on the published cross-sectional or reaction rate data for each reactions. The references of those data are mentioned in chapter 2 and table-4.1.

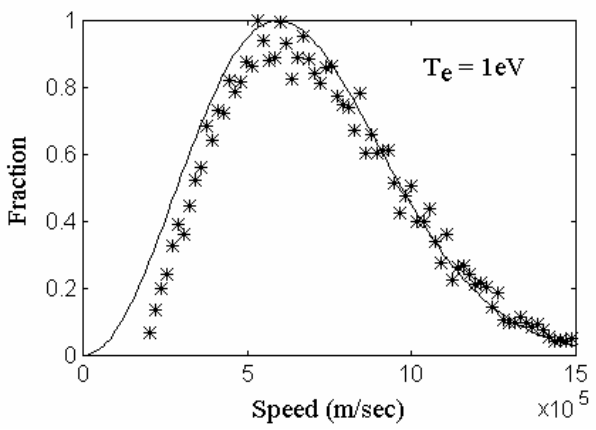

Fig. 4.3. Comparison of normalized Maxwell speed distribution (*) scheme adopted in the code, equatin (4.8) with that of theoretical formulation [5] (continuous line) for electron of temperature 1 eV. Fraction of particle having most probable speed v_m is considered as 1 in this graph.

c. Collisions with the wall

Collision length l is the distance between two successive collisions suffered by a test partcle and is defined as $l = -\lambda \cdot \ln(r)$, where λ is the mean free path of the collision and r is a random number. If the collision length l is greater than the distance of the nearest wall section in the same direction of the flight from a point where the test molecule starts or undergoes last collision, a wall collision is considered. At every collision with the chamber wall, a wall collision counter c_{wall} is increase by 1 unit. Depending upon the sticking coefficient of the wall the molecule will rebound. This incident is chosen by a random number generation. If the particle is reflected from the wall, its translational energy is unchanged after the wall collision and the direction is random with respect to the wall plane. If the wall is a pump surface, the test molecule is lost. The average number of bounce on the wall is estimated as,

$$c = \frac{c_{wall}}{N} \tag{4.7}$$

where N is the total number of test molecules. To estimate the wall loss, c is used.

d. Maxwell speed distribution

The mean free path of a collision depends on the energies of the particles which are involved. In a normal plasma discharge, electrons, ions and the neutral particles like atoms and molecules follow Maxwell's velocity distribution. In the present code, individual speed of each particle is chosen from a Maxwell's speed distribution. The local temperature of a particle (e.g. electron temperature T_e, ion temperature T_i and neutral gas temperature T_g) is considered as input in a subroutine called MAXWELL. As an output it gives the speed of that particle from the corresponding Maxwell's speed distribution. At the beginning or after a collision, the particle starts with a speed derived from Maxwell's speed distribution and correspondingly a random direction is chosen to continue the trajectory calculation.

The following scheme is used to generate the Maxwell speed distribution of the particles for the Monte-Carlo calculation.

$$\mathrm{v} = \mathrm{abs}\left[\left\{\mathrm{v_m} \times \sqrt{\ln\left(\frac{1}{r}\right)}\right\} + \left(\frac{\mathrm{v_m}}{3}\right)\right] \tag{4.8}$$

where r is a random number and $\mathrm{v_m} = \sqrt{\frac{2\mathrm{k_B}T}{m}}$ is the most probable speed of the particle having temperature T and mass m. A comparison of this scheme with the theoretical distribution [5] for electron of temperature 1 eV is shown in fig. 4.3.

e. Residence time

The average time, a molecule stays in that discharge cylinder is defined as the residence time. During trajectory calculation of a H_2 molecule, the collision with a particle or the wall is considered as step size. The time between two successive collisions (i^{th} and $i+1^{th}$) is calculated as,

$$\Delta \mathrm{t_i} = \frac{l_i}{\mathrm{v_g}} \tag{4.9}$$

where l_i is the distance between two successive collisions (i^{th} and $i+1^{th}$). The average residence time is calculated as,

$$\mathrm{t_{res}} = \frac{\sum_{\mathrm{col.no.}} \Delta \mathrm{t_i}}{\mathrm{N}} \tag{4.10}$$

where N is the total number of simulated molecules. The residence time is used to calculate the absolute density of H_2 molecules of having different vibrational levels.

f. Choice of detection point

To calculate spatial H_2^*(v") density profile in the driver, few tiny cubical spaces of volume ΔV_{det} = 1 cm^3 (called detector) are considered in some specified locations. H_2^*(v") molecules are created or destroyed due to collisions throughout the volume, but those are only accounted which are generated or destroyed in those tiny cubical volume only. During counting, vibrational levels (v") as well as the position of the detectors are also taken into account.

g. Estimation of density and vibrational spectrum of H_2^*(v") molecules

The absolute density profile of H_2^*(v") molecules are estimated as,

$$n_{v_{NEW}}(v'',x,y,z) = n_{v_{OLD}}(v'',x,y,z) \pm \left[C(v'',x,y,z) \times \frac{(Q \times t_{res})}{(N \times \Delta V_{det})} \times \exp\left(-\frac{c}{b(v'')} \right) \right] \quad (4.11)$$

where $n_{v_{NEW}}(v'',x,y,z)$ and $n_{v_{OLD}}(v'',x,y,z)$ are new and old H_2^* molecule density which are function of vibrational level v" and positional co-ordinate (x,y,z). $C(v'',x,y,z)$ is the count number inside a detector volume (1 cm^3) ΔV_{det} located at a position (x,y,z). The exponential term is added to incorporate the wall loss where c is the average number of wall collision suffered by N number of H_2^*(v") molecules during their test flights and b(v") is the wall loss coefficient. Details of wall loss are given in chapter 2. The term Q is the throughput of H_2 gas in terms of number of molecules, which is defined as,

$$Q = P \times S \times q \quad (4.12)$$

where P is the pressure in side the chamber just before the discharge (filling pressure), which is ~ 1Pa =7.5×10^{-3} torr. S is the pumping speed through the plasma grid, which ~ 2500 lit/sec and q is the number of molecules present in 1 torr-lit/sec gas throughput, which is ~3.5×10^{19} molecules/sec [5]. Please note that the conductance of the whole extraction system, which is made of three grids (plasma grid, extraction grid and acceleration grid) are not considered here. Only plasma grid conductance is considered because the molecules which pass through the plasma grid holes and stay in the inter grid spaces, are very unlikely to return in the discharge chamber again. Those molecules are considered as lost particles during trajectory calculation.

h. Magnetic field calculation

The complete topology of the magnetic field configuration of the ion source is calculated in a separate computer code (Magnetic field topology code) based upon magnetic charge

model [7]. The components of the resultant magnetic field are the algebraic sum of individual components of each permanent magnet sitting on the source wall. The detailed model and formulation to calculate the magnetic field components for each permanent magnet is given in appendix -4. The complete magnetic field map inside the ion source is shown in fig. 4.4.

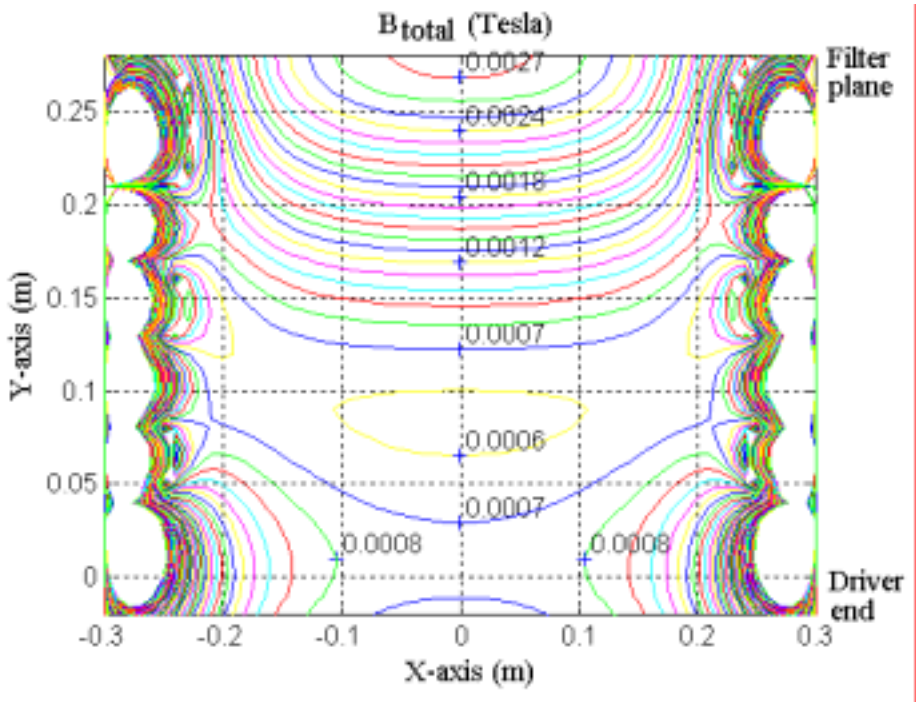

Fig. 4.4. The magnetic field contour map (in Tesla unit) inside the ion source (inside the rectangular expansion region).

4.4 Input and output structure of the computer code

a. Input Constants

All required fundamental constants, mass of electrons, H atoms H_2 molecules.
Polynomial fitting equations for the cross-sections and reaction rates for different reactions (mentioned in Ch-2) for different energies and vibrational levels.
Wall de-excitation constant.

b. Input Variables (Plasma and Gas)

1. Plasma density n_e and temperature T_e profile, which are obtained from Langmuir probe or Spectroscopic measurements.
2. Background gas pressure and gas temperature profile.
3. Atomic hydrogen (H) density (for Wall recombination and Vt reaction).
4. Fraction of H_2^+ and H_3^+ (for s-V process).

5. Plasma potential from Langmuir probe data.
6. Energy of the atoms.

c. Input Variables (Chamber)

1. Radius of the cylindrical discharge chamber (R).
2. Depth of the chamber.
3. The corner co-ordinates of each face of the rectangular expansion volume.
4. Identification of individual surface as reflecting surface or pump surface.
5. Pumping speed (for steady state throughput calculation)
6. Wall sticking coefficient.
7. Recombination coefficient of the wall.
8. Co-ordinates of detection locations (small volume ΔV in which particle count is done).

d. Outputs

1. The profile of $H_2^*(v'')$ molecules in the chamber.
2. The spatially resolved vibrational spectrum of $H_2^*(v'')$ molecules in the chamber.
3. The profile of negative H^- ion density.
4. Quantify the individual contributions of different reaction mechanisms.

4.5 Neutral transport code for volume process

The code estimates the spatially resolved density spectrum of vibrationally excited H_2 molecules n_v in the driver region, where the inductively driven RF discharge plasma is created. During trajectory calculation, it is considered that a test H_2 molecule suffers collisions with electrons and other particles like H atoms or H_2 molecules. It is assumed that between two successive collisions the test molecule moves in a straight line in a randomly specified direction and corresponding distance is defined as collision length '*l*' , which is estimated as, $l = -\lambda \ln r$, where λ is the mean free path of a reaction and r is a random number ($0 \leq r \leq 1$). From the launching point or from the collision point, the test particle starts with a new speed, derived from its Maxwell's speed distribution, (equation. 4.8) corresponding to the energy of the test molecule at that moment. The mean free path λ for individual reaction is calculated from the corresponding reaction rate or from the reaction cross-section (equation 4.6). Since the reaction rates and the cross-sections are energy dependent, Maxwell's speed distributions of the electrons and the test H_2 molecules are considered. The vibrational levels (v") are also taken into account because the reaction cross-sections are v" dependent [8, 9, 10] too. The plasma density n_e profile inside the driver is Gaussian (equation 4.1). The electron temperature T_e profile is an exponential (equation 4.2). These n_e and T_e values are taken from an independent spectroscopic measurement and these profiles are inputs in the code. After dissociation or ionization, the test molecule is destroyed and trajectory calculation for that molecule is stopped. A new molecule will start from the source surface, the gas inlet. If the molecule

survived after a collision, a random direction is chosen to fly further till it is destroyed or pumped off by the pump surface or stick to the wall according to sticking coefficient of the wall, which is determined by a random number. If it does not stick to the wall, it collides elastically with the wall and rebounds in a random direction with the same translational energy. During the test flight of each molecule, the residence time (time of flight) and the number of wall collision is enumerated. The average number of wall collision is used to estimate the wall de-excitation of the vibrational level (v") [12]. The wall de-excited molecules are then re-distributed among lower lying vibrational states according to a exponential weight factor w ($0<w<1$). The maximum value of w corresponds to v"=0 (ground level) and the minimum value corresponds to (v"-1) level. By knowing the gas throughput and pumping speed through the extraction grid, the average residence time (equation 4.10) is used to calculate the absolute density value of H_2 molecules having different vibrational level (equation 4.11). The short flow chart of the neutral transport calculation is shown in fig. 4.5. For detailed flow chart please see appendix-5.

4.6 Negative ion production code for volume process

This code calculates the spatially resolved production and the distribution of H^- ion density (n_-) in the expansion volume (see fig.4.2). It also calculates the spatial distribution of $H_2^*(v")$ molecules in that region from driver to the extraction grid. The rectangular vessel is modeled by the equations A3.1, A3.2 and A3.3 respectively given in appendix-2. The basic scheme of this code is same as that of neutral transport code, except few reactions are not considered as electron temperature is lower than that of driver. For example, in this section E-V reaction is not included, because in the expansion region the electron temperature T_e, is low ($\leq$ 10 eV) and so the E-V reactions are unlikely. The inputs are the experimental n_e and T_e values as a function of positional co-ordinate measured by Langmuir probes whose profiles are approximated by equations 4.3 and 4.4 respectively.

4.7 Volume produced H^- ion transport code

The H^- ion trajectories are calculated numerically by solving the 3-D equation of motion, $M\mathbf{v}/dt=q(\mathbf{E}+\mathbf{v}\times\mathbf{B})$. M, **v**, q, **E**, **B** are the ion mass, velocity, charge, electric field and magnetic field respectively. The magnetic field due to all the permanent magnets, which are situated on the source body, is calculated [13] at each time-step. Reactions having number 10-13 in table-4.1 are included in this code.

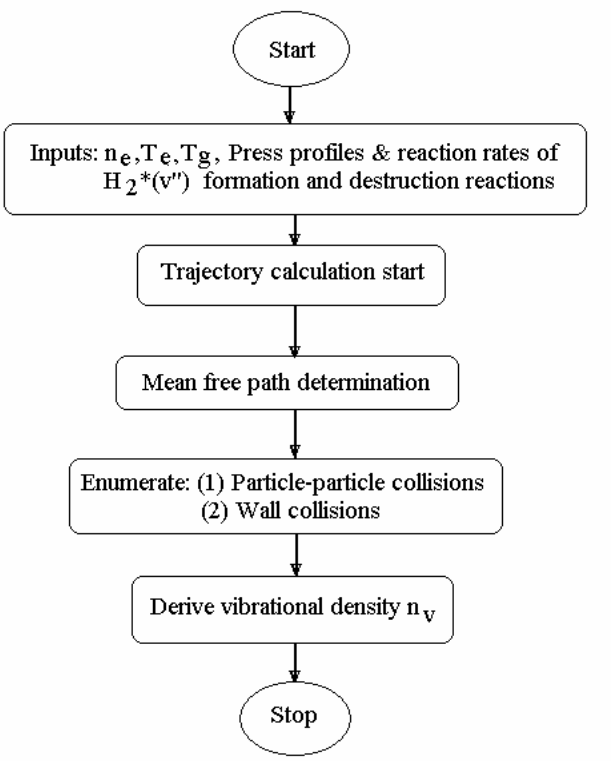

Fig. 4.5. Schematic flow chart diagram of neutral transport code (details see appendix-5).

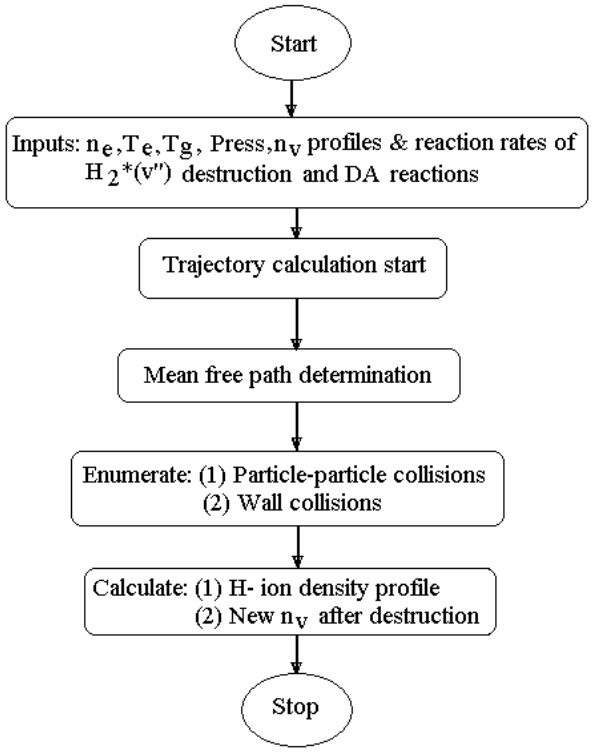

Fig.4.6. Schematic flow chart diagram of negative ion production code (details see appendix-5).

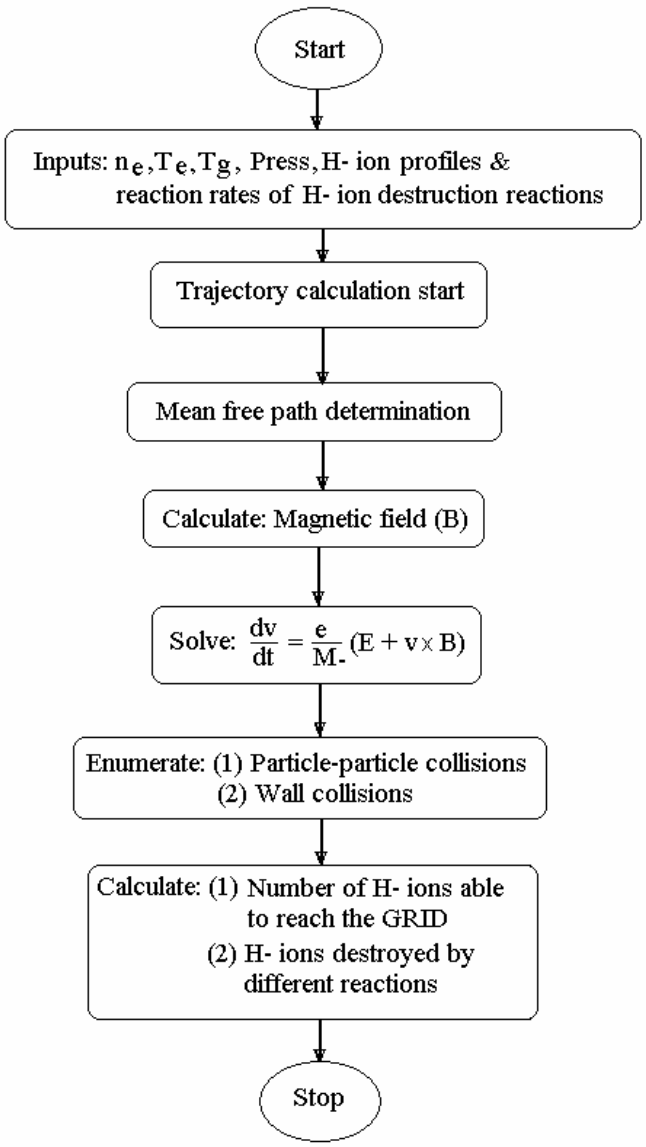

Fig. 4.7. Schematic flow chart diagram of volume produced negative ion transport (details see appendix-5).

Table-4.1 Nomenclature of different reactions and their typical reaction rates

Reactions	Type	Label	$\langle\sigma v\rangle$ $m^{-3}s^{-1}$	Ref
1. $e+H_2(v') \rightarrow e+H_2(v'')$; $(v''>v')$.	$H_2^*(v'')$ formation	e-V	2×10^{-15}	[15]
2. $e+H_2(v') \rightarrow e+ {}_2(B^1\Sigma_u^+, C^1\Sigma_u^+)$ $\rightarrow e + H_2(v'') + h\nu$.	$H_2^*(v'')$ formation	E-V	5×10^{-17}	[9],[15]
3. Wall+ $H^+_n \rightarrow H_2(v'')$; n=1,2,3.	$H_2^*(v'')$ formation	s-V		[16]
4. H(wall)+H (plasma) $\rightarrow H_2(v'')$.	$H_2^*(v'')$ formation	Recom		[17]
5. $e+H_2(v'') \rightarrow e+H_2(b^3\Sigma_u^+,)$ $\rightarrow e+2H$	$H_2^*(v'')$ destruction	Dis	3×10^{-16}	[18]
6. $e+H_2(v'') \rightarrow 2e+H_2^+$.	$H_2^*(v'')$ destruction	Ion	9×10^{-16}	[15]
7. $H_2(v'')+H_2(v')$ $\rightarrow H_2(v''-1)+H_2(v'+1)$; $(v''>v')$.	$H_2^*(v'')$ destruction	V-T	1×10^{-16}	[19],[20]
8. $H_2(v'')+H \rightarrow H_2(v')+H$; $(v''>v')$.	$H_2^*(v'')$ destruction	V-t	8×10^{-17}	[15],[19]
9. $H_2(v'')+wall \rightarrow H_2(v')$; $(v''>v')$.	$H_2^*(v'')$ destruction	Wall relax		[12]
10. $e+H_2(v') \rightarrow H^-+H$.	$H_2^*(v'')$ destruction and H^- ion formation	DA	5×10^{-15}	[21],[22]
11. $H^-+H^+_n \rightarrow H$.	H^- ion destruction	MN	1×10^{-13}	[23],[36]
12. $H^-+e \rightarrow H+2e$	H^- ion destruction	ED	5×10^{-14}	[14],[36]
13. $H^-+H \rightarrow 2H+e$.	H^- ion destruction	AD	2×10^{-15}	[23]

4.8 Particle balance model

As an analytic approach, and for comparison of the code results, 0-D particle balance rate equation for H^- ion production is solved considering the reactions having number 10-12 in table-4.1. Plasma neutrality i.e. $n_+ = n_e + n_-$ is considered here. There are two parts in the particle balance model. The first part calculates the vibrational density of H_2 molecules and second part calculates the negative ion density.

In the first part EV process is taken as the $H_2^*(v'')$ production mechanism and dissociation (Dis), ionization (Ion), dissociative attachment (DA) and general decay due to due wall loss are taken as destruction processes. In steady state condition, the balance equation for $H_2^*(v'')$ molecules is,

$$f_f n_{H_2} n_e \langle \sigma v \rangle_{EV} = (1 - f_f) n_e n_v \langle \sigma v \rangle_{DA} + f_f n_e n_v \left[\langle \sigma v \rangle_{Dis} + \langle \sigma v \rangle_{Ion} \right] + \frac{n_v}{\tau_v} \tag{4.13}$$

where f_f is the fraction of fast electrons present in the electron density. EV, dissociation and ionization processes depend only on the population of fast electrons. Slow electrons' contribution for vibrational excitation of H_2 molecules is negligible. The background gas density is denoted by n_{H_2} and τ_v is the residence time of the molecule, ~ 50 μs for the present experimental scenario. The solution becomes,

$$n_v = n_{H_2} \frac{f_f \langle \sigma v \rangle_{EV}}{\left[(1 - f_f) \langle \sigma v \rangle_{DA} + f_f \left(\langle \sigma v \rangle_{Dis} + \langle \sigma v \rangle_{Ion} \right) \right] + \frac{1}{n_e \tau_v}} \tag{4.14}$$

In the second part, dissociative attachment (DA) is taken as the only H^- ion production process. Since Mutual neutralization (MN) and Electron detachment (ED) are the dominant H^- ion destruction mechanism, only their contributions are included. The balance equation can be written as,

$$n_v n_e \langle \sigma v \rangle_{DA} = n_- n_+ \langle \sigma v \rangle_{MN} + n_- n_e \langle \sigma v \rangle_{ED} + \frac{n_-}{\tau_-} \tag{4.15}$$

The real positive density solution is,

$$n_- = n_e \frac{-\left[\langle \sigma v \rangle_{dest} + \frac{1}{n_e \tau_-} \right] + \sqrt{\left(\left[\langle \sigma v \rangle_{dest} + \frac{1}{n_e \tau_-} \right]^2 + 4 \langle \sigma v \rangle_{MN} \langle \sigma v \rangle_{DA} \frac{n_v}{n_e} \right)}}{2 \langle \sigma v \rangle_{MN}} \tag{4.16}$$

where $\langle \sigma v \rangle_{dest} = [\langle \sigma v \rangle_{MN} + \langle \sigma v \rangle_{ED}]$, the H^- ion destruction reaction rate and τ_- is the confinement time of negative ions, which is much longer than that of electrons because negative ions are massive and less energetic (~ 0.5 eV or less), so better confined in the plasma electro-statically by the plasma potential. The typical confinement time for H^- ion in the present experimental setup is ~ 100 μs or more.

To find the effect of the electron temperature on the H^- ion density, ED reaction rate, $\langle \sigma v \rangle_{ED}$ as a function of electron temperature is calculated from the ED cross-section [14] with a fitting equation [see equation (4.17)]. The equation (4.17) is valid between 0.75 eV and 10 eV only, because above 10eV the ED cross-section is almost constant ~ 3.4×10^{-19} m^2 and 0.75 eV is the threshold energy for ED reaction.

$$\sigma_{ED} = \frac{(T_e - 0.75)^2 \times 10^{-19}}{2.4 T_e} \quad m^2 \tag{4.17}$$

4.9 Results and discussion on simulation and model

The simulation and the 0-D particle balance model produce similar results (with in the error limit) regarding density of vibrationally excited H_2 molecules n_v, H^- ion density n_-. The discrepancy between the simulation result and that of particle balance model is because 0-D model is based upon local average conditions and it does not taken into account the motion of the particles, where as in the simulation motions are considered.

The spatial distribution of density spectrum of the H_2 molecules calculated with the help of MOCASINIS is shown in fig.4.8. The density of the higher vibrational states (v"=5-14) of H_2 molecules, which are relevant for the H^- ion production goes down with the distance from the driver. This is because, away from the driver, T_e falls below 10eV. So $H_2^*(v")$ production reactions are not large anymore. At a distance of 30 cm from the driver, the average effective vibrational density n_v decreases by a factor of four. It is also found that wall loss is dominant. The average life time or residence time of an excited molecule τ_V, before colliding with a wall is ~ 50μs for 1200 K gas temperature, where as for ionization and dissociation, the life time is ~ 200μs. The solution of the particle balance equation (4.14) also gives the similar results, which are shown in fig. 4.9 and fig. 4.10. If the chamber volume is small, then τ_V become shorter due to wall de-excitation and n_v is increasing with n_e. If the volume is very big, the wall de-excitation can be neglected and the ionization/dissociation lost term makes n_v saturate in spite of increase of n_e. Fig. 4.10 shows a comparison of the simulation result and the particle balance model for vibrationally excited H_2 molecules along the source axis in the expansion region of BATMAN. To solve equation (4.14) along the axis, equations (4.3) and (4.4) are used to calculate the local n_e and T_e with 20% as f_f .

It is shown in fig.4.11 and 4.12 that the effective negative ion density is almost uniform from the driver to the grid although both n_e and T_e changes along that chord. Near the driver n_e is 5×10^{18} m^{-3} and T_e is 20eV and near the extraction grid n_e is 5×10^{17} m^{-3} and T_e is between 2-5eV. Fig. 4.13 shows that only those H^- ions, which are produced within 1-2 centimeters from the grid, are able to reach the extraction hole. This result indicates that the surface produced H^- ions have better opportunity to be extracted. This simulation is in agreement with the experiments of the BATMAN source which produces 2-4 mA/cm^2 H^- current densities (calorimetrically) when it is operated without Cs [24]. The H^- ion current density (j_-) from the simulated H^- ion density is estimated as ~ 2 mA/cm^2.

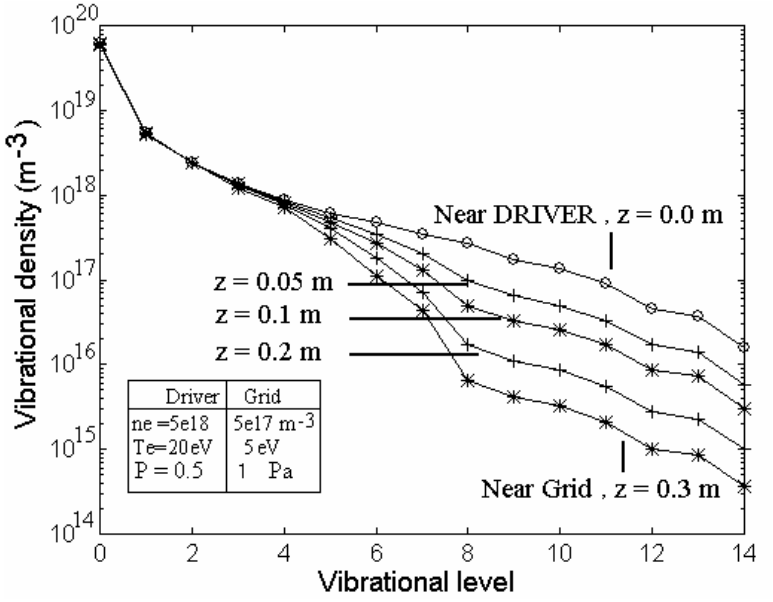

Fig.4.8. Density profile of vibrationally excited H_2 molecules along the source axis in the expansion region of BATMAN. The inputs which are used in the simulation are given in the inset.

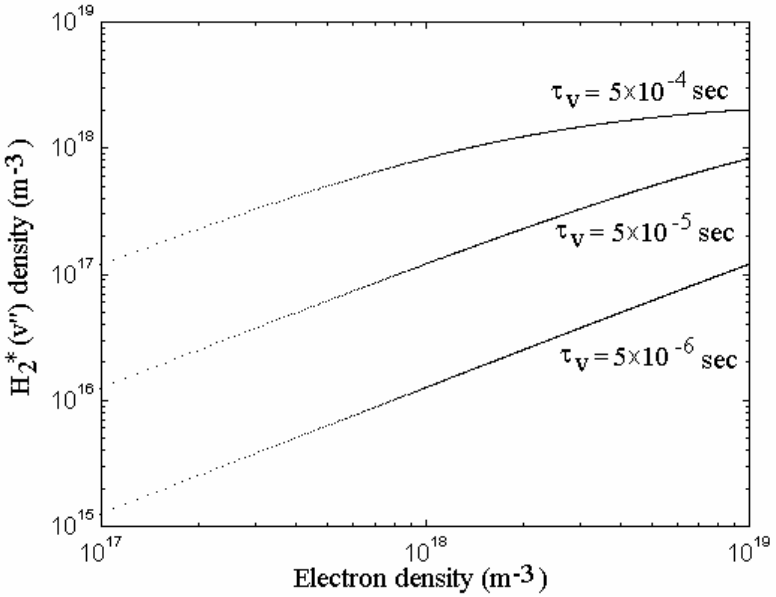

Fig. 4.9. Vibrationally excited H_2 molecules vs. electron density in the driver for different life time of excited molecules.

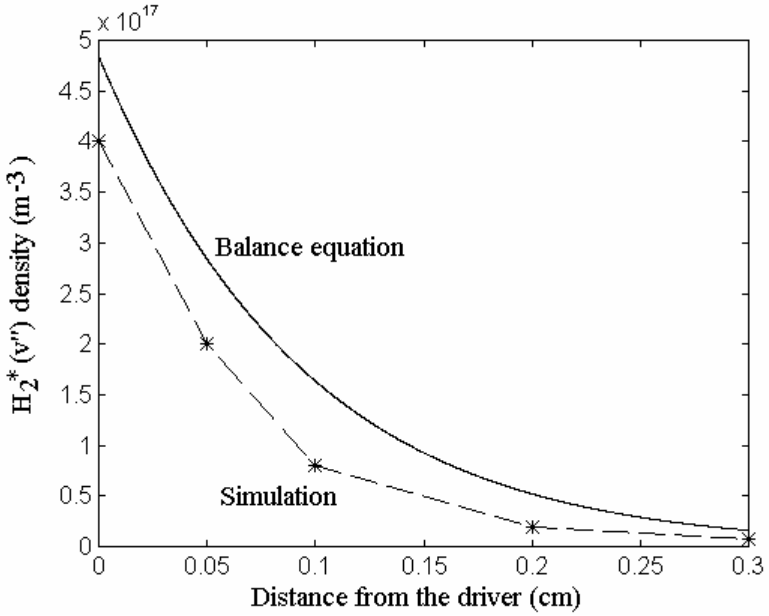

Fig. 4.10. Comparison between the simulation and the particle balance model [equation (3.18)], regarding density profile of vibrationally excited H_2 molecules ($\sum$v"=5-14) along the source axis in the expansion region of BATMAN. Background pressure is 1 Pa.

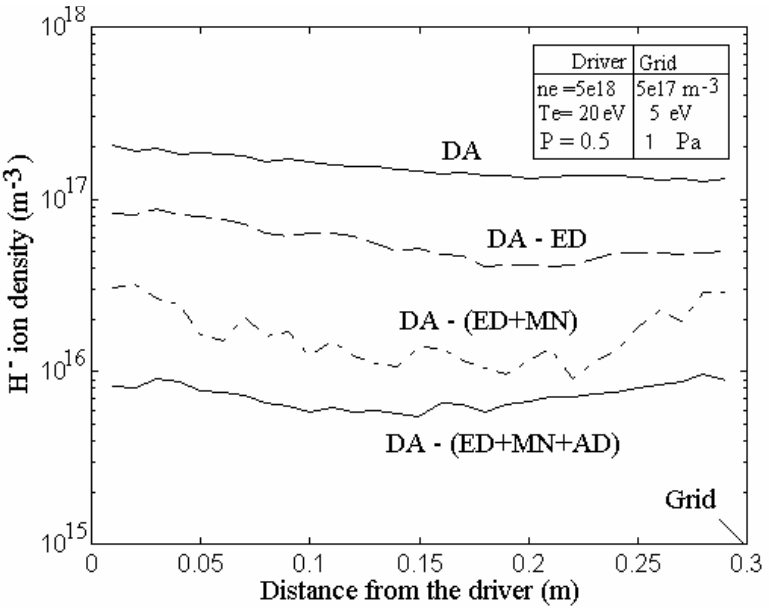

Fig. 4.11. Density profile of H^- ions along the source axis in the expansion region of BATMAN. The inputs which are used in the simulation are given in the inset. The contribution of different reactions are also shown.

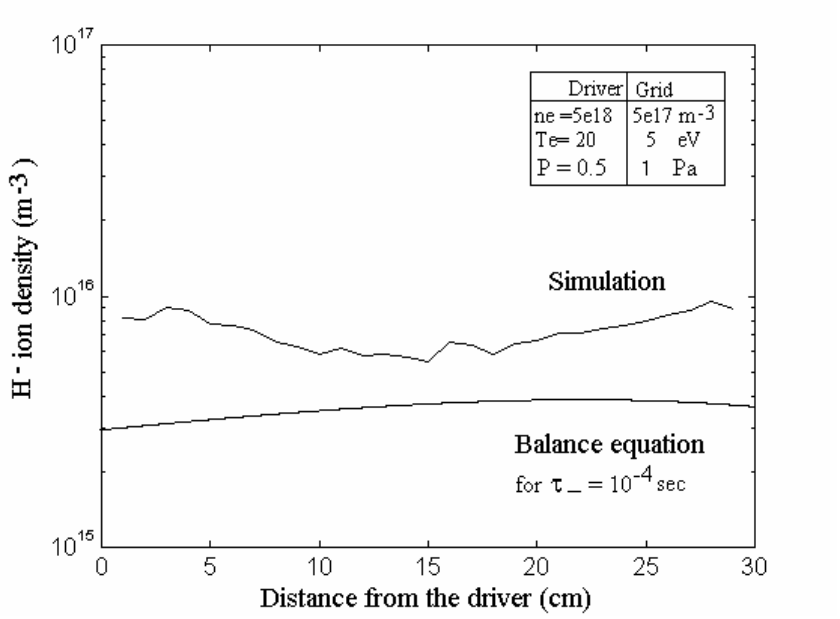

Fig. 4.12. Comparison of calculated H^- ion density profile along the source axis by the simulation and the particle balance equation (3.20). Inputs for simulation are shown in inset. Equations (3.6) and (3.7) and fig. 3.10 are used for n_e, T_e and n_v profiles for particle balance solution.

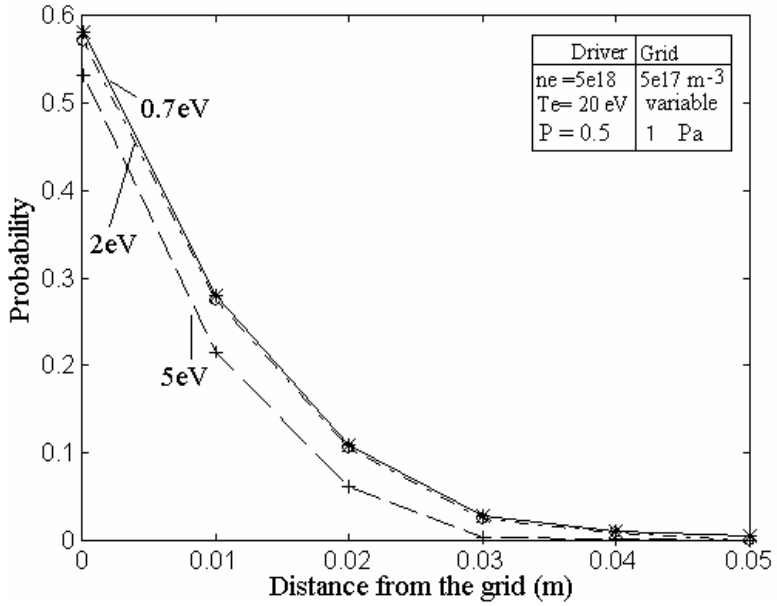

Fig.4.13. Probability of H^- ions to reach the extraction grid surface for three different T_e values near the grid region. Inputs for the simulation are given in the inset.

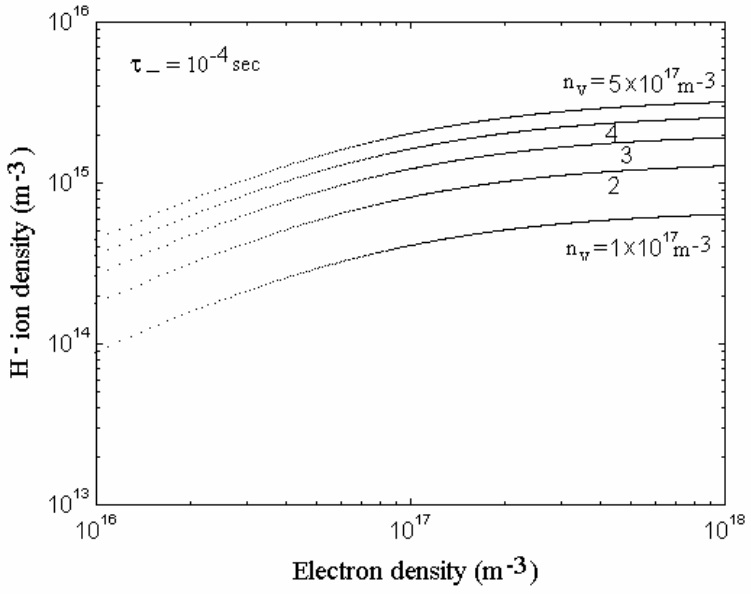

Fig.4.14. The solution of particle balance equation (3.20) as a function of electron density n_e for different densities of vibrationally excited H_2 molecules n_v.

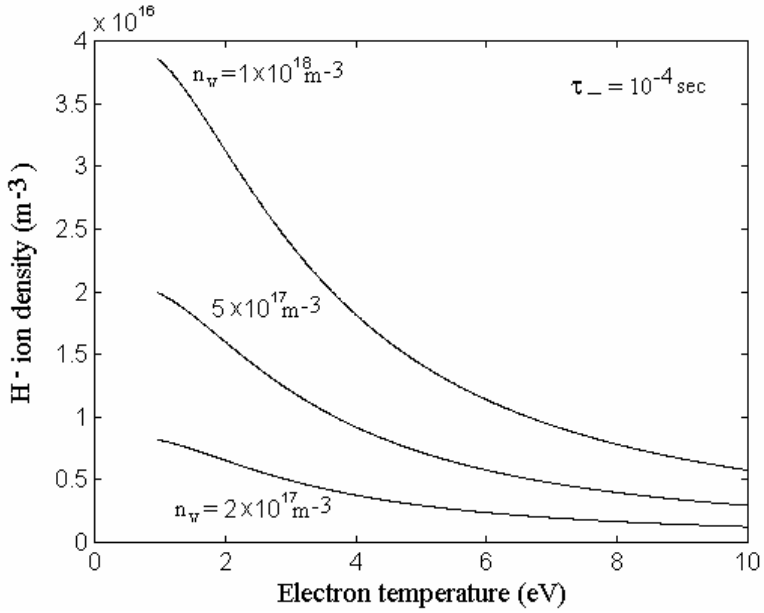

Fig.4.15. The solution of particle balance equation (3.20) as a function of electron temperature T_e for different densities of vibrationally excited H_2 molecules n_v. If T_e reduces from 5 eV to 1eV, H^- ion density is improved by factor of 2-3 only.

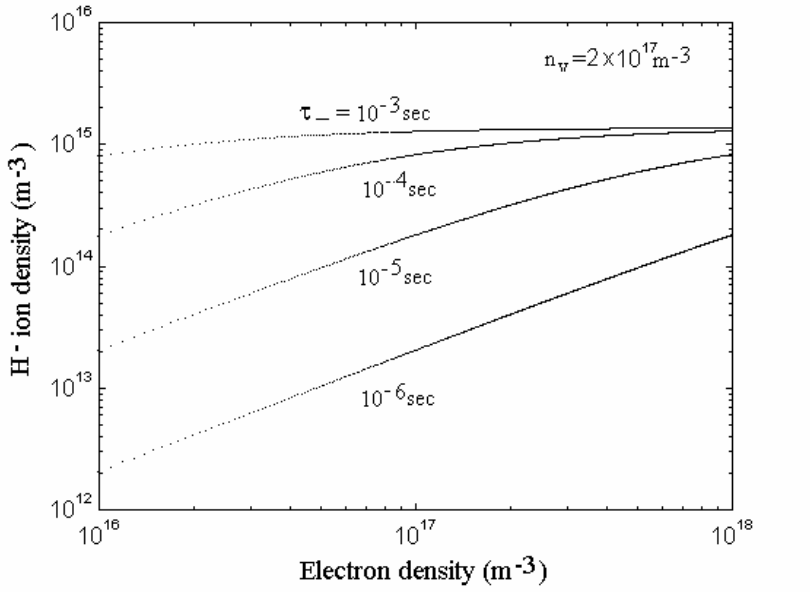

Fig.4.16. The solution of particle balance equation (3.20) for different negative ion confinement time τ_-. For $\tau_- > 10^{-4}$ sec, H^- ions are lost mainly by ED and MN reaction collisions and make the function insensitive to τ_-.

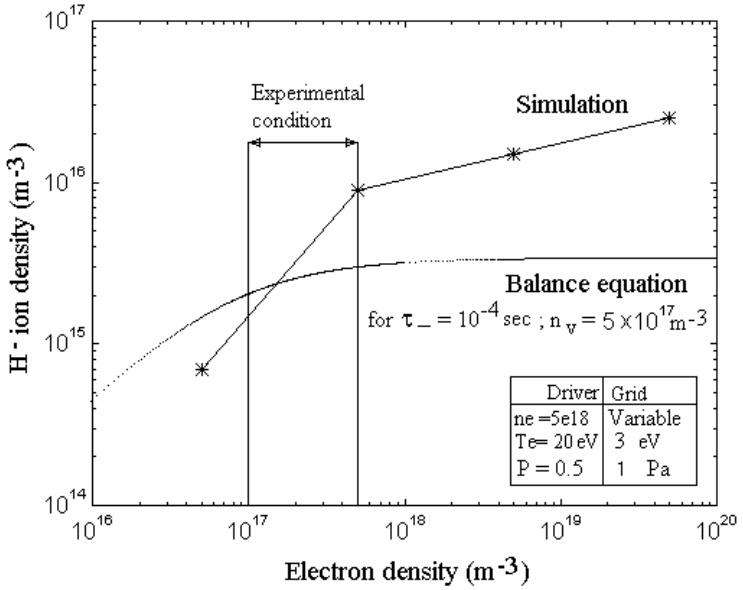

Fig. 4.17. Comparison between the simulation and the particle balance model regarding H^- ion density vs. electron density. In inset the input conditions for the simulation are given.

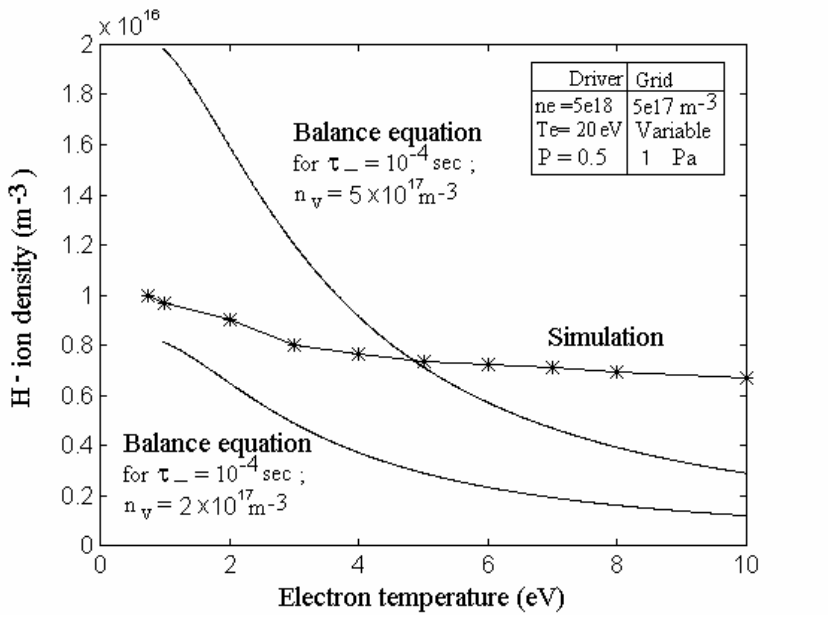

Fig.4.18. Comparison between the simulation and the particle balance model regarding H^- ion density vs. electron temperature. In inset the input conditions for the simulation are given.

In the case of volume production mechanism, equation (4.16); the H^- ion density near the grid increases with the local electron density n_e until n_e becomes equal to n_v as shown in figures 4.14, 4.16 and 4.17. Beyond that point, n_e dependency becomes flat slowly. For higher vibrational density values, n_- increases with the local n_v value only, which are shown in figures 4.14 – 4.17. In fig.4.17 the simulation results and the solution of the balance equation (4.16) are compared. Fig.4.18 indicates that near the extraction grid n_- increases when T_e decreases. The balance equation is valid locally whereas the simulation includes non-local phenomena also. This is the main reason for the discrepancy in fig.4.17 and 4.18.

4.10 Transport of surface produced H^- ions

In most of the powerful negative ion sources, cesium (Cs) is used [25, 26] to improve the negative ion current. It is very clear that Cs improves the surface production of negative ions by reducing the surface work-function [27, 28, 29]. Most of the H^- ions which are produced only on the plasma grid (PG) surface are extracted effectively because the distance the H^- ions can travel near the plasma grid is very small ~ 2 cm [1] due to the destructive collisions. The initial directions of the surface produced H^- ions are away from the PG i.e. towards the main plasma because negative ions are accelerated by the plasma sheath. So to develop an efficient negative ion extraction code it is very important to know how the directions of motion of those surface produced negative ions are changed and able to reach the grid holes. This simulation code is also developed for BATMAN ion source. The geometrical model used for this calculation is shown in fig. 4.19 and fig. 4.20.

Recently a two-dimensional (2D) attempt [30] has been made with a simplified plasma model, without considering electron diffusion across the magnetic field and collisions. In that report it was tried to see the effects of weak magnetic field due to the electron suppression magnets present in the extraction grid (EG) on the transport of the volume produced H^- ions through the PG hole.

The present code is a 3D Monte Carlo simulation code developed by me. In this code elastic collisions (EC) and charge exchange (CX) collisions between H^- ions and the background neutral atoms and molecules are taken into account. It also includes all the H^- ion destruction collisions: electron detachment (ED), mutual neutralization (MN) and associated detachment (AD). The experimental observed plasma parameters (plasma density n_e, electron temperature T_e, gas pressure P, gas temperature T_g) are used as input.

The trajectories of the H^- ions produced on the plasma grid surface are calculated numerically by solving the same 3D equation of motion, $M.d\mathbf{v}/dt=q(\mathbf{E}+\mathbf{v}\times\mathbf{B})$. The total field **B** is shown in fig. 4.21 for two cases: (1) with electron suppression magnets in EG and (2) without magnets inside EG. The maximum field on the PG surface is ~ 220 gauss due to the EG magnets. The electric field due to plasma sheath is calculated by differentiating the sheath potential ϕ_{sh} profile with respect to (w.r.t.) the distance. The sheath potential ϕ_{sh} profile is modeled as,

$$\phi_{sh} = \phi_{pp}\left[1 - \exp\left(-\,x/\lambda_D\right)\right] \tag{4.18}$$

Here ϕ_{pp} is the plasma potential ~ 15V, λ_D is the Debye length and x is the distance from the source chamber wall which is in ground potential (0V).

During the beam operation, few kV positive potential is applied to the the EG w.r.t. the ion source (actually the ion source is connected to few kV negative potential w.r.t. the EG). This configuration is same as an electron gun. The positive extraction potential profile $\phi_E(z)$ penetrates into the plasma through the PG holes. The profile of $\phi_E(z)$ in the extraction gap (between PG and EG) varies as [31],

$$\phi_E(z) = \phi_{EG}\left(\frac{z}{d_{eff}}\right)^{4/3} \tag{4.19}$$

where z is the distance from the EG. The penetration depth d_{eff} of $\phi_E(z)$ is determined by the space charge limited electron current (Child law) which is calculated as [31],

$$d_{eff} = \left[\left(\frac{4\in_0}{9}\right)\left(\frac{2e}{m_e}\right)^{1/2}\left(\frac{\phi^{3/2}{}_{EG}}{j_e}\right)\right]^{1/2} \tag{4.20}$$

where $\in_0$ is the free space permittivity e and m_e are the electronic charge and mass respectively, ϕ_{EG} is the extraction voltage applied on the EG w.r.t. the ion source (w.r.t. PG) and j_e is the electron current density through the PG hole which can be calculated as ($n_e e v_e/4$). The electron temperature (T_e) near the PG determines velocity of the electrons v_e. The magnetic field due to the electron suppression magnets in the EG has an effect on electron density n_e near the PG holes. Lower the j_e, deeper would be the positive potential penetration and help to extract more negative ions along with the electrons from the region further deep inside of the ion source. The $\phi_E(z)$ inside the plasma (beyond PG) is modeled by an empirical formula as,

$$\phi_E(z) = \phi_{PG} \exp\left[-\left\{ \frac{(z-G)}{\delta} \right\}^2 \right] \text{ when } d_{eff} > G \text{ and } \phi_E(z) = 0 \text{ when } d_{eff} \le G \quad (4.21)$$

where $\delta = (d_{eff} - G)$, G is the gap between the inner surface of the PG and the EG, taken as 6.5mm. ϕ_{PG} is the extraction potential obtained from equation (4.19) putting $z = G$. It is experimentally observed [6] that if a positive bias potential is applied to the PG, it sucks the local electrons and reduces the n_e considerably near the PG and forms a double layer [32, 33]. The experimentally observed potential profile of that positive bias of the PG in the plasma can be approximated by a Gaussian profile. The extraction voltage which can penetrate through the PG holes can be assumed similar to PG bias with different magnitude according to applied ϕ_{EG}.

The n_e and T_e values along the source axis (z-axis) are obtained from Langmuire probe data [34] which are approximated by two separate exponential functions. From the driver to the grid it is assumed that n_e varies from $1\times10^{18}m^{-3}$ to $1\times10^{17}m^{-3}$, T_e varies from 15eV to 2eV and the background H_2 gas pressure varies from 0.6 Pa to 1.2 Pa. Gas temperature is taken as 1200K. The H atom density is taken as 10% of the local background gas density. The mean free path (MFP) λ of individual collision is calculated from the corresponding reaction rates. Since the reaction rates are energy dependent, Maxwell's speed distributions of electrons, H^- ions, atoms and the molecules are included in the simulation (discussed in 4.3.d.). The collision reactions considered in the calculations are listed in table-4.2.

If the magnetic field near the PG due to electron suppression magnets in EG is removed, the gyration radius (r_c) of H^- ions changes from ~ 3 mm to ~ 3 cm, which has a significant influence on the H^- ion extraction. The local plasma parameters are also changed due to the changes in the magnetic field. To see the effect of the magnetic field on the plasma parameters, n_e and T_e profiles are approximated by two fitting equations based on the calculated data available in ref. 35. The model in ref. 35 considers both heat and particle diffusion through a transverse magnetic field. The change in n_e and T_e has an effect on d_{eff} and therefore on the extraction probability.

Table-4.2. Nature, nomenclature and typical values of reaction cross-sections

Reactions	Type	Label	σ (cm^2)	Reference
1. $H^- + e\ (>1eV) \rightarrow H + 2e$	H^- destruction	ED	2×10^{-16}	[36]
2. $H^- + H^+_n \rightarrow H$	H^- destruction	MN	2×10^{-13}	[36]
3. $H^- + H \rightarrow H_2 + e$	H^- destruction	AD	2×10^{-15}	[36]
4. $H^- + H_2 \rightarrow H^- + H_2$	Direction change	EC	2×10^{-15}	[37]
5. $H^- + H \rightarrow H + H^-$	Direction change	CX	1×10^{-17}	[36]

4.11 Results and discussion on surface produced H^- ion transport

In the case of surface production, H- ions are generated on the plasma grid (PG) surface due to the flux of energetic atoms and positive ions. After that H^- ions are accelerated towards the plasma in the sheath region due to positive plasma potential with respect to the PG and so moving away from the PG. This initial direction is wrong from H^- ion extraction point of view. The extraction of H^- ions is significantly improved by increasing the extraction voltage. The presence of magnetic field due to the electron suppression magnets inside the extraction grid (EG) has a considerable influence on the radius of curvature of the trajectory of the H^- ions. It changes the wrong direction of surface produced H^- ions into the favorable direction for extraction. The magnetic field also reduces the electron density near PG and correspondingly the co-extracted electron current. As a result of this, the extraction field penetration moves deeper into the plasma through the PG hole and therefore the extraction probability of H^- ions is also increased.

Fig.4.22 shows the effect of extraction voltage on the negative ion extraction probability. In the figure, two regions are clearly visible, space charge limited (SCL) region where extraction probability increases proportional to $(\phi_{EG})^{3/2}$ and source limited (SL) region. The maximum possible fraction of surface produced H^- ions can be extracted is ~ 35% and 3.5kV is the optimum extraction voltage where the transition from SCL region to SL occurs.

Fig.4.23 shows the effect of collisions, particularly the elastic collision (EC) with the background neutrals, which can change the direction of motion of a surface produced H^- ions. It is found that due to the elastic collisions ~ 8% of the total surface produce H^- ions go back to the grid wall and are distributed on the surface randomly, of which only few H^- ions can be extracted through other nearby holes. The percentage of the loss due to the collisions in the plasma is bigger if the elastic collisions are not considered. Extraction probability "passed grid hole" is nearly unaffected. The losses on the side wall are negligible because H^- ions are well confined by the sheath potential on the wall and are reflected from the sheath-plasma interface.

Fig.4.24 shows the effect of the initial energy of the H^- ions, just after its birth. There is an uncertainty about this information in the available literature. In this simulation it is found that the initial energy of the surface produced H^- ions have less effect on the extraction and the loss terms. Because the energy gained in the plasma sheath, is more important. If the plasma potential is less positive with respect to the wall, the extraction probability would be higher and the loss due to collisions would be less. Because if the H^- ions are accelerated less in the sheath, it would penetrate less into the plasma and therefore effectively bend its trajectories more due to EG magnetic field and could be extracted more effectively. For details see fig. 4.25.

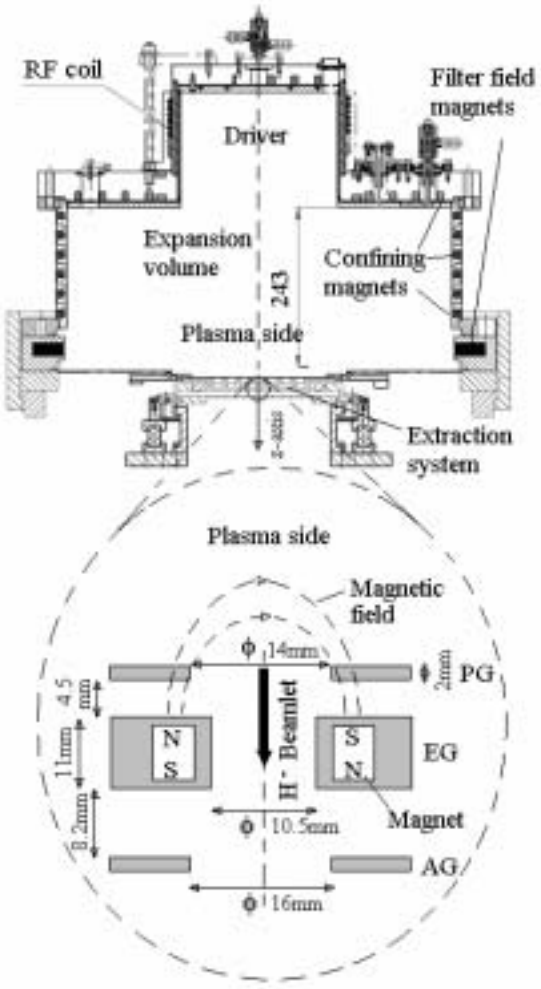

Fig.4.19. Schematic diagram of BATMAN ion source with enlarged extraction system showing the orientation and magnetic field lines of the electron suppression magnets situated inside the EG.

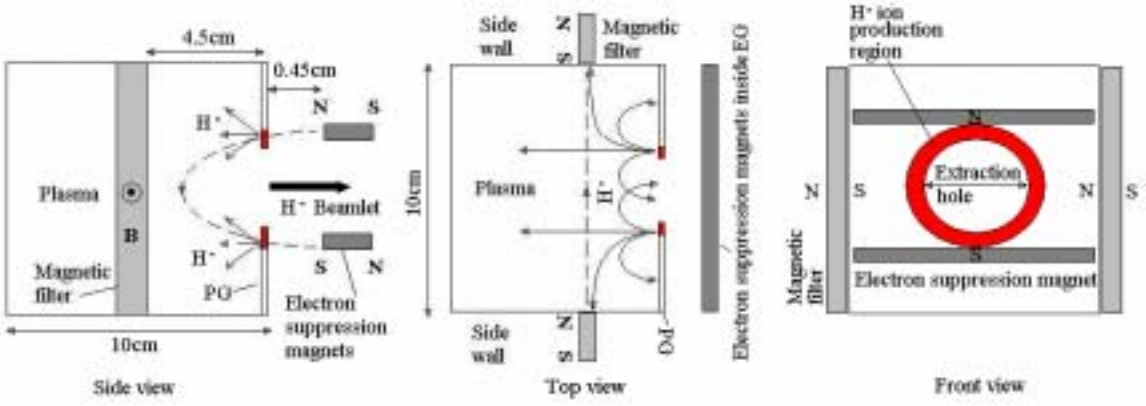

Fig.4.20. Schematic picture of the present 3D particle simulation model. H^- ions are produced in an annular region of width 1mm around the periphery of the hole on PG. Different possible H^- ions trajectories are also shown in the figure.

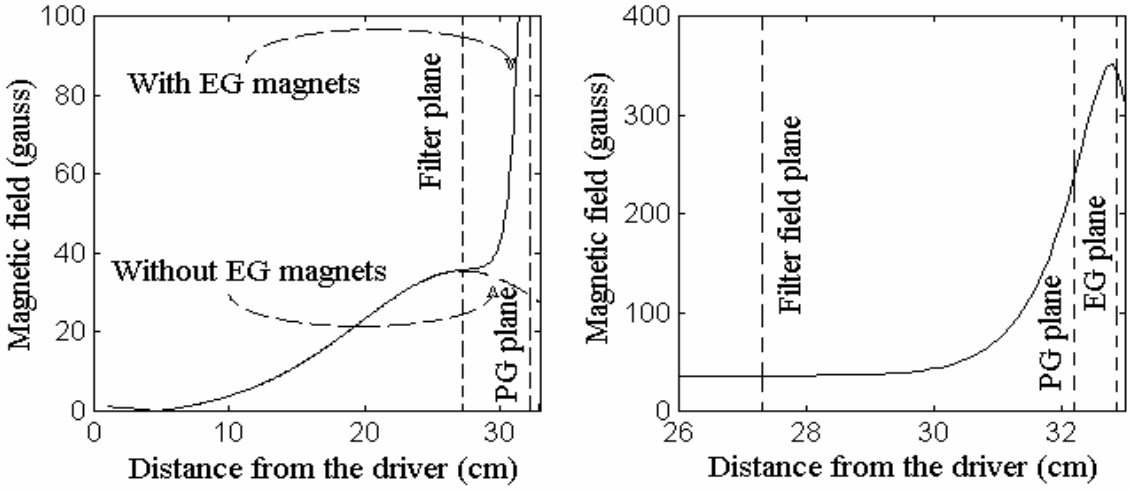

Fig.4.21. Total magnetic field profile in BATMAN ion source. Magnetic field near the PG is ~ 220 Gauss due to EG electron suppression magnets.

Fig.4.26 shows the effect of magnetic field strength on the PG due to the electron suppression magnets inside the EG on the H^- ions extraction. It shows that there is an optimum value of magnetic field strength ~ 400 Gauss. When magnetic field is stronger (> 1kG), the negative ions are strongly magnetized and confined in the magnetic field near the PG hole. Therefore the loss of H^- ions due to the collisions increases. Most of the H^- ions are lost within 5 cm from the PG. When magnetic field in very low (~ 20G), the H^- ions are not magnetized, therefore not confined near the hole and it can go deep into the plasma and lost there. In detail analysis of the H^- ion trajectories (see in the fig.4.27), it is observed that the half of the ions which are generated on the one side of the periphery of the hole fall into the hole. This selection is due to the magnetic field orientation with respect to the H^- ions velocity direction. The ions which are originated on the other side of the periphery of the hole would be fallen into the neighboring hole

and could be extracted. The potential contour inside the plasma, penetrates through the PG hole due to the EG voltage is not considered as a spherical (meniscus) shape but as a cylindrical one for simplicity, having a sharp transition of electric field along the edge of the hole. This simplified assumption may contribute some over-estimation on extraction probability and also explains the sharpness of the fig.4.27 (final location of H^- ions inside the hole).

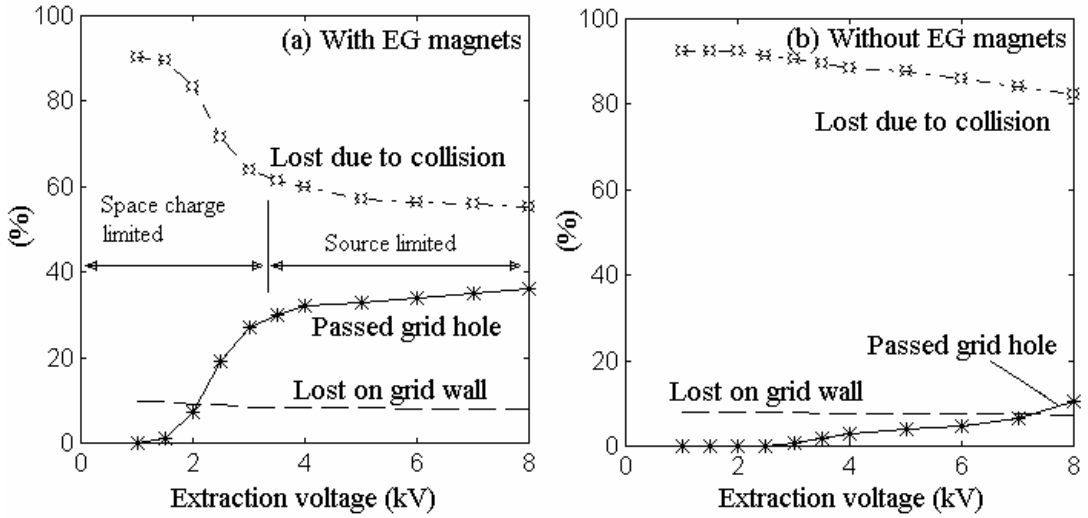

Fig.4.22. Fraction of the surface produced H^- ions to be extracted (Passed grid hole), lost due to collision in the plasma (Lost due to collision) and lost on the PG wall for different ϕ_{EG}. Lost to the side wall of the chamber is negligible. It is observed that ~35% of the total H^- ions lost due to collisions are occurred within 5 cm from the PG. In fig. (a) "Passed grid hole" data can be compared qualitatively with the experimentally obtained data (fig. 3.8 in chapter 3).

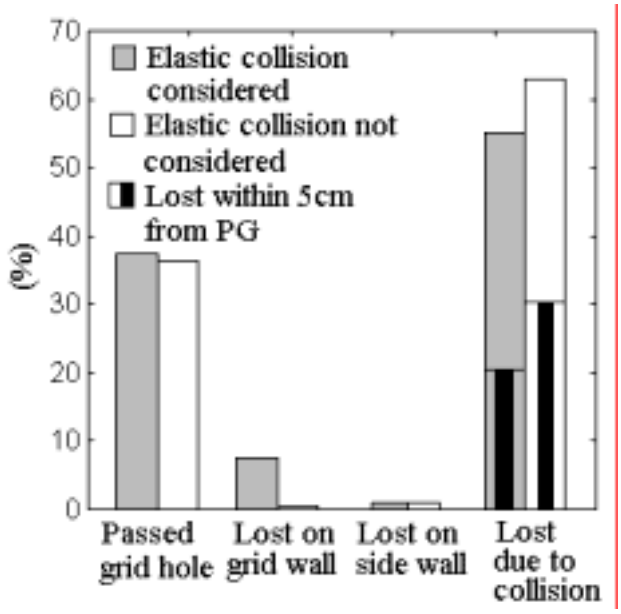

Fig.4.23. Effect of elastic collision between H^- ions and the background neutrals on the extraction and loss processes of the H^- ions.

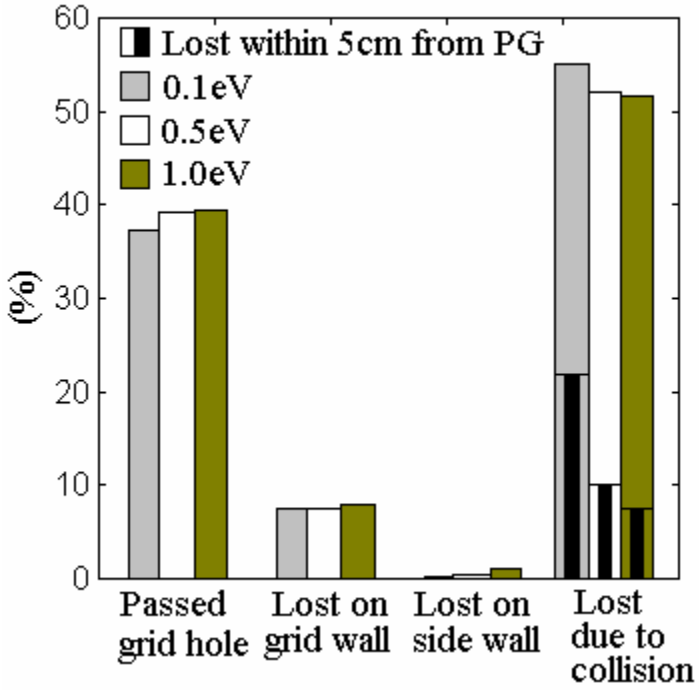

Fig.4.24. Effect of initial kinetic energy of H^- ions. Extraction and loss terms are nearly independent

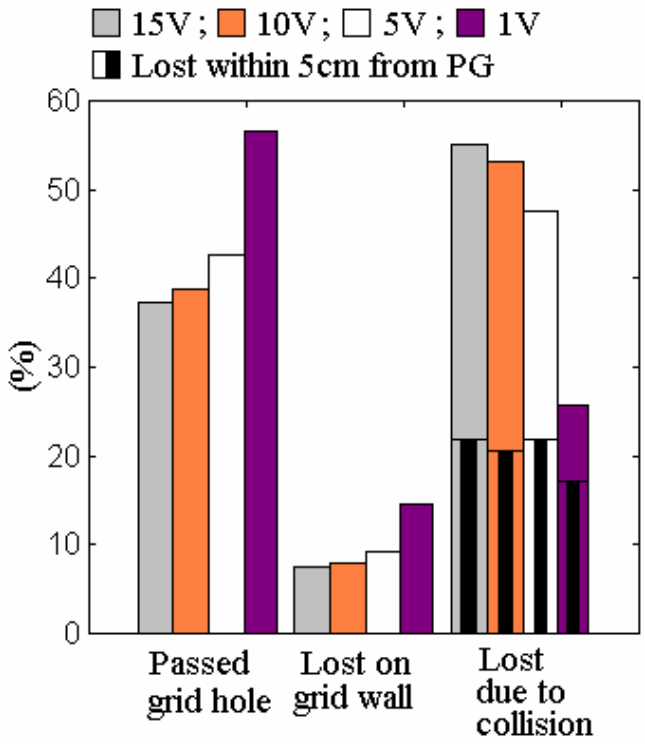

Fig.4.25. Effect of plasma potential ϕ_{pp}. For lower ϕ_{pp}, H^- ions are less accelerated towards plasma and correspondingly extraction term increases and loss term decreases.

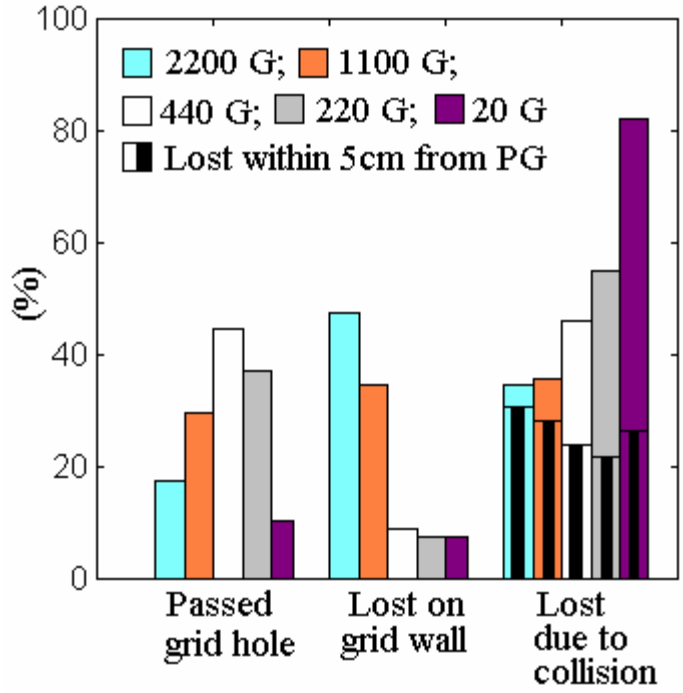

Fig.4.26. Effect of magnetic field strength due to electron suppression magnets in the EG on the PG.

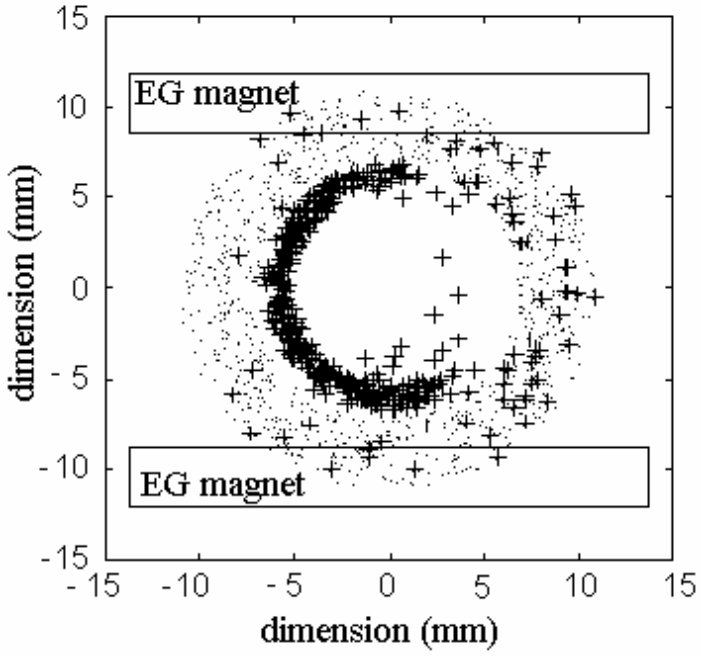

Fig.4.27. Birth locations of H^- ions on the periphery of the PG hole (·) and final locations of those H^- ions inside the hole for extraction and on the PG plane (+) during trajectory calculation. Relative positions of EG magnets are also shown.

4.12 Conclusion

The results of the computer simulation based on volume process clearly shows that the pure volume production for H^- ions are not sufficient to reach the ITER target (28 mA/cm^2 H^- ion current, which roughly corresponds to ~10^{12} cm^{-3} H^- ion density in front of the plasma grid). Volume produced H^- ion density profile inside the source is nearly uniform although the electron density and temperature is not uniform. The distance in the ion source, the H^- ion can travel before it is destroyed by collisions is only few centimeters (~ 1-2 cm). Therefore only those ions can be extracted effectively, which are generated very close to the grid surface. This indicates that surface produced H^- ions can be extracted more effectively. The amount of H^- ions can be produced by surface process depends upon the flux of the energetic H atoms and the positive ions, but their direction is towards the plasma due to the plasma sheath potential and not towards the plasma grid holes. The strong magnetic field (~220 Gauss) coming from the extraction grid magnets helps to bend the direction of motion of those H^- ions which are produced on the plasma grid surface. It is observed that a considerable amount (~ 35%) of the H^- ions which are produced on the plasma grid surface, can reach the plasma grid hole for extraction.

References

[1] M. Bandyopadhyay, R. Wilhelm, Rev. Sci . Instrum, **75**, 1720, (2004).
[2] C. Gorce, M. Capitelli, J. Bretagne, M. Bacal, Chem. Phys., **93**, 1, (1985).
[3] O. Vollmer, B. Heinemann, W. Kraus, P. McNeely, R. Riedl, E .Speth, R. Trainham, R. Wilhelm, Fus. Eng. Des, **56-57**, 465, (2001).
[4] U. Fantz , Internal report, (2003).
[5] A. Roth, *Vacuum technology*, North-holland, (1976).
[6] M. Bandyopadhyay et.al., to be published in Oct. issue in J. Appl. Phys., (2004).
[7] Y. Ohara, et.al., J. Appl. Phys., **61**, 1323, (1987).
[8] J. R. Hiskes, J. Appl. Phys., **70**, 3409, (1991).
[9] D. T. Stibbe, J. Tennyson, New J. Phys., **1**, 2.1-2.9, (1998).
[10] M. Cacciatore, M. Capitelli, C. Gorse, J. Phys. D, **13**, 575, (1980).
[11] U. Fantz, internal memo, Unpublished, June, (2003).
[12] J. R.Hiskes, A. M. Karo, Appl. Phys. Lett., **54**, 508, (1989).
[13] Y. Ohara, M. Akiba, H. Horiike, H. Inami, Y. Okumura, S. Tanaka, J. Appl. Phys., **61**, 1323, (1987).
[14] D. S. Walton, B. Peart, K. T. Dolder, J. Phys. B: Atom .Molec. Phys., **4**, 1343, (1971).
[15] P. Berlemont, D. A. Skinner, M. Bacal, , Rev. Sci. Instrum., **64**, 2721, (1993).
[16] J. R. Hiskes, A. M. Karo, J. Appl. Phys., **67**, 6621, (1990).
[17] M. Bacal, M. Glass-Maujean, A. A. Ivanov Jr., M. Nishiura, M. Sasao, M. Wada, AIP Conf. Proc., **639**, 13, (2002).
[18] M. A. Khakoo, J. Segura, J.Phys. B: At. Mol. Opt. Phys., **27**, 2355, (1994).
[19] J. R. Hiskes, A. M. Karo, J. Appl. Phys., **56**, 1927, (1984).
[20] J. Loureiro, C.M. Ferreira, J. Phys. D: Appl. Phys., **22**, 1680, (1989).
[21] A. P. Hickmann, Phys. Rev. A, **43**, 3495, (1991).
[22] J. M. Wadehra, Phys. Rev. A, **29**, 106, (1984).
[23] A. A. Matveyev, V. P. Silakov, Plasma Sources Sci. Technol., **4**, 606, (1995).
[24] W. Kraus, et.al. Fusion Eng. Design, **66-68**, 491, (2003).
[25] O. Vollmer, et.al. Rev. Sci. Instrum., **71**, 939, (2000).
[26] Y. Okumura, et.al. Rev. Sci. Instrum., **71**, 1219, (2000).
[27] V. G. Dudnikov, Rev. Sci. Instrum., **63**, 2660, (1992).
[28] M. L. Yu, Phys. Rev. Lett., **40**, 574, (1978).
[29] Yu. Belchenko, Rev. Sci. Instrum., **64**, 1385, (1993).
[30] T. Sakurabayashi, A. Hatayama and M. Bacal, J. Appl. Phys., **95**, 3937, (2004).
[31] S. Humphries, Jr., *Charged Partcle Beams*, Wiley, New York, p. 199, (1990).
[32] L. A. Schwager and C. K. Birdsall, Phys. Fluids B, **2**, 1057, (1990).
[33] S. R. Majumdar, A. Roy Chowdhury and S. N. Paul, Phys. Scripta, 69, 335, (2004).
[34] P. McNeely, B. Heineman, W. Kraus, R. Riedl, E. Speth and O. Vollmer, Fusion Eng. Design, **56-57**, 493, (2001).
[35] A. Fukano and M. Ogasawara, Jpn. J. Appl. Phys., **40**, 7072, (2001).
[36] R. K. Janev, W. D. Langer, K. Evans Jr., D. E. Post Jr., *Elementary Processes in Hydrogen-Helium Plasmas*, Springer-Verlag, (1987).
[37] A. V. Phelps, J. Phys. Chem. Ref. Data, 19, 653, (1990).

Chapter 5

Plasma flow measurements

Summary: Measurements of ion flow in an ion source made for negative ion extraction are described in this chapter. The plasma flow has been measured using Mach probe. The flow shows a dominant direction toward the extraction grid; however the flow pattern, away from the central axis of the source, shows a direction reversal and therefore convection. The plasma flow along the axis is due to the electric field created by the plasma potential gradient. The force on the plasma created by the electric field is mainly balanced by the collisional drag force. The collision between the plasma and the background gas creates a pressure gradient along the flow direction. The one dimensional plasma dynamic analysis supports the consistency of the experimental observations. Presence of transverse magnetic filter reduces the plasma flow velocity, which must have an impact on the negative ion production on the Cesiated (Cs coated) grid surface. The analysis shows there is no plasma current exists in the source. The Mach probe is also used as two single probes and compared with the results as double probe to measure other plasma parameters, like n_e and T_e. The presence of an ion flow has a strong influence on negative ion motion toward the extraction grid and on the sheath potential. It would play a dominant role in the ion dynamics and negative ion production and beam over all efficiency.

5.1 Introduction

In many ion sources, especially those, which are developed for NBI systems in fusion devices, considerable gradients plasma density and temperature are present along the axis [1]. In a fluid dynamic description of such ion sources, these gradients need to be balanced by the spatial distribution of electric field and by the changes in plasma momentum [2, 3]. These changes have been measured by measuring the ion fluxes using a Mach probe [4, 5], in BATMAN source [6]. A Mach probe is basically a double probe [7], with a wall situated in between two probe heads. The schematic diagrams of a Mach probe which is used in the experiment are shown in fig. 5.1. The Mach probe is aligned in such a way that one probe tip faces the flow of the plasma and the other one which is situated behind the barrier and does not receives the flow. If I_{sat_1} and I_{sat_2} are the ion saturation currents collected between the two probe tips for opposite double probe bias conditions, the Mach number M has been defined as [8],

$$M = \log\left(\frac{I_{sat1}}{I_{sat2}}\right) \Big/ 2.22 \tag{5.1}$$

From the double probe characteristic obtained from a Mach probe, it is possible to estimate plasma density n_e from I_{sat} and electron temperature T_e by fitting a curve using an analytical formula [7] on the characteristic with a fitting value of T_e. The plasma density n_e can be measured also by using the individual probe tips as single probe separately [9]. An example of measuring T_e is shown in fig. 5.2.

A negative ion plasma source is a complex device, in which the negative ions are generated mainly from a surface interaction, which are located in the regions where the plasma parameters are strongly non-uniform and often away from the main area of plasma ionization [10]. In this situation it is therefore to be expected that the pressure gradient are accompanied by fluid plasma movements, which are conveniently studied using a Mach probe [11]. Additionally the fact is that, the negative ions are mostly surface generated in all bigger and having higher current delivers capability sources because Cesium is used in all those sources [12, 13, 14]. Since the survival length of negative ions is relatively short (~ 1-2 cm) [15, 16], mostly the negative ions which are generated on the plasma facing grid surface, are extracted effectively. So the probe analysis, very close to the plasma grid is important to understand the complex mechanism of generation-extraction. In agreement to these statements, this chapter describes the results of the measurements of plasma flow done in BATMAN source [17]. The plasma dynamics has been analyzed along an axis of symmetry (source axis) using the measurement data of plasma temperature, density and the fluid velocity. In this analysis, the interaction of the plasma flow with background gas creates a gas pressure gradient along the source axis which has been measured as a function of plasma discharge parameters. The one dimensional plasma dynamic analysis shows the consistency of the experimental observations. It is observed that addition of a strong transverse magnetic field reduces the plasma flow velocity and the other plasma parameters in agreement with the basic plasma force balance equation and transverse diffusion model [18, 19]. The analysis and those experimental results suggest improvement in performance and efficiency in the development of a negative ion sources.

5.2 Plasma flow measurements

In BATMAN ion source plasma is created in the *driver* and then it expands in the *expansion* volume. Due to this basic mechanism, it is very likely that the plasma has a flow from the *driver* towards the plasma grid. The plasma flow should have a considerable influence on the transport of molecules, ions, atoms and also on the yield of surface produced negative ions.

There are two types of Mach probe used to determine the flow in BATMAN ion source. In the first case, the Mach probe (Mach probe-I) has single probe head which is comprised of two identical, opposite facing, 0.5 mm diameter and 1 cm long cylindrical tips made of Tungsten, separated by a 6-mm thick Al_2O_3 ceramic wall. In the second case two orthogonal Mach probe heads (Mach probe-II with four identical opposite facing rectangular flat Tungsten strips of width 0.6mm and length 5mm). With the orthogonal Mach probes it is possible to determine two directional components of the flow. The schematic diagrams of the geometry of those two Mach probes are presented in fig.5.1. The Mach probe tips are installed on the end of an L-shaped vacuum tight stainless tube and capable to explore the expansion region as shown in fig.5.3. The radial scans near the driver and axial scans across the source by Mach probe-I are shown in fig.5.4 and fig.5.5 respectively. In fig.5.4 it is observed that the plasma density in front of the driver is relatively constant and it decays radially away from the driver region. Outside the driver the ratio of the ion saturation currents between the two opposite probes

reverses itself. This indicates a reversal of the flow direction, this time toward the driver and away from the grid. In fig.5.5, it is observed that due to the magnetic filter field plasma density and temperature go down and Mach profile more or less uniform, with a small dip at the center. Near the plasma grid the radial scan measurements of parallel and axial flow together with the density are measured independently by the axial and parallel probe heads of Mach probe-II and are shown in fig.5.6.

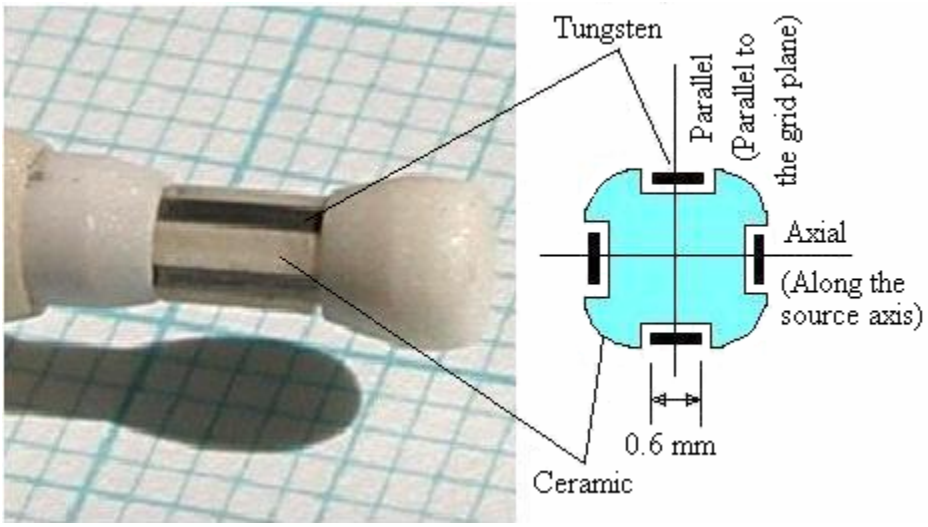

Fig. 5.1. Picture and schematic diagram of the Mach probe-II with two orthogonal heads.

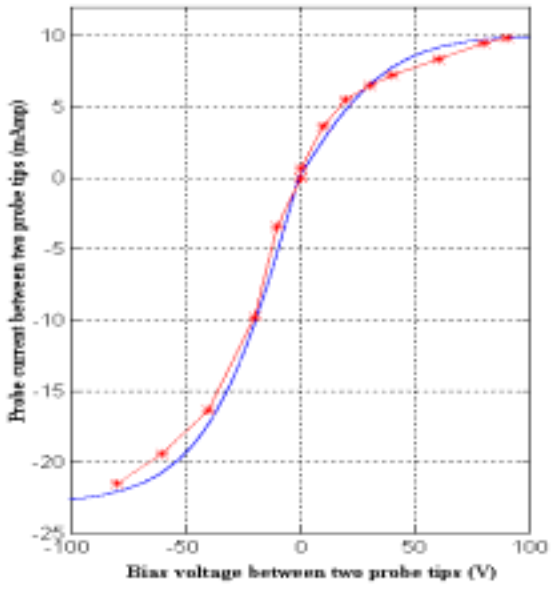

Fig. 5.2 Double probe characteristic on the source axis, near the driver. (*) are the measured data and the continuous curve is the fitting equation [7]. T_e obtained is ~ 20 eV.

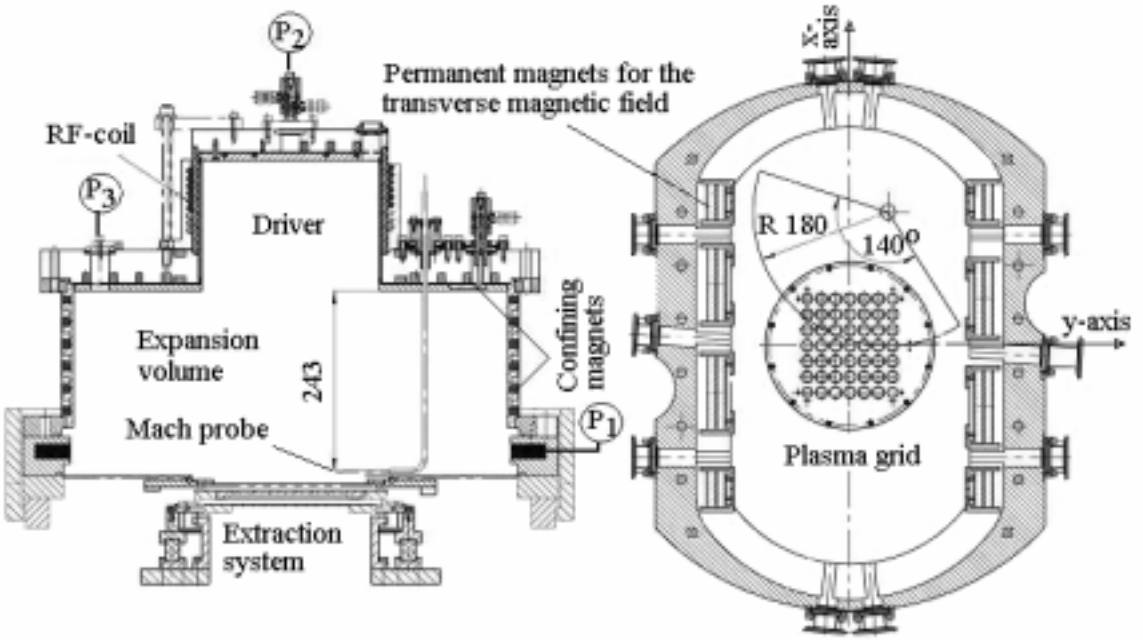

Fig.5.3. Scanning arrangement of the Mach probe inside BATMAN

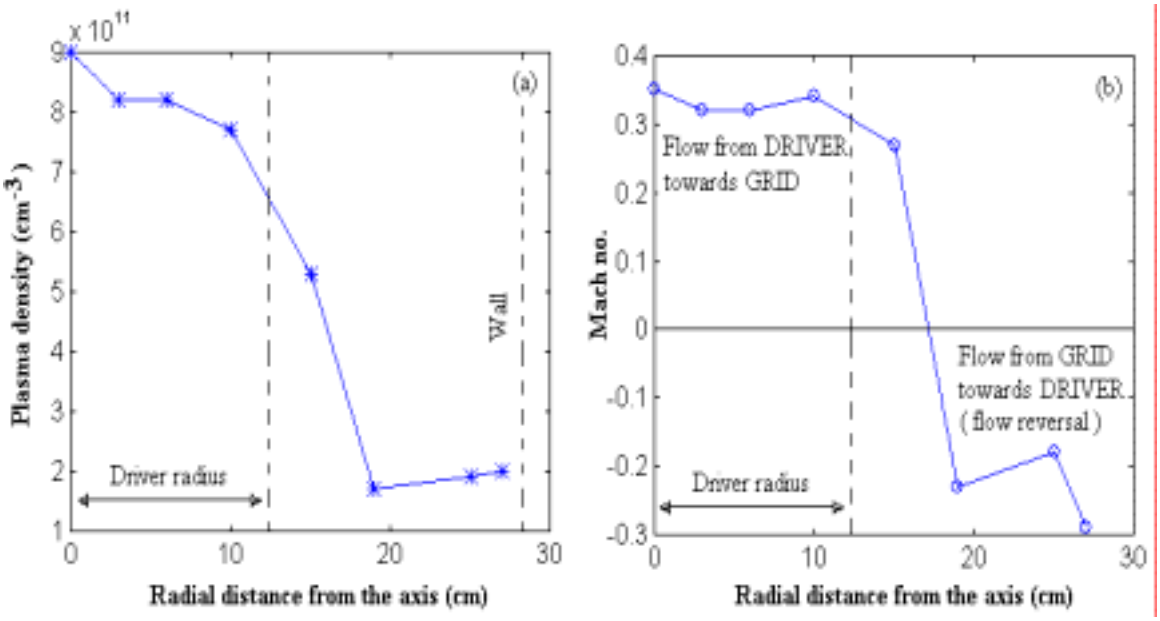

Fig.5.4. Relative plasma density and the flow velocity in terms of Mach number near the driver. Measurements are done with Mach probe-I.

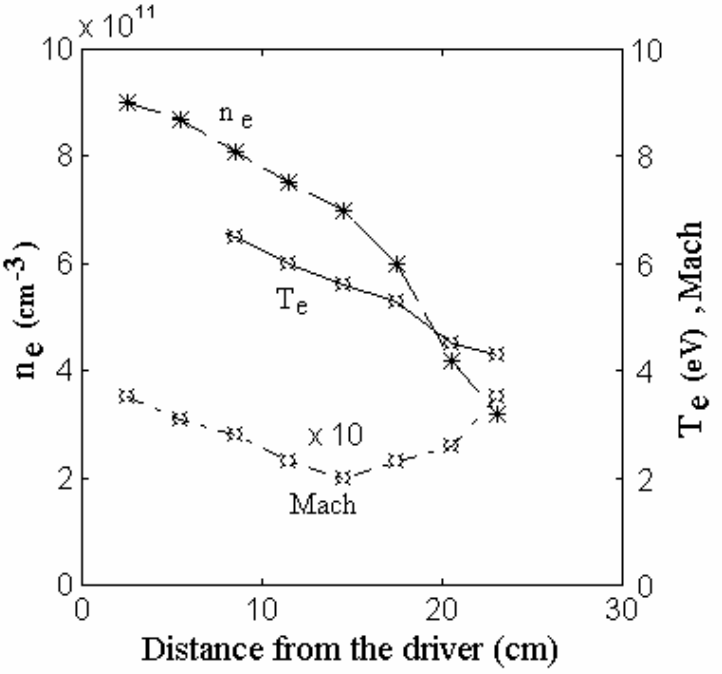

Fig. 5.5. Axial plasma density, temperature and the flow velocity profiles measured with Mach probe-I.

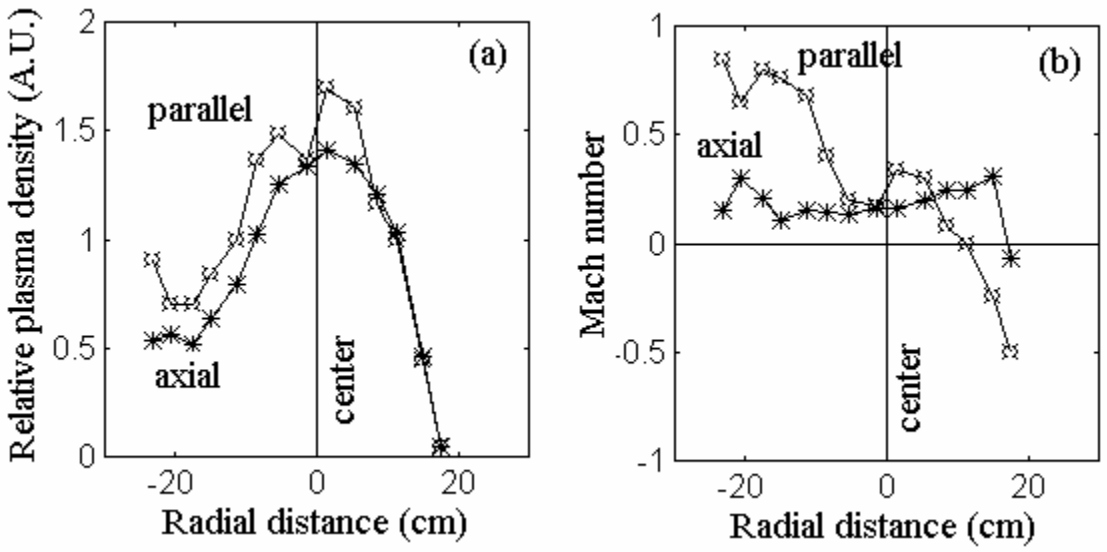

Fig.5.6. Relative plasma density and the flow velocity in terms of Mach number near the grid. Measurements are done with individual probe heads of the Mach probe-II independently.

From the above results fig. 5.4, fig. 5.5 and fig. 5.6., it is concluded that the flow in the source develops a convection pattern, which is shown qualitatively in fig. 5.7. The axial flow depends on the magnetic field topology of the confinement magnets situated externally on the source wall. Two different magnet configurations, as shown in fig. 5.8 and fig. 5.9 are examined.

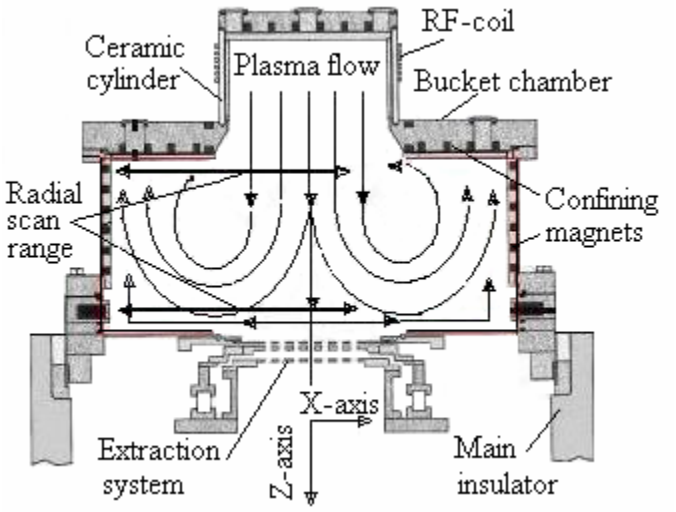

Fig. 5.7. Schematic plasma flow pattern in BATMAN ion source with reference co-ordinate system

5.3 Force balance

In order to gain a better understanding of the properties of the ion source, an analysis using the force balance [18] on the source axis is presented. The relevant parameters have been investigated in two configurations and without grid bias and H^- ion beam extraction as shown in fig.5.8. These two configurations are not same as normal operational bucket type source configuration [20]. In one of the configuration a strong transverse magnetic filter was applied along the y-axis of the reference frame. From the changes in the plasma parameters due to this transverse field, which acts as a filter field, a consistent picture emerges. The measurements were carried out along the source axis (z-axis) as shown in fig.5.7. The total field profiles along the z-axis are shown in fig.5.9**.** The relevant plasma profiles along the axis are shown in fig. 5.10 and 5.11. The insertion of two Baratrons, one with a reading in the grid region (P_1) and a second one in the driver region (P_2), (see in fig.5.3) give the measurement of the pressure difference between these two positions as shown as a time dependent graph in fig. 5.12(a). Fig. 5.12(b)-(d) also show the pressure difference as a function of the filling pressure and as a function of the applied power levels. It is evident a pretty good linear trend of the pressure difference as a function of the filling pressure and applied RF power as well.

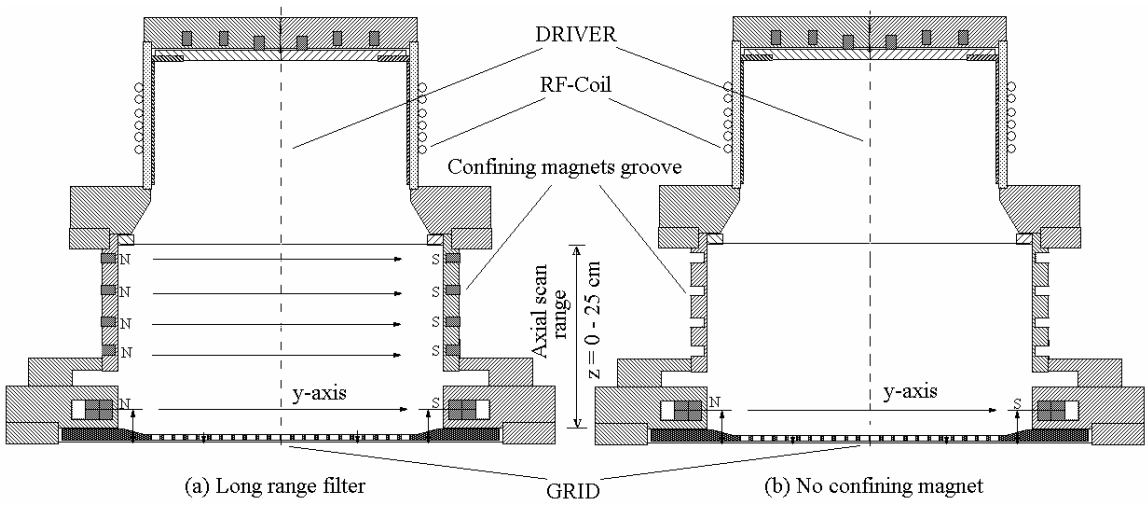

Fig.5.8. Magnet arrangements in BATMAN for the study of two cases. The magnetic filter field direction is along the y-axis.

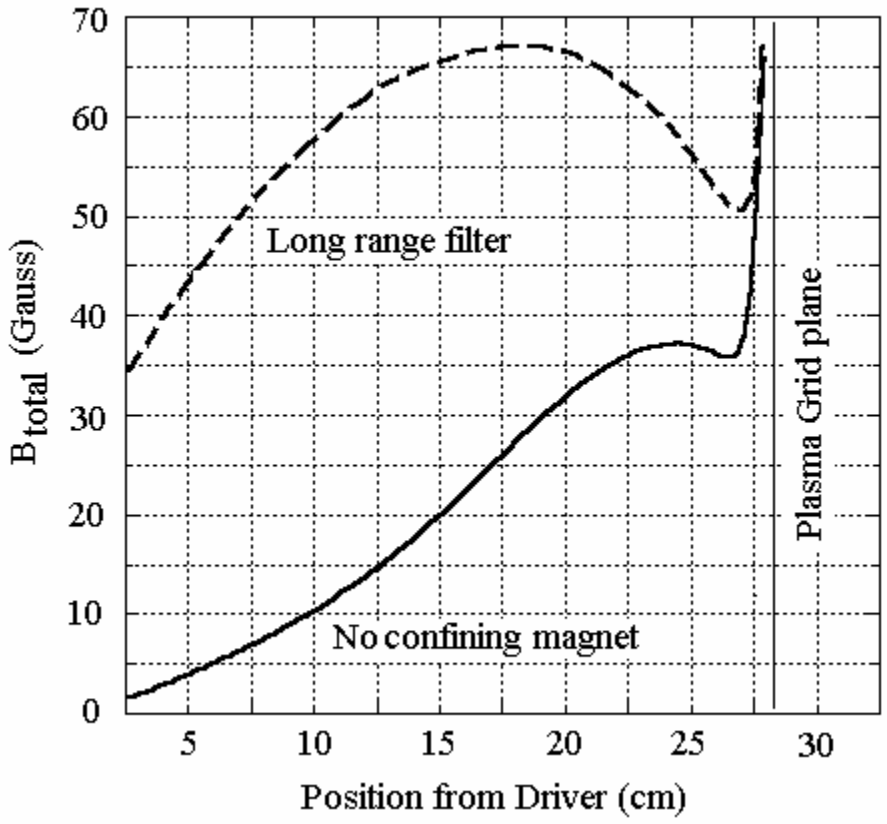

Fig.5.9. Total magnetic field profiles along the axis of BATMAN for the two cases.

In order to analyze the experimental data of the force balance, the force balance equation for ion [18] is,

$$mn_i\left[\frac{\partial \vec{u}}{\partial t}+\left(\vec{u}\cdot\vec{\nabla}\right)\vec{u}\right]=qn_i\left[\vec{E}+\left(\vec{u}\times\vec{B}\right)\right]+f\big|_c \tag{5.2}$$

where m is the mass of the ion, $n_i = n_e$ is the plasma density, u is the fluid velocity, q is the charge of the ion, E is the ambipolar electric field calculated from the axial gradient of the measured plasma potential, B is the externally applied magnetic field along y-axis and f_c is the drag force term due to different collisions.

The ion temperature T_i is small compare to the electron temperature T_e , the pressure gradient $\nabla\Pi_i$ term for ion can be neglected. As a steady-state case, $\partial u/\partial t = 0$. It is assumed that on the z-axis the fluid velocity has an axial symmetry, because ions are not magnetized; therefore the (u×B) term can be neglected. The equation (5.2) along the z-axis can be written,

$$mn_i u_z\frac{\partial u_z}{\partial z}=qn_i E_z+f\big|_c \tag{5.3}$$

Here u_z is the plasma fluid velocity, $u_z=Mu_{ac}$, where M is the measured Mach number and u_{ac} is the ion acoustic velocity calculated from electron temperature T_e.

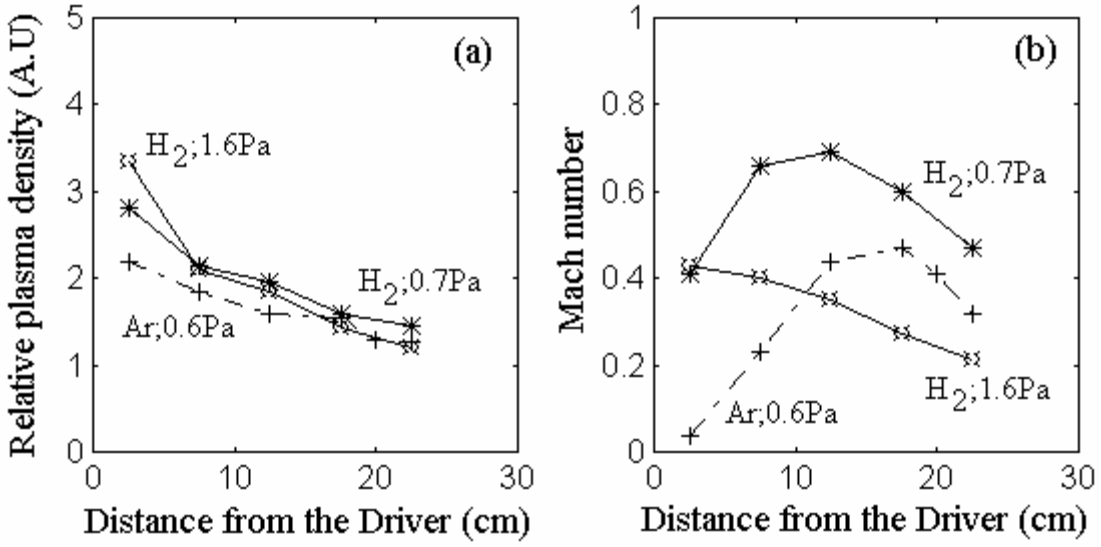

Fig.5.10. Relative plasma density in arbitrary unit (A.U) and corresponding plasma flow in the case of no confining magnet configuration for different background gas pressure and different types of gases.

In the geometry of BATMAN different forces are,

1. The force due to ambipolar electric field E caused by the electron pressure gradient is $F_E = qn_eE$ and the direction of that force is directed toward the Grid for +ve ions.
2. The drag force, F_c due to collision with neutrals [22] is directed toward the Driver.

3. The force due to inertia $F_I = mn_e$ (u.∇)u = $mn_e u_z \partial u_z/\partial z$, is directed toward the Grid direction if the velocity gradient is towards Driver.
4. The drag force, due to momentum transfer by charge exchange reaction [23] F_X is directed toward the Driver.

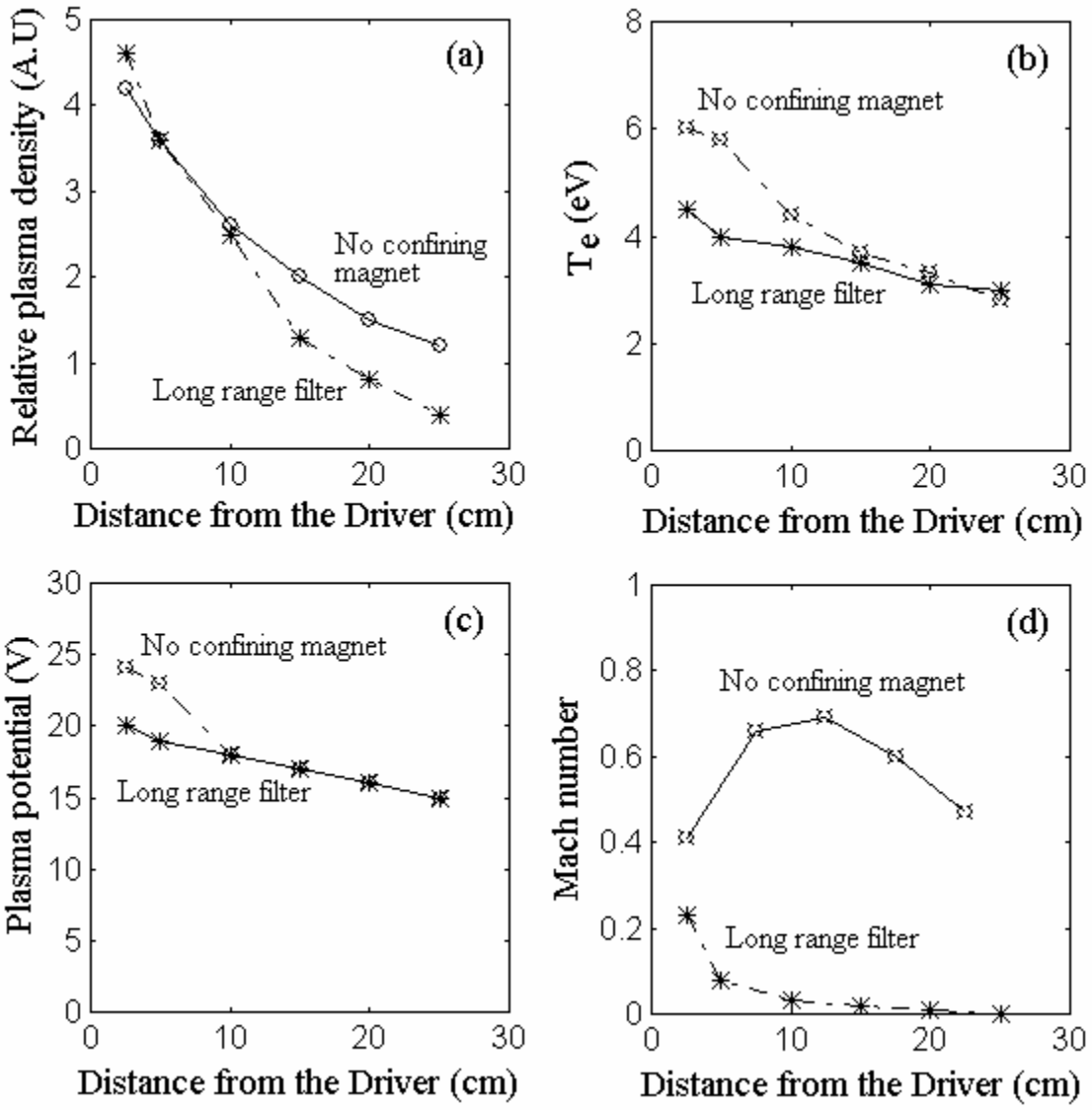

Fig.5.11. Relative plasma parameters and plasma flow for two different source configurations.

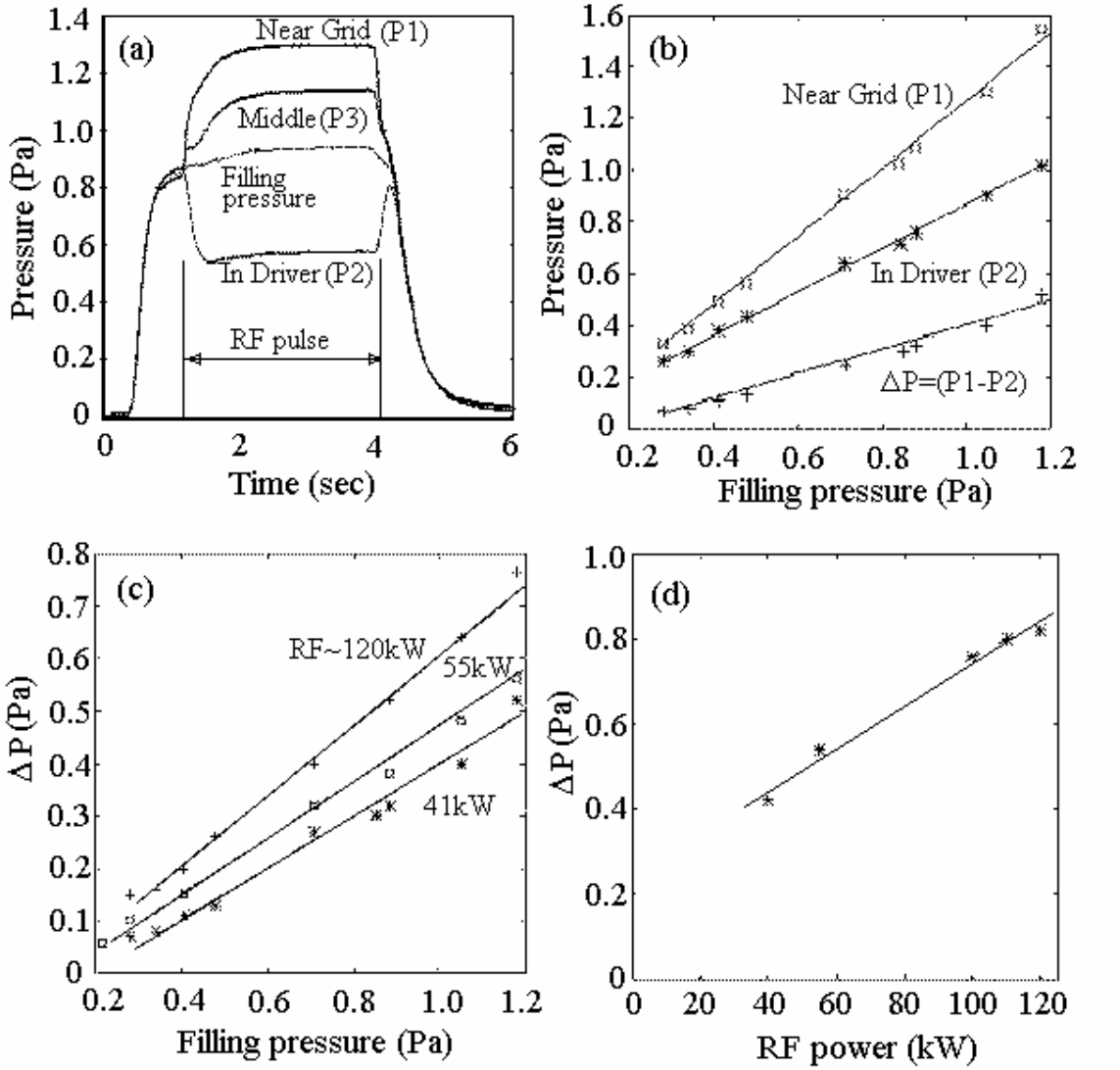

Fig. 5.12. (a) Variation of gas pressure with time at different location in BATMAN during the plasma shot. (b) Variation of pressure at different location in the source for different filling pressure, (c) and (d) Pressure difference ΔP occurred between the grid region and the driver region for different filling pressure and RF power respectively.

For the two described source configurations, assuming plasma ion composition [24] as $H^+ : H_2^+ : H_3^+ = 0.6 : 0.3 : 0.1$, the results of the calculation of the force balance are shown in fig. 13. The following can be stated.

1. From the measurement the force balance equation is verified within the error bar.
2. As already evident from the experimental data, at higher pressure the drag with the background gas increases while at higher power the driving force also increases.

3. All the forces in the source are ultimately driven by the heating of the electrons in the driver region, which gives rise to an electron pressure gradient. In the absence of a strong magnetic field this force is transferred to the ions, mainly via ambipolar electric field. The force imparted thereby on the ions results to the smaller part in their acceleration (the inertia force F_I) but is mainly transferred to the neutral particles, via collisions (F_c) and charge exchange (F_X). It should therefore ultimately result in a neutral pressure gradient in the direction away from the driver towards the grid. The observed differences (fig.5.12), distributed evenly over a distance 0.3m corresponds indeed nearly same to the value (F_c+F_X) in fig.5.13, which confirms the self-consistency of the measurement and of this model.
4. In the parameter regime of the source when $\omega_{ic} << \nu$ where ω_{ic} is the ion-cyclotron frequency and ν is the ion-neutral momentum transfer collision frequency, the applied magnetic filter field acts mainly onto the electrons. Their pressure gradient can now be balanced not only by the magnetic field, but also by the currents in the direction perpendicular to the magnetic field. The magnitude of these currents depends not only on the plasma properties but also on the boundary conditions at the source wall (e.g. suppression of electron flow by confining magnets). As the electric field, produced inside the source due to the complex electron dynamics during the pulse is measured directly; it is still possible to establish a force balance on ions irrespective of electron dynamics. The effect of a transverse magnetic field leads to a substantial reduction of ion flow toward the grid.

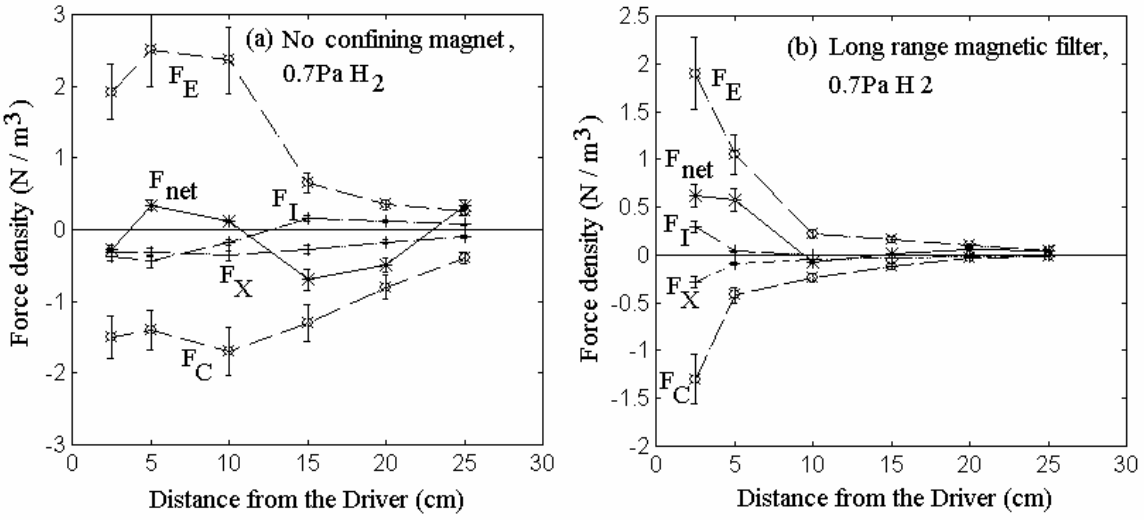

Fig. 5.13. Calculated net force F_{net} acting on the plasma. F_{net} is nearly zero along the axis.

In presence of a magnetic filter field, it is possible to write force balance in terms of transverse velocity of ions in the drift approximation [18] as,

$$v_{\perp} = \mu_{\perp} E - D_{\perp} \left(\nabla n_e / n_e \right) + \left[\frac{\left(v_E + v_D \right)}{\left\{ 1 + \left(\nu^2 / \omega_{ic}{}^2 \right) \right\}} \right] \tag{5.4}$$

where ν is the ion-neutral momentum transfer collision frequency, ω_{ic} is the ion-cyclotron frequency, $\mu_{\perp}$ and $D_{\perp}$ are the ion-mobility and diffusion coefficient respectively in the perpendicular direction with respect to the transverse magnetic field B along y-axis. The first term in the right hand side of equation (5.4) is the velocity due to the ambipolar electric field, the second term is the velocity due to diffusion, v_{diff} and the third term is due to the drift, v_{drift}. In the drift velocity term v_E corresponds to E×B drift and v_D corresponds to the diamagnetic drift due to the plasma pressure gradient and the magnetic field. The direction of v_{drift} is along x-axis and orthogonal to the source axis (z-axis). The diffusion term and the diamagnetic term for ions can be neglected because the ion temperature is very low compare to the electron temperature. The electron dynamics enters only indirectly, as it determines the E_x electric field due to the presence of magnetic filter field. In case of ions, equation (5.4) can be written in two orthogonal components as,

$$u_z = \mu_{\perp} E_z + \frac{\left(E_x / B \right)}{\left[1 + \left(\nu / \omega_{ic} \right)^2 \right]} \tag{5.5}$$

$$u_x = \mu_{\perp} E_x - \frac{\left(E_z / B \right)}{\left[1 + \left(\nu / \omega_{ic} \right)^2 \right]} \tag{5.6}$$

The effect of E_x on the axial flow velocity u_z can be estimated by examining two extreme cases: short-circuited electric field (E_x=0) and suppressed flow (u_x=0). In the first case after solving equations (5.5) and (5.6),

$$u_z = \mu_{\perp} E_z \left[1 + \frac{\left(\nu / \omega_{ic} \right)^2}{\left\{ 1 + \left(\nu / \omega_{ic} \right)^2 \right\}^2} \right] \tag{5.7}$$

and in the second case equation (5.4) become,

$$u_z = \mu_{\perp} E_z \tag{5.8}$$

Comparing equations (5.7) and (5.8), it is observed that the effect of E_x produce a correction term (~ 20%) on u_z. Since electric field driven drift is small, it confirms that the magnetic filter field acts primarily through a reduction of the ambipolar electric field, which now does not have to balance the total electron pressure gradient.

A comparison between the measured plasma flow velocities with the help of Mach probe and the calculated fluid velocities, which are derived from the equation (5.8) for two source configurations are shown in fig. 5.14. By close inspection one finds that the two values agree within a factor of 2-3 for all the cases examined. The one dimensional

plasma dynamic analysis supports the consistency of the experimental observations. The possible existence of other components of the plasma flow and the measurement errors in the observations may attribute to the discrepancies.

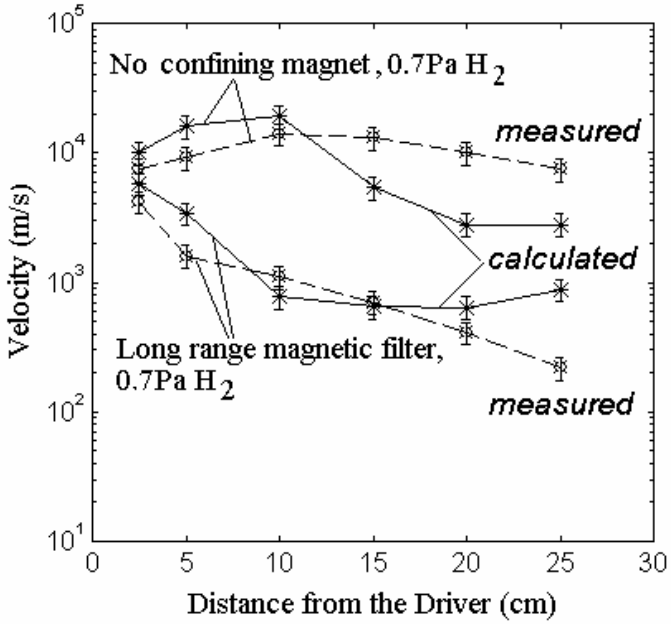

Fig.5.14. Comparison of measured plasma flow velocity with the help of Mach probe and the calculated plasma flow velocity profile with the help of equation (5.8) along the source axis (z-axis) in two cases.

5.4 Effect of plasma flow on the plasma sheath

The plasma flow changes the ion dynamic and the physics of ion extraction in at least two ways.

a. It directly modifies the plasma sheath. The Poisson's equation in the sheath can be written as,

$$\frac{d^2V}{dx^2} = -\frac{n_s e}{\varepsilon_0}\left[\left\{1-\frac{V}{V_0+(\mathrm{KE}/e)}\right\}^{-\frac{1}{2}} - \exp\left(\frac{eV}{k_B T_e}\right)\right] \tag{5.9}$$

The first part inside the square bracket is the ion part, where potential V is negative. The kinetic energy, which the ions acquire in the pre-sheath according to Bohm criteria, is denoted by eV_0. (V_0 is not the potential at the plasma-sheath boundary). The kinetic energy of the ions due to plasma flow is written as KE. Assuming the conservation of mono-energetic ion flux, no new ions are produced inside the sheath and the electric field at the plasma-sheath boundary is very small; after integrating once analytically the equation (5.9) becomes,

$$\frac{1}{2}\left(\frac{dV}{dx}\right)^2 = \frac{n_s}{\varepsilon_0}\left[2(eV_0 + \mathrm{KE})\left\{1 - \frac{V}{V_0 + (\mathrm{KE}/e)}\right\}^{\frac{1}{2}} + k_B T_e \exp\left(\frac{eV}{k_B T_e}\right) - 2(eV_0 + \mathrm{KE}) - k_B T_e\right] \quad (5.10)$$

Equation (5.10) can be written in a dimensionless form, considering $eV_0 = k_B T_e / 2$,

$$\frac{d\eta}{ds} = \left[(1+f)\left(1 - \frac{2\eta}{1+f}\right)^{\frac{1}{2}} + \exp(\eta) - (2+f)\right]^{\frac{1}{2}} \quad (5.11)$$

where η is the normalized potential (eV/k_BT_e), negative in this case, f is the normalized flow energy ($2\mathrm{KE}/k_BT_e$) and s is the normalized distance (x/λ_D). λ_D is the Debye length, defined as,

$$\lambda_D = \left\{(\varepsilon_0 k_B T_e)/(2 n_s e^2)\right\}^{\frac{1}{2}} \quad (5.12)$$

Equation (5.11) is solved numerically and the results are shown in fig. 5.15.

b. It will modify the ion flux to the grid by adding a term to the Bohm flux as shown in equation (5.9).

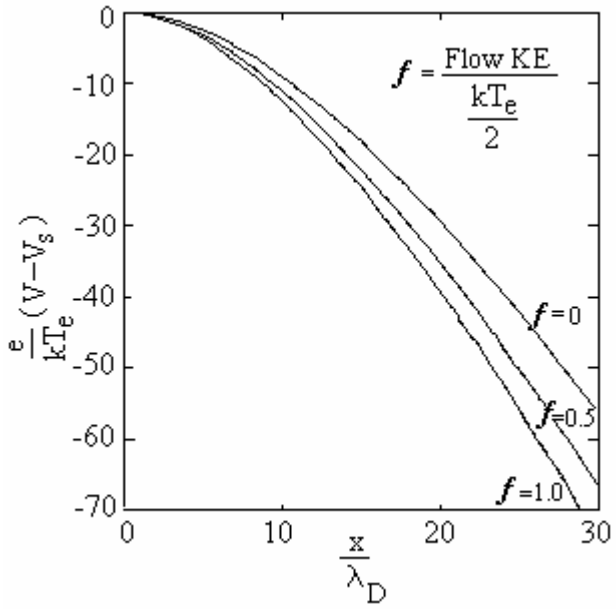

Fig.5.15. Plot of normalized potential $e(V - V_s)/k_B T$ as a function of normalized distance x/λ_D. The potential of the plasma-sheath boundary is denoted as V_s.

5.5 Influence of plasma flow on negative ion production

The surface production of H^- ions depends on the flux of energetic H atoms and positive ions [24, 25]. In this process electrons have to be attached with that impinging atoms and ions by overcoming the work-function of the metal surface. This mechanism leads to a requirement of kinetic energy (KE) of the atoms and ions, which should be greater than the work-function of the metallic surface [25]. So less the work-function of the surface is, more will be the surface production. In case of Cs covered Mo or W surface, the minimum work-function can be achieved as [25] ~ 1.6 eV.

In the plasma discharge, due to the dissociation of the H_2 molecules by electrons, energetic atoms (~ 2 eV) are formed initially [26], but due to the collisions with background gas molecules, walls and due to the recombination, the energetic part of the atomic population is expected to be 1% of the background gas density n_g. The bulk H atoms are thermalized with energy of ~ 0.1 eV, or less, which are not useful for surface production. Due to the presence of plasma flow, the ions have a directional KE of ~ few eV, as electron temperature is of the same order. These energetic ions could be converted into energetic atoms by charge exchange collisions [22]. The typical mean free path of charge exchange collision is ~ 2-5 cm for the experimental conditions near the plasma grid. To estimate the negative ions yield from charge exchanged neutral atoms, the ion flux Γ_i and the corresponding atom flux Γ_a on the cesiated surface to be calculated.

The KE of an ion due to the plasma flow is ~ $M^2T_e/2$; where M is the Mach number and T_e is the electron temperature near the grid. The H^- ion yield on a cesiated surface having work-function ~ 1.6 eV by the energetic atoms as a function of plasma flow velocity in terms of Mach number is shown in fig.5.16. This calculation is carried out using the formulation and data used in Ref. 27.

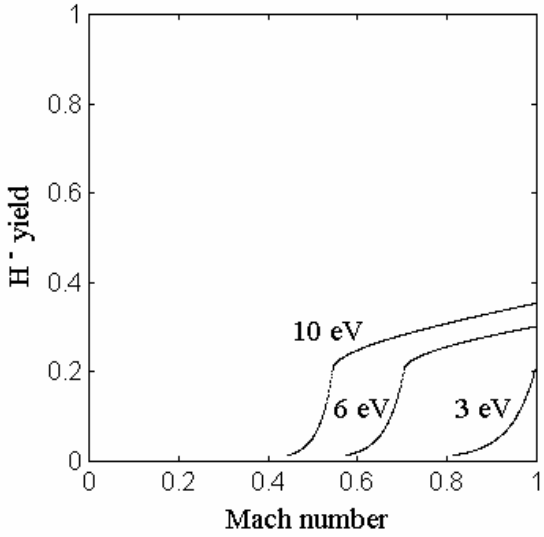

Fig.5.16. Total H^- ion yield due to energetic atoms bombardment as a function of plasma flow velocity in terms of Mach number on a Cs covered Mo/W surface having work-function 1.6 eV .

From the bohm criterion, equation (5.9) it is pointed out that due to the presence of the plasma flow the sheath structure is changed from the case when the plasma flow is absent and therefore the positive ion flux is consequently altered. The same formulation (presented in ref.11) is used to estimate the variation of positive ion flux on the wall for different plasma flow velocity. The variation of the normalized positive ion density with the normalized sheath potential is shown in fig. 5.17. The normalized spatial positive ion density profile inside the sheath is shown in fig. 5.18. The surface production of negative ions depends both on the ionic and the atomic flux on the wall. The ionic flux on the wall is calculated with the help of the same formulation, equation 5.11.

Fig.5.19 shows an estimated H^- ion current density (normalized with respect to the Mach number = 0 in each case) due to the surface production in BATMAN ion source using the H^- ion surface production yield values from ref. 24 and 25. The first part before the step (see in fig.5.19) in each curve is due to the contributions of positive ions which are accelerated in the sheath and the background H atoms impinging on the surface. The step arises due to the atomic contribution after charge exchange collision. The threshold Mach number originates due to the threshold KE (W-A, A is the electron affinity) of the atom to produce negative ion. The work-function of the surface is assumed as W=1.6eV and the electron affinity of an H^- ion is A=0.75eV. The conclusion of this simple calculation shows that if a strong plasma flow is present, directed toward the PG up to a distance shorter than the neutral collision mean free path, a considerable enhancement of the H^- ion production could result.

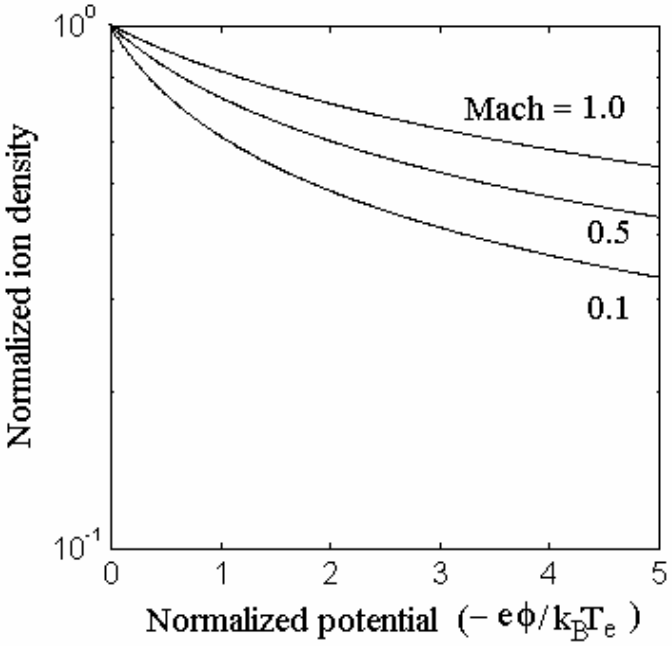

Fig.5.17. Effect of plasma flow on normalized positive ion density inside a sheath due to different normalized potential.

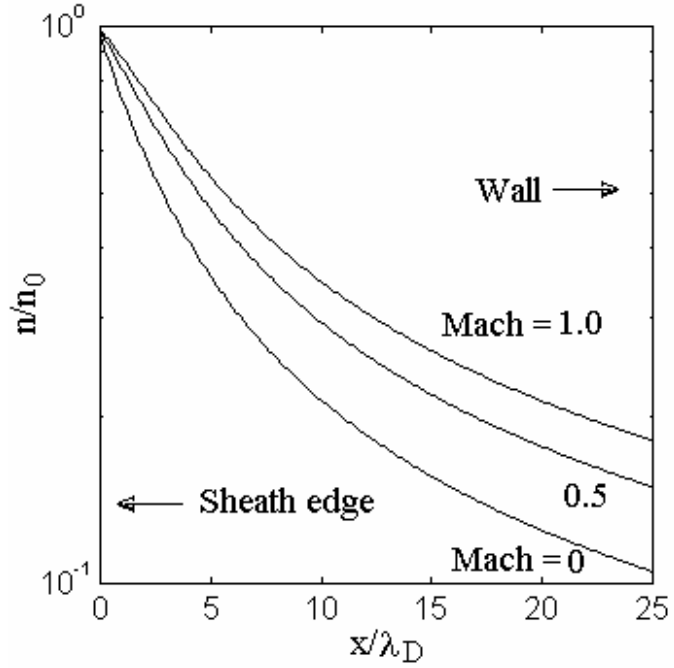

Fig.5.18. Effect of plasma flow on normalized positive ion density inside a sheath at different normalized distance from the wall due to different normalized potential.

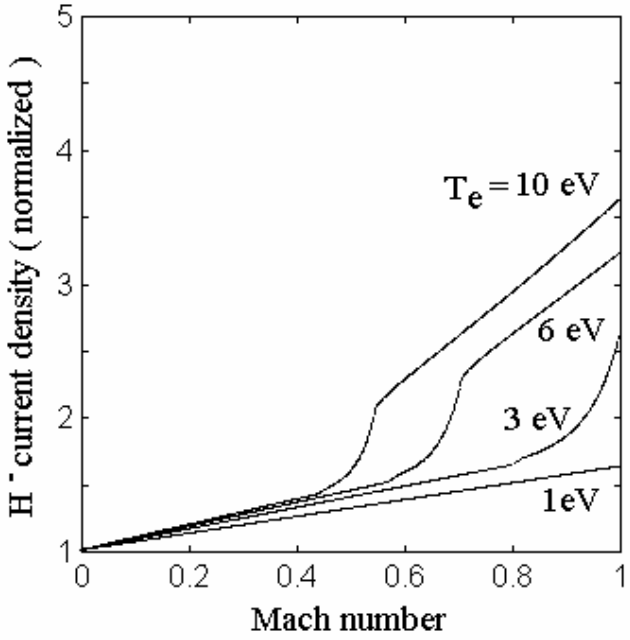

Fig.5.19. Effect of plasma flow on the estimated negative ion current density, normalized to Mach number = 0 due to the surface production for different T_e.

5.6 Conclusion

The experiment and analysis show that plasma flow is an important characteristic of a ion source where there is a large gradient of plasma potential exists due to ambipolar diffusion. It has been shown that the plasma flow velocity can approach Mach number of 1 and it is strongly dependent on the transverse magnetic fields. The measurements done in BATMAN ion source using a Mach probe along the axis comprehend plasma density, plasma potential, electron temperature and the barometrically measured background gas pressure. This consistent set of experimental observations has been used to solve the one-dimensional force balance equation in its differential form. The collisions due to the charge exchange and with the neutrals have been considered as frictional terms. At steady state condition the force on the plasma created by the ambipolar electric field is balanced by the frictional forces. In the case of ions, collisions with neutrals represent the dominant drag force term. The $u_z \times B$ force, due to the transverse filter field does not contribute because its direction is orthogonal to the axis. The effect of electron motion on the ions comes through the ambipolar electric field which is measured in this case and so included in the present analysis. The electron dynamics can be changed by the presence of confining magnets. The presence of confining magnets does not allow the flow of hall current (in the x-direction) which makes a 20% correction term on the axial ion flow velocity with respect to the case when there are no confining magnets sitting on the source wall. The analysis shows that plasma flow is an important characteristic of a plasma source where there is a large gradient of plasma potential exists. The collisions between the plasma ions and the background gas molecules create a pressure gradient along the flow direction. This pressure gradient along the axis is proportional to the radio frequency (RF) power and the filling gas pressure. The one dimensional plasma dynamic analysis supports the consistency of the experimental observations. Presence of transverse magnetic filter reduces the plasma flow velocity, which could effect the negative ion production on the Cesiated grid surface, given that the surface production of negative ions also depends on the flux of the positive ions and energetic atoms impinging the surface. It is expected to improve the negative ion extraction up to a factor two due to the change in ion flux from isotropic nature to a directional one and an additional term in Bohm flux as shown in equation (5.9). The presence of plasma flow could also play an important role by influencing the extraction current by modifying the sheath near the extraction grid. The flow will modify the effective distance from which the negative ions are able to reach the grid, before getting destroyed. Since transverse magnetic filter field reduces the plasma flow towards the extraction grid, it is therefore obvious that the optimization of the ion flux by changing the filter field strength could be an important parameter in the development of efficient negative ion sources.

References

[1] P.McNeely, B.Heineman, W.Kraus, R.Riedl, E.Speth, O.Vollmer, Fus.Eng. Des, **56-57**, 493 (2001).

[2] R.N.Franklin, J.Phys.D: Appl.Phys.,**35**, 536 (2002).

[3] F.A.Hass, L.M.Lee and A.J.T.Holmes, J.Phys.D: Appl.Phys.,**24**, 1541 (1991).

[4] P.C.Stangeby, Phys.Fluids, **27**, 2699 (1984).

[5] I.H.Hutchinson, Phys.Fluids, **30**, 3777, (1988).

[6] O.Vollmer, B.Heinemann,W.Kraus, P.McNeely, R.Riedl, E.Speth, R.Trainham and R.Wilhelm, Fus.Eng. Des, **56-57**, 465 (2001).

[7] B. M. Annaratone, et.al., Plasma Sources Sci. Technol., **1**, 232, (1992).

[8] B. J. Peterson, et. al., Rev. Sci. Instrum., **65**, 2599, (1994).

[9] B.M.Annaratone, M.W.Allen and J.E.Allen, J.Phys.D: Appl.Phys.,**25**, 417 (1992).

[10] P. McNeely, M. Bandyopadhyay, P. Franzen, B. Heinemann, C. Hu, W. , R. Riedl, E. Speth, and R. Wilhelm, AIP Conf. Proc. **639**, 90, (2002).

[11] A. Tanga, M. Bandyopadhyay and P. McNeely, Appl. Phys. Lett., **84**, 182, (2004).

[12] D. Riz and J. Pamela, Rev. Sci. Instrum., **69**, 914, (1998).

[13] Y. Oka, et.al.., Rev. Sci. Instrum., **73**, 1054, (2002).

[14] T. Ohga et. al., Rev. Sci. Instrum., **73**, 1058, (2002).

[15] M. Bandyopadhyay and R. Wilhelm, Rev. Sci. Instrum., **75**, 1720, (2004).

[16] O. Fukumasa, T. Fujioka and T. Fukuchi, AIP Conf. Proc. **639**, 75, (2002).

[17] M. Bandyopadhyay, et.al., to be published in Oct. issue in J. Appl. Phys (2004).

[18] F. F. Chen, Introduction to Plasma Physics, Plenum Press, New York, (1974).

[19] S. I. Braginskii, Reviews of Plasma physics, Vol.1, Edited by M. A. Leontovich, Consultants Bureau, New York, (1965).

[20] O. Vollmer, H. Falter, P Frank, B. Heinemann, W. Kraus, P. Massmann, P. McNeely, R. Riedl, E. Speth, R. Trainham, R. Wilhelm, Rev. Sci. Instrum., **71**, 939, (2000).

[21] A. V. Phelps, J. Phys. Chem. Ref. Data, 19, 653, (1990).

[22] R. K. Janev, W. D. Langer, K. Evans Jr., D. E. Post Jr., *Elementary Processes in Hydrogen-Helium Plasmas*, Springer-Verlag, (1987).

[23] W. Kraus, P Franzen, B. Heinemann, E. Speth, O. Vollmer, Fus. Eng. Des., **56-57**, 493, (2001).

[24] B. S. Lee, M. Seidl, Appl. Phys. Lett., **61**, 2857, (1992).

[25] M. Seidl, H. L. Cui, J. D. Isenberg, H. J. Kwon, B. S. Lee, Proc. 6th Int. Symp. Prod. & Neutralization of Neg. Ion, 25, (1992).

[26] J. Geddes, R.W. McCullough, A. Donnelly, H. B. Gilbody, Plasma Sources Sci. Technol., **2**, 93, (1993).

[27] H. L. Cui, J. Vac. Sci. Technol. A, **9**, 1823, (1991).

Chapter 6

Grid bias experiments

Summary: Positively biased plasma grid reduces the electron density near it and therefore reduces the co-extracted electron current. The negative ion current is nearly unaffected. The effect of applied bias voltage in terms of plasma density variation is observed up to ~ 5 cm into the plasma and form a double layer in the vicinity of the grid. The H^- ions which are produced on the plasma grid surface are present inside the double layer. Therefore those ions are not confined inside the plasma volume by the positive plasma potential (plasma sheath). Formation of the double layer due to the positively biased grid may help those H^- ions which are produced on the plasma grid surface to be extracted more efficiently. The effect of extraction potential which is applied to the extraction grid (second grid) is equivalent to the effect of the positively biased grid because the extraction potential is few kV positive with respect to the plasma. The field due to the extraction potential may penetrate into the plasma through the plasma grid (first grid) holes.

6.1 Introduction

To understand the extraction mechanisms of negative ions and to develop an extraction code, it is important to know the plasma behavior near the plasma grid. In negative ion extraction system, due to the similar sign of charges, the electrons are co-extracted with the negative ions. The electrons are lighter than the negative ions and therefore the amount of co-extracted electron current is few orders more than the negative ion current. Lower electron current is always desirable. It is observed in an experiment [1] done by M. Bacal and her group that the positively biased plasma grid reduces the co-extracted electron current considerably during the negative ion extraction and also helps to increase the H^- ion density near the grid, (see the fig.6.1.[1]). In their experiment the optimum plasma grid bias potential is ~2V positive with respect to the wall (ground) potential. The plasma potential in that experiment is lying between 2 to 3 V only.

6.2 Experimental setup

The plasma grid bias experiment is carried out with CEA grid (obtained from CEA, Cadarach, France). This CEA grid has relatively smaller area ~ 70 cm^2, which is isolated from the rest of the source body and can be floated or biased so that load on the bias power supply will be within the tolerable limit. The electrical setup is shown in figure 6.2. Measurements of plasma parameters are carried out by Mach probe-II (described in chapter-5, fig. 5.1). The plasma flow near the plasma grid is measured directly with this probe. To measure the plasma density, Mach probe-II is used as a double probe and as a single Langmuir probe too. Due to the geometrical restrictions it is not possible by the probe tip to reach closer than 1.5cm towards the plasma grid surface. The input RF power is 60 kW and pressure is 0.6 Pa. The biasing is done with a DC power supply (commercial batteries). The confining magnets are placed in their grooves on the bucket chamber in line cusp configuration and a permanent magnetic filter is present ~ 4.5 cm

from the plasma grid (inside the diagnostic flange). The present magnetic field configuration is the normal BATMAN operational configuration.

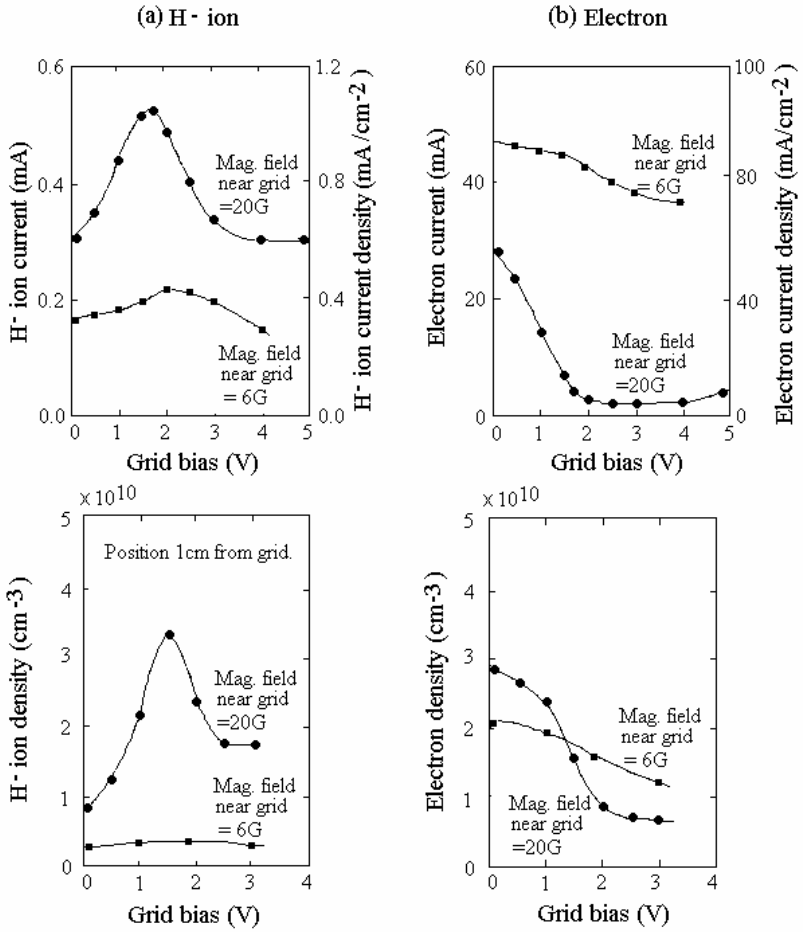

Fig.6.1 (a) H^- ion current and H^- ion density increased and (b) electron current and electron density decreased with proper grid bias and magnetic field. The plasma source is a conventional arc source having the plasma potential ~2-3 V [1].

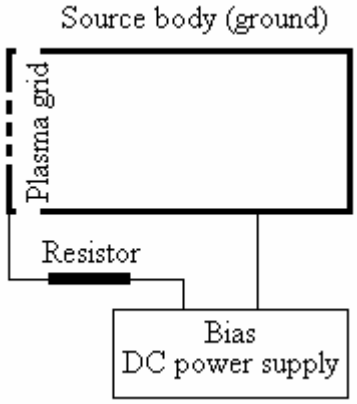

Fig. 6.2. Schematic plasma grid bias diagram

6.3 Results

The relative plasma density (in terms of ion saturation current in the electrical probe) is measured on the source axis in front of the grid with positive and negative plasma grid bias (see fig. 6.3). For positively biased grid, plasma density is reduced drastically, because the grid sucks the electrons. This would explain why co-extracted electron current goes down when plasma grid is biased positively [2]. Regarding the plasma flow only the axial flow is experienced some retardation effect due to the positive bias as expected whereas parallel flow is unaffected. For details of axial and parallel flow please refer chapter-5. The depletion of electron due to the positive grid bias is extended couple of centimeters inside the plasma from the plasma grid as shown in figure 6.4.

Fig. 6.5(a) suggests that a double layer [3] is formed in the vicinity of positively biased plasma grid. It is expected that the H^- ions which are produced due to the surface production process lie in that region [4]. The surface produced H^- ions are confined in the first layer of thickness between 0 – 2 cm from the plasma grid and then extracted. The positive bias potential on the plasma grid can be considered as an extraction field for H^- ions. The raw probe characteristics data, taken in that region are also shown in fig. 6.5 (b). At higher grid bias voltage and at a distance of only 2 cm from the plasma grid, the strong electron depletion is evident from the very low value of the probe current in the electron side (positive probe voltage) of the Langmuir probe characteristic.

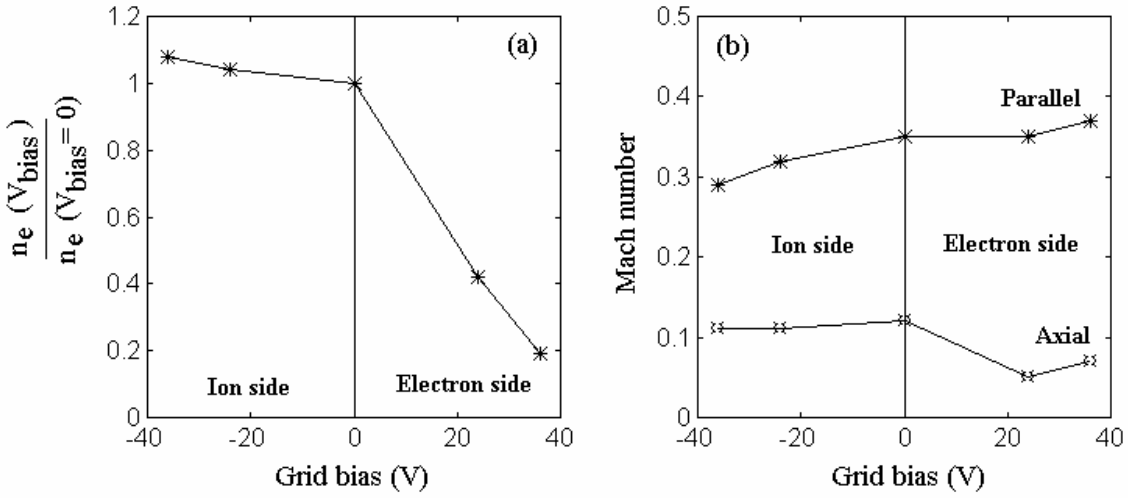

Fig. 6.3 (a) Normalized plasma density in front of the plasma grid for different plasma grid bias voltages. (b) Axial and parallel components of the flow velocity of the plasma near the plasma grid (see chapter -5 for details). The "electron side" corresponds to the positive grid bias because then electrons are attracted towards the grid whereas negative grid bias corresponds to "ion side" because it attracts positive ions.

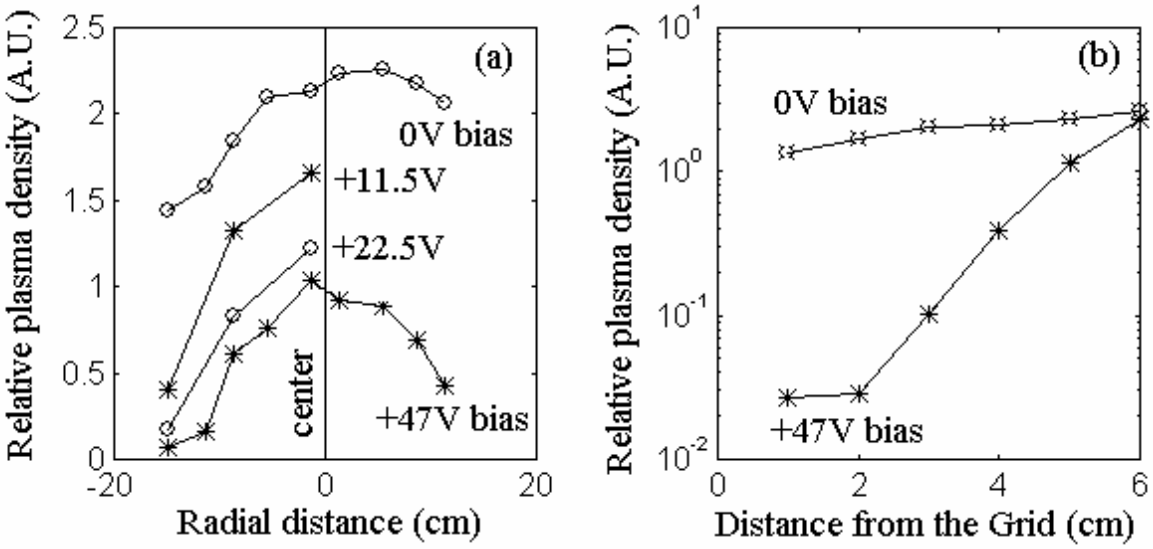

Fig. 6.4 (a) The depletion profile of the electron density in front of the grid due to the plasma grid bias. (b) The extent of the bias effect from the grid, observed inside the plasma along the source axis in terms of the plasma density depletion.

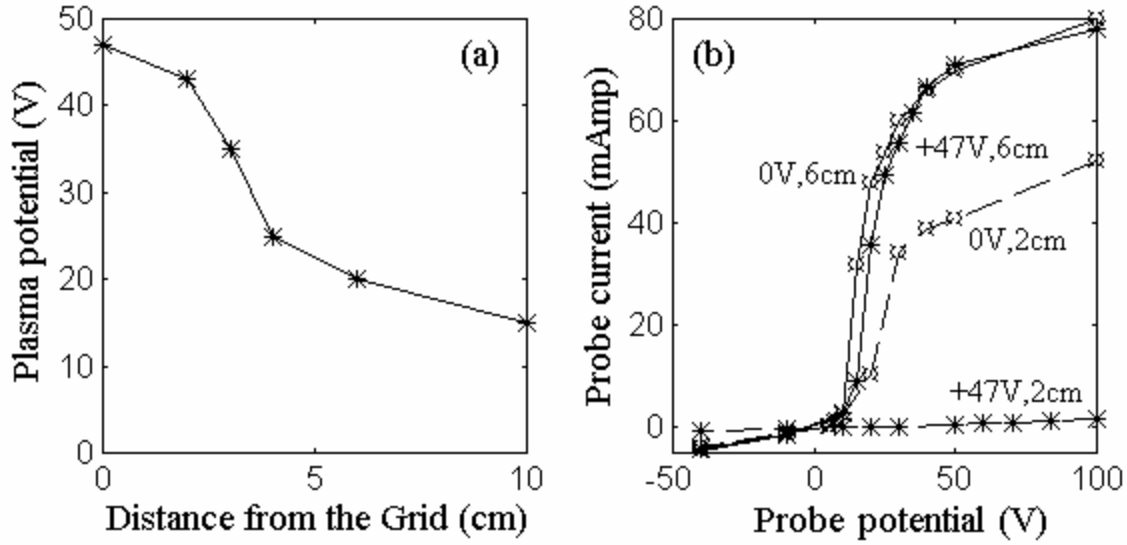

Fig. 6.5 (a) The double layer formation near the plasma grid due to the positive grid bias potential. (b) The Langmuir probe characteristics of the plasma at different positions and for different grid bias conditions.

6.4 Conclusions

Positively biased plasma grid reduces the electron density in the vicinity of the plasma grid and decreases the co-extracted electron current. To compensate the loss of electrons near the grid, the density of H^- ions may increase locally to make the plasma neutral. The double layer formation may improve the surface produced H^- ions extraction probability because towards the plasma grid, the negative ions are not confined by the plasma sheath; rather they are attracted by the positive grid potential. The effect of the positively biased grid is equivalent to the positive extraction voltage (~kV) applied to the extraction grid (2^{nd} grid, after the plasma grid, see chapter-3), which can penetrate into the plasma through the plasma grid hole.

References

[1] M.Bacal et.al. Rev.Sci.Instrum.**59**, 2152, (1988).

[2] O. Vollmer, B. Heineman, W. Kraus, P. McNeely, R. Riedl, E. Speth, R. Trainham, R. Wilhelm, Fus. Eng. Des., **56-57**, 465, (2001).

[3] C. Charles, Appl. Phys. Lett., **84**, 332, (2004).

[4] B. S. Lee and M. Seidl, Appl. Phys. Lett., **61**, 2857, (1992).

Chapter 7

Ion source diagnostics by modulation technique

Summary: The conventional negative ion density measurement is based on the measurement of the extra electrons, which are created from the negative ions after the photo-detachment. The density of the extra electrons, which is measured by a Langmuir probe, is equal to the density of the negative ions. In high power rf source, any diagnostic based on absolute measurement of electron densities is difficult due to the presence rf fluctuations. Relative measurements of densities at different phases during a modulation cycle have better signal-to-nose ratio. Based on this idea a new diagnostic method is introduced and some preliminary results are presented in this chapter. The modulation of the bias voltage of the plasma grid would modulate the plasma density near the grid and therefore it would modulate the negative ion density also. If a laser beam is passed through the modulated region, the light intensity of the laser beam would also be modulated due to the photo-detachment absorption by the H^- ions because H^- ion density is modulated there. The modulation of the laser beam is detected by a fast photo diode whose signal is fed into a Lock-in-amplifier. The density modulation of negative ions is calibrated with the density modulation of the plasma. The modulation of the plasma density is proportional to the plasma light modulation which is detected by the same photo-diode system.

A new diagnostic method is developed to measure the plasma electron temperature T_e. This T_e measurement technique is based on the same modulation principle and it uses the dispersion relations of the phase velocity or damping of ion-acoustic waves (modulated signal) in the plasma. The T_e measurement by the ion-acoustic detection technique is more useful in the high power rf sources where rf noise is high and the data from a conventional T_e measurement by a Langmuir probe is uncertain. The present measurements are in the range of 1kHz - 40kHz in H_2+Cs and Xe+Cs plasmas. In deriving the formulation it is assumed that negative ion concentration in the volume of the plasma is much less compare to the electron density. The T_e measurements, derived from ion-acoustic wave dispersion relation, are carried out in two different experimental setups and compared with the T_e value derived from the Langmuir probe characteristic.

7.1 Negative ion density measurement

7.1.1 Introduction

The conventional negative ion density measurement is done by the laser photo-detachment method [1]. The energy of the laser photon must be greater than the electron affinity of the extra electron of that negative ion. If a photon of that laser collides with a negative ion, it can detach that extra electron from its orbit. The detached electrons are then collected by a positively biased Langmuir probe which is placed co-axially to the laser beam. If the probe potential is above the plasma potential (electron saturation regime) it is assumed that all the detached electrons near the probe are collected by the probe. These detached electrons are created suddenly in the laser beam path by that laser pulse and therefore there is a sudden increase of probe current which is proportional to the detached electron density is observed. Since the detached electrons are created from the negative ions, the detached

electron density is equal to the negative ion density. In presence of strong rf noise the probe current oscillates which introduces some uncertainties in the absolute measurement of photo-detachment signal. To overcome this problem a new negative ion density measurement is developed. It is a phase sensitive diagnostic method based on the relative density measurement by a modulation signal.

This part of the chapter describes the principle, technique and measurement results (preliminary) of H^- ion density by the modulation technique. The modulation of the plasma and therefore the modulation of the H^- ion density are created by an oscillating electric field (2 – 10 kHz). A cw green ($\lambda \sim 532$ nm) laser (battery operated laser pointer) is passed through the plasma where modulation is taking place. Due to photo-detachment mechanism of the H^- ions [1], the absorption of the laser light is also modulated in the same frequency of the applied electric field. The modulated absorption light signal is then detected by a photo-diode and a Lock-in-amplifier system. The use of a lock-in-amplifier (LIA) makes this phase sensitive measurement technique very powerful and less susceptible to the noise. The principle of LIA operation is depicted in appendix-6, where it also describes, why measurement with LIA is less sensitive to noise. The set of measurements comprehend, (a) the modulation of the plasma (visible) light emission due to the plasma density oscillation. The plasma density oscillation is created by an alternating potential applied on the diagnostic plate. (b) The modulation of the green ($\lambda \sim$ 532 nm) laser pointer light due to the fluctuation of photo-detachment absorption because the negative ion density near the diagnostic flange is also oscillating by the applied alternating potential. Plasma light modulation is used for calibration of density modulation because the plasma density is proportional to the intensity of the plasma light emission.

7.1.2 Principle of the H^- ion diagnostic system

If an oscillation is created in the plasma, it is assumed that the densities of all the individual components of the plasma also oscillate in the same frequency. It is also assumed that the amplitudes of the modulation of the individual densities are proportional to the amplitude of modulation of the main plasma density. The negative ion is a component of the plasma. Therefore under these assumptions one can write,

$$\frac{\Delta n_-}{n_-} = \frac{\Delta n_e}{n_e} \tag{7.1.1}$$

The modulation of the H^- ion population can be determined by measuring the modulation of the laser photo-detachment absorption signal,

$$\Delta n_- = \frac{\Delta \mathrm{I}_{\mathrm{laser}}}{\mathrm{I}_{\mathrm{laser}}} \cdot \frac{1}{\sigma\, l} \tag{7.1.2}$$

where Δn_- is the H- ion density modulation, $\Delta \mathrm{I}_{\mathrm{laser}}$ is the laser light modulation signal due to H^- ion photo-detachment absorption, $\mathrm{I}_{\mathrm{laser}}$ is the background DC laser signal, σ is the laser photo-detachment cross-section of the H^- ions ($3\times10^{-17}\mathrm{cm}^2$ at 532 nm laser light wavelength [2]) and l is the absorption path length of the laser.

In order to obtain the density of negative ions n_-, one needs a calibration of the modulation. The required calibration can be done by measuring the plasma density modulation ($\Delta n_e/n_e$) by a Langmuir probe or by measuring the modulation of the plasma light intensity ($\Delta I_{plasma}/I_{plasma}$). The relation between the plasma density modulation and the plasma emission light intensity modulation is given as,

$$\frac{n_e}{\Delta n_e} = \frac{I_{plasma}}{\Delta I_{plasma}} \text{ if } I_{plasma} \propto n_e \qquad (7.1.3)$$

I_{plasma} is the background plasma light intensity and ΔI_{plasma} is the amplitude of the plasma light modulation signal. Using equations (7.1.1), (7.1.2) and (7.1.3) it is possible to determine the absolute value of the negative ion density.

7.1.3 Experimental setup

The modulation of electric potential was applied between the diagnostic plate (DP) and the source body, which is electrically connected to ground. The picture of DP is shown in fig.7.1.1. The DP is installed in the source through the diagnostic flange. The position of DP is very close and parallel to the plasma grid (PG). During the experiment, PG is also connected to the ground. The frequency range (2 – 10 kHz) is limited by the operability of the impedance matching step-down transformer. The current at the DP is in the range of 0 – 50A with typical working values, 20-30A. The peak-to-peak oscillating voltage applied between the DP and the source body or the mesh, attached to the DP is ~ 50V. A Lock-in-Amplifier (LIA; Signal Recovery, model - 5209) is used in high stability pass band 12dB mode with integration time of 1 - 3 seconds. For details of LIA please see the appendix-6. The duration of plasma pulses are of 3.5–5 seconds at 50 kW RF power. The H_2 pressure is 0.55 Pa in the driver during the pulse. A 12 meter twisted and bipolar copper screened cable is used to connect the amplifier having output impedance ~ 4Ω and the (4Ω -0.5Ω) step-down transformer. The transformer is required in order to match the impedance of the DP ~ 0.5Ω in the plasma with the amplifier output. This arrangement helps to transfer maximum possible power to the DP from the amplifier and therefore it is possible to get maximum possible modulation of the plasma in front of the DP. The schematic diagram of the diagnostic experimental setup is shown in fig.7.1.2.

Noise rejection is a key problem faced by us to detect our small amplitude (~ 10nV) of signal from the photo-detachment absorption. All cables is needed to be appropriately screened and the optical collection at the output of the fiber is necessary to avoid electrical pick-up on the detector (photo-diode), induced by the metal casing of the fiber. Given the excessive acceptance of the fiber, purposely build collimator (black tube) is installed at the fiber entrance to ensure that the plasma light is collected from the same region from where the laser photo-detachment absorption signal is collected. A cw laser having wavelength 532 nm (laser pointer) is used for the photo-detachment purpose. A narrow band interference filter for 532 nm wavelength is used at the output of the fiber during the collection of the laser photo-detachment absorption signal to reject the plasma light falling on the detector.

7.1.4 Results of the H^- ion diagnostic system

The phase relationships between the applied reference signal (from the oscillator) and the detected signals (diode) due to the plasma light modulation and the laser absorption modulation are shown in fig.7.1.3.

The maximum amplitude of the plasma light modulation signals was ~ 55μV (ΔI_{plasma} signal) detected by the LIA. The separately measured background DC signal of the plasma light is 250mV (I_{plasma}).

The actual value of the modulated signal must be increased by ~ 15% due to the limitation of the pulse length compared to the integration time. During the plasma light modulation signal measurement, a relatively large signal at double frequency was also observed.

The modulation amplitude of the laser light was much smaller. The maximum amplitude of the laser light modulation signal was only ~ 70nV (ΔI_{laser} signal). The separately measured background DC signal of the laser light is 3V (I_{laser}).

Using l = 20cm, the DP length in equation (7.1.2), $\Delta n_- = 4\times10^7$ particles cm^{-3} is obtained. and from equation (7.1.3), $n_e/\Delta n_e = 4.5\times10^3$ is obtained. Putting the values of ($n_e/\Delta n_e$) and Δn_- in equation (7.1.1) give the negative ion density is obtained as,

$$n_- = 1.8\times10^{11}\ cm^{-3} \qquad (7.1.4)$$

It is assumed that the production rate of the H^- ions on the DP surface and its nearby region is considerably more than that of the production rate in the plasma volume present outside the DP but in the same laser beam path. The reason behind this assumption is, some amount of Cesium is already present in the source when this experiment is conducted and therefore it is expected that on the DP surface, the possibility of the surface production of H^- ions is very high. In chapter-2, 4 and 5 it is discussed several times that surface production mechanism of negative ions is more efficient than that of the volume production.

Both the signals from the plasma light modulation and that of the laser light are nearly sinusoidal functions with no measurable offset. One expects that those two signals must not have the same phase because of their different mobility. However the observed ~ 90 degree phase difference between the two signals is yet to be understood.

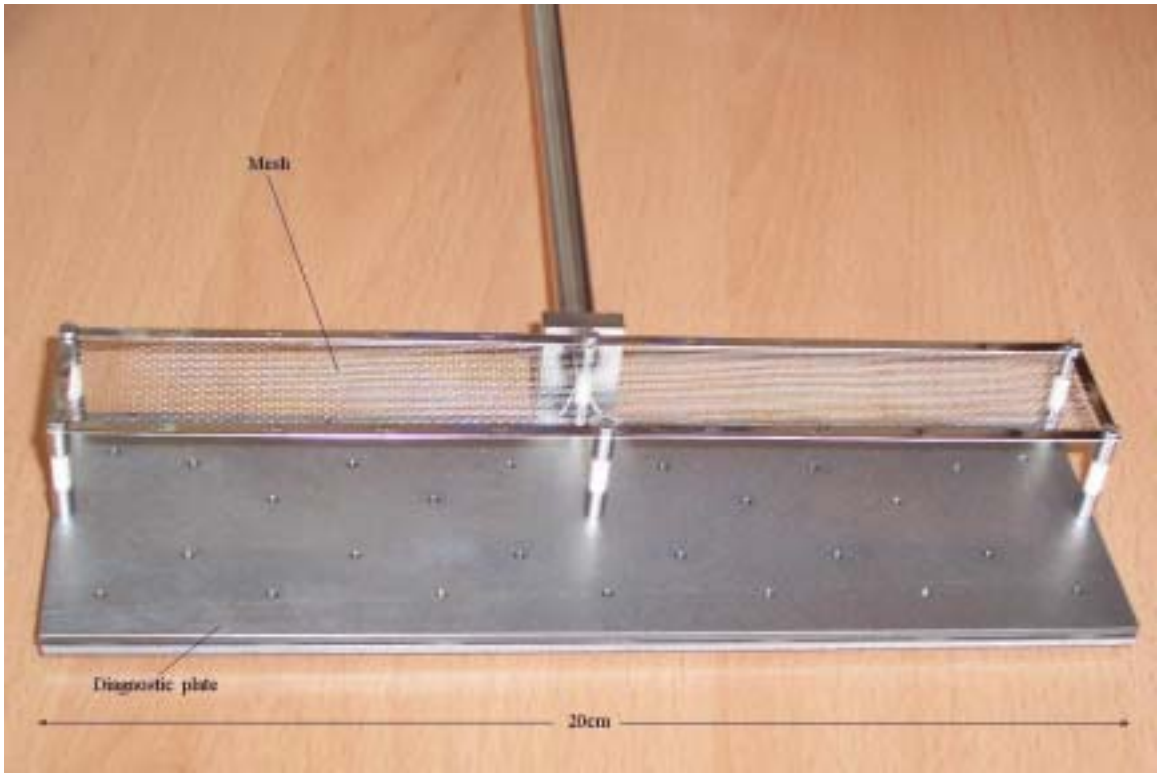

Fig.7.1.1. Photograph of diagnostic plate (DP) made of Molybdenum.

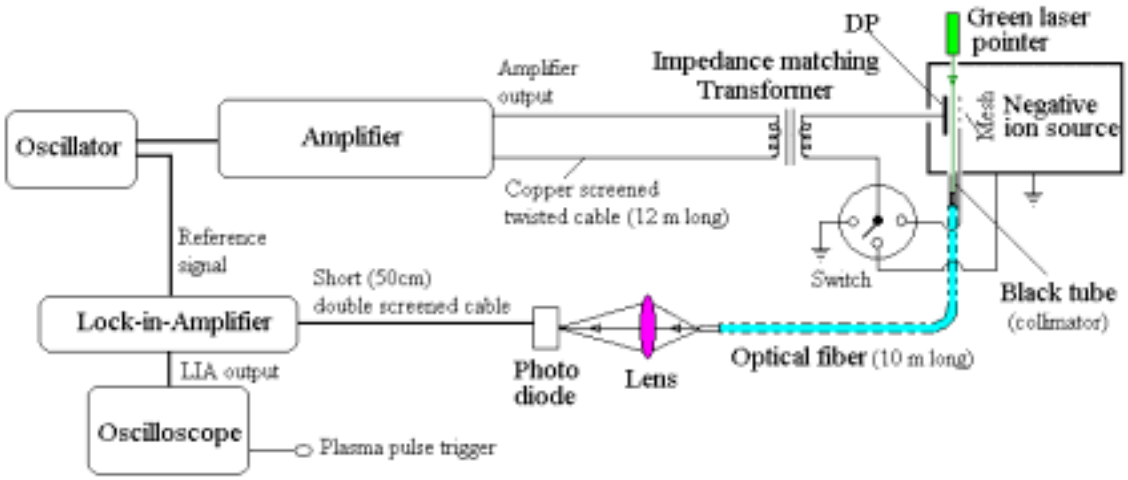

Fig.7.1.2. Schematic diagram of negative ion density measurement by modulation technique experimental setup.

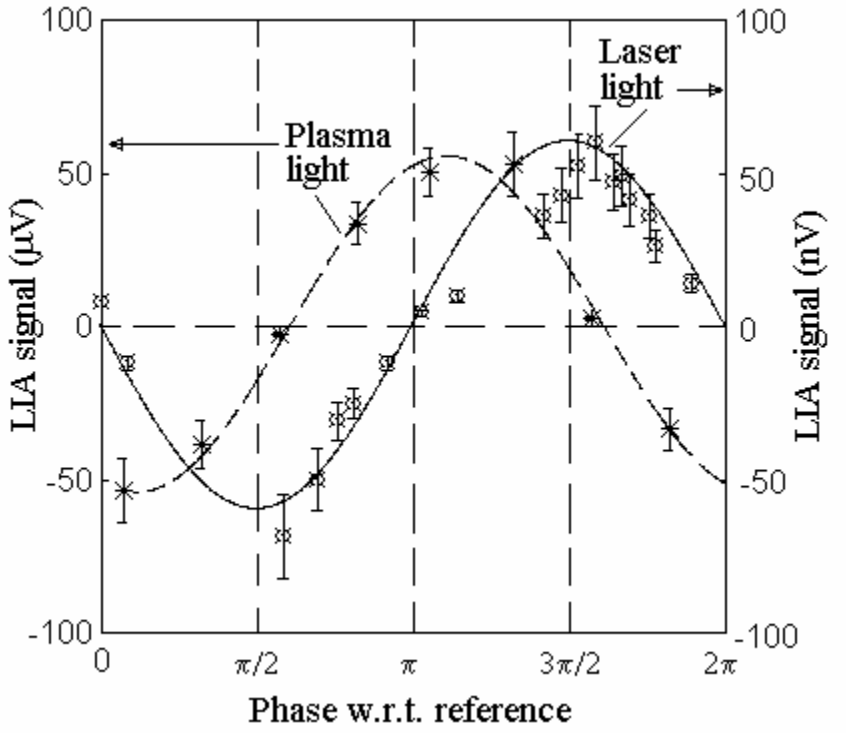

Fig.7.1.3. Phase relation of Plasma light and Laser (λ=532 nm) absorption modulation signal detected by a Lock-in-Amplifier (LIA) with respect to (w.r.t.) the reference signal.

7.1.5 Discussion of the H^- ion diagnostic system

The results presented here are preliminary measurements. Few uncertainties in the absolute density value of H^- ions have to be sorted out which are discussed below. In order to obtain the density of negative ions n_-, one needs a calibration of the modulation. The calibration of the modulation can be carried out by measuring the plasma density modulation with a Langmuir probe or by the plasma light. In the present case, modulation of the plasma light is used for the calibration. The assumptions behind this calibration technique are,

1. Most of the plasma light collected by the fiber is collinear with the laser beam and is from the same region where laser absorption is taken place.
2. The dominant laser light absorption species at 532 nm are the H- ions only.
3. The degree of modulation of the negative ion density is same as that of the plasma density.

The uncertainty of these assumptions may lead to discrepancy in the absolute H^- ion density value. The possible weaknesses of the assumptions are,

1. The plasma light which is collected by the optical fiber may contain considerable amount of photons which are actually originated at different regions of the source. In that case the measurement of the plasma light modulation is underestimated

because the photons which are originated outside of the modulated region do not carry the modulation information. The underestimated calibration factor may lead to an overestimated negative ion density. To avoid the collection of plasma light from the outside region and to collect the plasma light from a small region near the DP only, a black tube of inner diameter 0.5cm and length 5cm is attached with the optical fiber at its light entrance end. This tube reduces the acceptance angle of the optical fiber.

2. The plasma may contains other particles which may also absorb the green laser light (λ=532nm). For example O^- ions and H_2^+ ions also absorb light having wavelength of 532nm. The cross-sections of such absorptions at 532nm wavelength are, $6.4\times10^{-18}cm^2$ for O^- ions and 9.0×10^{-19} cm^2 for H_2^+ ions [2], whereas for H^- ions it is 3.0×10^{-17} cm^2. In this experiment it is expected that the concentration of O^- ions is negligible but the concentration of H_2^+ ions is unknown. This result has to be verified with other wavelengths to ensure that the modulation of laser light absorption is done by only due to photo detachment of H^- ions and not by other particles. In this regard Xe arc lamp having broadband spectra with different optical wavelength selection filters is under installation.

A better way to calibrate the plasma modulation is with a Langmuir probe installed in that region where the modulation of the plasma is occurring. The calibration with a Langmuir probe would minimize those uncertainties discussed above.

The advantages of this diagnostic method are,

1. Experimental setup is very simple, less expensive and insensitive to noise.
2. Due to the application of LIA, it is possible to detect very small signal level also (~10 nV range) in the presence of large noise (~μV).
3. Expensive and powerful laser is not required.
4. Can be applicable to detect and quantify the individual components in plasma or in a gas mixture, if the proper wavelength is known which is absorbed by that component.

7.2 Electron temperature measurement

7.2.1 Introduction

Ion-acoustic wave propagation in low temperature plasmas has been widely investigated in strongly electronegative plasmas [3,4,5]. The ion-acoustic wave has two modes of propagation in negative ion enriched plasmas. The phase velocity of "fast" mode increases and damping decreases with increasing negative ion concentration [3,4]. The "slow" mode is highly damped. Measurement in the range of 1kHz-40kHz in Hydrogen and Xenon plasmas show that slow wave propagates according to the dispersion relation.

In the case of Hydrogen (H_2) the presence of Cs affects considerably the excited waves in the plasma. Using a Mach probe [6,7] detection technique, it has been possible to measure the relevant parameters of the plasma, which are related to wave propagation both in terms of damping as well by measuring phase shift [8].

In case of Xe gas instead of the mixture of H_2 and Cs in the same situation, given that the ion mass approximate the Cs ion mass, the plasma behaved as a single-species plasma and correspondingly the dispersion relation is reduced to a single species. The solution of the dispersion relation gives an independent determination of the electron temperature T_e [9].

The H_2+Cs mixture can be treated in first approximation as two-species plasma. The low frequency part of the spectrum shows dependence of the phase velocity to the relative ion concentration of the two species. From the phase velocity, an estimate of the relative ionic concentration can be obtained [10].

7.2.2 Experimental setup

The present experiment for the ion acoustic study is carried out in two setups in the BATMAN 6-1 type ion source [11], and shown in fig.7.2.1. Ion-acoustic wave (in the range of 1-40 kHz) have been excited using the plasma grid (CEA grid) of diameter ~ 20cm in setup-I with a combination of function generator and a power amplifier of maximum power 80 Watt. To receive the signal due to propagated wave in the plasma at different positions, a Mach probe is used [12] in setup-I. It is also used to measure the plasma flow velocity. During the experiment with setup-I the Mach probe has been mostly operated as double probe for measuring the plasma density to increase the signal/noise ration. We have also operated it, as single probe for the same run of measurements, but the RF and peak up noise was much larger. All the measurements were made at input voltages of 25-Volt *rms.* to the exciter (output of the amplifier). The 5Ω resistor in setup-I limits the current through the exciter. The value of the grid current in setup-I is independently measured through inductive way and found to be independent of frequency and proportional to the applied voltage. Wave response measurements are carried out using an oscilloscope and a spectrum analyzer. By moving the probe away from the exciter, both the phase delay and the wave attenuation are measured.

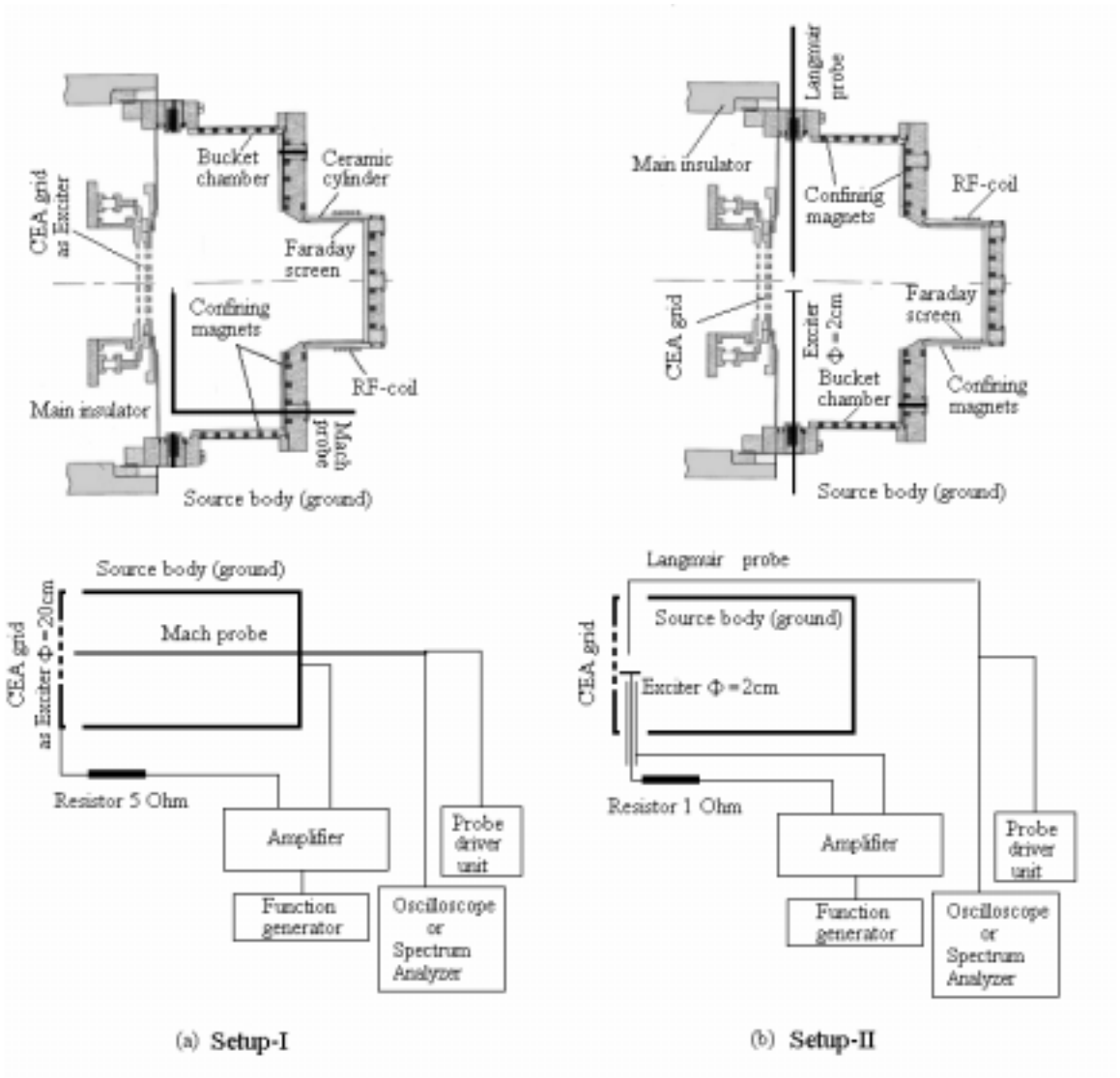

Fig.7.2.1. Schematic diagram of setup-I and setup-II with corresponding electrical circuit for ion-acoustic T_e measurement.

In setup-II, ion-acoustic wave have been launched using a circular disc of diameter ~ 2 cm, made of Molybdenum mesh. The function generator and the amplifier are the same as setup-I. An uncompensated Langmuir probe is used to detect the wave signal in the plasma. The exciter device in setup-II is floating with respect to the ion source body.

Plasma conditions are made to be the same: pressure 0.6 Pa and the RF coupled power ~ 50 kW in both the setup.

7.2.3 Principle and formulation of the electron temperature measurement system

The ion-acoustic velocity in plasma is proportional to the square root of the electron temperature T_e and can be expressed as $A \propto \sqrt{\frac{k_B T_e}{m_+}}$. Here m_+ is the mass of the ion and k_B is the Boltzmann constant. If the ion-acoustic velocity is measured inside the plasma, it is possible to derive the electron temperature from that measurement. In the present study, the formulations of T_e measurement for two different plasma cases are derived.

Case 1: Plasma with two or more ion species

For plasma having two or more ion species, the general dispersion relation can be written as [8],

$$1 = \sum_j \frac{\omega^2_{Pj}}{\left[(\omega - kv_j)^2 - k^2 v^2_{th\,j}\right]} \tag{7.2.1}$$

The summation is over all charged particles i.e. electrons and different ions. ω_{Pj}, v_j, and $v_{th\,j}$ are the plasma frequency, the drift velocity and the thermal velocity of the jth charged particle respectively. $k = 2\pi/\lambda$ is the wave number and λ is the wavelength of the excited wave. If we consider plasma has no drift or flow velocity, the equation (7.2.1) can be written as,

$$1 = \sum_j \frac{\omega^2_{Pj}}{\left[\omega^2 - k^2 v^2_{th\,j}\right]} \tag{7.2.2}$$

The thermal velocity of the electron is much larger than the phase velocity $V_{Ph} = \frac{\omega}{k}$. For two component ion species (H^+ and Cs^+), the equation (7.2.2) can be written as,

$$1 + \frac{\omega^2_{Pe}}{v^2_{th_e} k^2} = \frac{\omega^2_{P1}}{\left(\omega^2 - v^2_{th_1} k^2\right)} + \frac{\omega^2_{P2}}{\left(\omega^2 - v^2_{th_2} k^2\right)} \tag{7.2.3}$$

"1" stands for H^+ ion and "2" stands for Cs^+ ion. Due to heavy mass of Cs^+ ion, $v_{th\,2}$ is very small compare to the phase velocity and H^+ ion thermal velocity $v_{th\,1}$. After simplification, the equation (7.2.3) become,

$$1+\frac{k^2{}_D}{k^2}=\frac{\frac{\omega^2{}_{P1}}{k^2}}{\left(\frac{\omega^2}{k^2}-v^2{}_{th_1}\right)}+\frac{\frac{\omega^2{}_{P2}}{k^2}}{\left(\frac{\omega^2}{k^2}\right)} \tag{7.2.4}$$

where $k_D=\frac{\omega^2{}_{Pe}}{v^2{}_{th_e}}=\frac{2\pi}{\lambda_D}$, where λ_D is the *Debye length*.

During experiment, the wavelength of the excited wave is ~ 10 cm which is much longer than that of $\lambda_D \sim 10^{-3}$ cm. So the equation (7.2.4) becomes,

$$\frac{k^2{}_D}{k^2}=\frac{\frac{\omega^2{}_{P1}}{k^2}}{\left(V^2{}_{Ph}-v^2{}_{th_1}\right)}+\frac{\frac{\omega^2{}_{P2}}{k^2}}{V^2{}_{Ph}} \tag{7.2.5}$$

$$1=\frac{A^2{}_1}{\left(V^2{}_{Ph}-v^2{}_{th_1}\right)}+\frac{A^2{}_2}{V^2{}_{Ph}} \tag{7.2.6}$$

where $A_1=\frac{\omega_{P1}}{k_D}$ and $A_2=\frac{\omega_{P2}}{k_D}$ are the ion-acoustic velocity of H^+ and Cs^+ ion respectively.

The equation (7.2.6) has four solutions for the phase velocity V_{Ph}. The only positive and real solution is,

$$V_{Ph}=\sqrt{A^2{}_1+A^2{}_2+v^2{}_{th_1}} \tag{7.2.7}$$

Ion-acoustic velocity for two different ion species are denoted by A_1 and A_2, where $A_j=\sqrt{\frac{n_j}{n_e}\frac{kT_e}{m_j}}$. If we consider the plasma flow having flow velocity V_0 too, the solution become,

$$V_{Ph}=\sqrt{A^2{}_1+A^2{}_2+v^2{}_{th_1}+V^2{}_0} \tag{7.2.8}$$

Note that in the referred paper [10] last two terms (thermal and plasma flow [12]) were not included. The present solution is more general. To find the ionic fraction inside multi-species plasma, equation (7.2.7) or (7.2.8) can be used.

Case 2: Plasma with only one ion species

In the case of a single ion species plasma, from these data and using the following equations, the ion acoustic velocity and the wavelength of the excited wave in the plasma can be calculated [8].

$$V_{Ph} = \frac{\omega}{\kappa} = \left(1.45 \pm \frac{V_0}{A} + \frac{0.36}{1.45 \pm \frac{V_0}{A}} \right) A \qquad (7.2.9)$$

where A is the ion-acoustic speed, $\frac{V_0}{A}$ is the *Mach* number of the flow. The +ve sign corresponds to the case when probe is in the upstream direction and –ve sign corresponds to the downstream case. To find T_e in terms of ion-acoustic velocity, two methods of detection technique can be used: (a) The attenuation length δ measurement and (b) time delay Δt of a particular phase of the excited wave measurement.

(a) The attenuation length δ of the excited ion-acoustic wave in the plasma can be written as [8],

$$\frac{\delta}{\lambda} = \left(0.39 \pm 0.27 \frac{V_0}{A} \right) \qquad (7.2.10)$$

In equation (7.2.10), the attenuation length δ is defined as the distance from the exciter where the signal strength decreases by *e*-times of the input signal. The wavelength of the wave is denoted by λ. In equation (7.2.10), the +ve sign corresponds to the downstream and –ve sign corresponds to the upstream case. Here δ and *Mach* number (V_0/A) are measured quantities, which can give the value of A, using equations (7.2.10) and (7.2.9).

(b) The time delay Δt of a particular phase of the excited wave, measured between the exciter and the probe gives the phase velocity of that wave, V_{ph}=Δx/Δt. The distance between the probe and the exciter is denoted as Δx. Ion-acoustic velocity A can be derived by using equation (7.2.9).

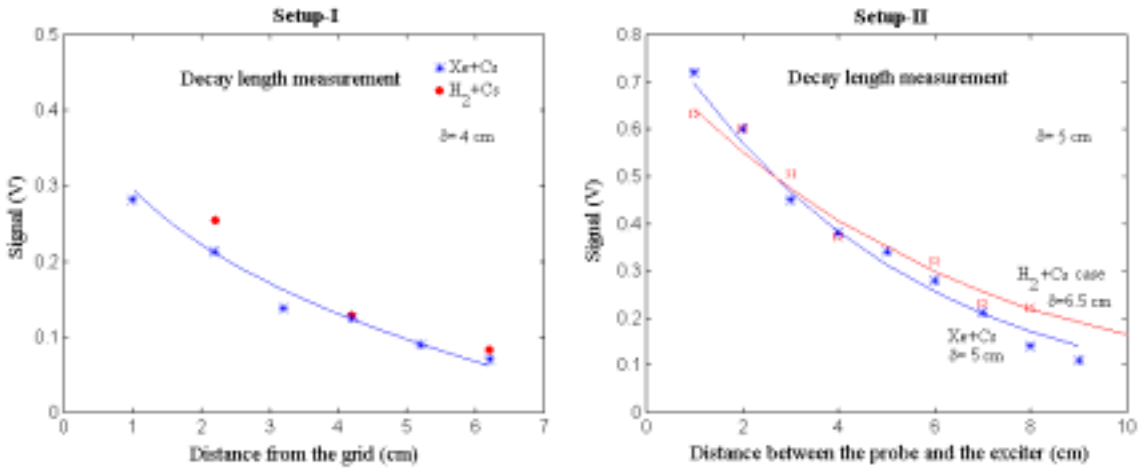

Fig.7.2.2. Attenuation of wave in the plasma

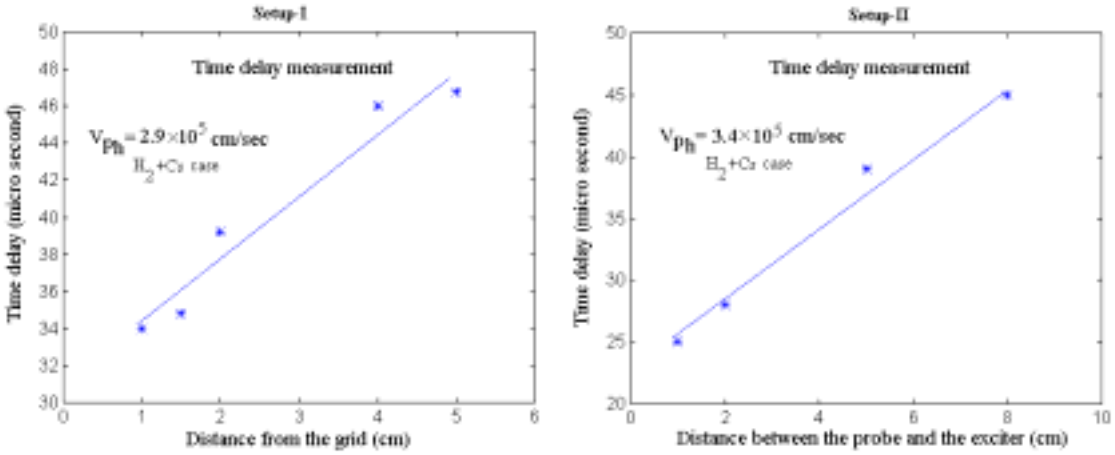

Fig.7.2.3. Time delay with distance between the exciter and the probe for H_2 + Cs plasma in setup-I.

7.2.4 Results and discussion

The fig.7.2.2 shows, the decay length measurements in setup-I and setup-II in H_2 + Cs and Xe+Cs plasma respectively. In the case of Xe+Cs, the plasma is as if it is single component as already mentioned, because Xe^+ and Cs^+ ions have almost the same mass (131.3 and 132.9 amu respectively). The ion-acoustic speed can be calculated from equations (7.2.10) and (7.2.9), neglecting the possible contribution of Cs^{++} ions.

The ion-acoustic velocity can also be written in terms of electron temperature T_e for the present experimental case as,

$$A = \sqrt{\frac{k_B T_e}{m_+}} \tag{7.2.11}$$

In case of Xe+Cs gas mixture, the results including T_e from the experiments performed in setup-I and setup-II and the comparison of T_e value with Langmuir probe are given in table -7.1.

Table-7.1 Comparison of T_e value measured by ion-acoustic wave detection technique and Langmuir probe method

Quantity	**Setup-I**	**Setup-II**	**Langmuir probe** (uncompensated)
Decay length (δ)	4 cm	5 cm	
Mach number $\left(\frac{V_0}{A}\right)$	0.37	0.05	
Phase velocity (V_{Ph}) Acoustic velocity (A)	2.5×10^5 cm/s 1.4×10^5 cm/s	2.3×10^5 cm/s 1.3×10^5 cm/s	
Electron temperature T_e	2.5 eV±10%	2.2 eV±10%	3 eV±50%

Based on the results obtained so far, it is planned to extend the frequency range to higher value and in particular to the accessibility of the "fast" branch of the dispersion relation [3,4]. Due to the specificity of our experimental apparatus, it will be possible to modulate the ratio between negative H^- ion density and positive H^+ ion density by positive grid biasing, hence exploring the "fast" branch in a situation of mass equality.

7.3 Conclusions of two different diagnostic systems

This chapter presents a modulation technique (in ion-acoustic wave range) to measure the negative ion density and electron temperature in an inductively coupled RF source. This novel modulation technique method is used for the first time in negative ion density measurement and has to be verified with different wavelengths of the photon and with a separate standard technique (conventional laser photo-detachment). This diagnostic method can be applicable to detect and quantify the individual components in a plasma or in a gas mixture, if the proper wavelength is known which is absorbed by that component. The diagnostic setup for measurement of density of the H^- ions, based on modulation technique is simple and less expensive than that of conventional laser photo-detachment system because it does not need high power laser.

In the case of electron temperature measurement, this technique gives an alternative method of T_e measurement in plasma having single species ion. The standard Langmuir probe method needs noise rejection techniques in RF environment which normally are complex and even uncertain. In the case of plasma, having two ion species, the dispersion relation analysis leads to the determination of the ratio of the two ion species.

References

[1] M.Bacal, Rev. Sci. Instrum.,**71**, 3981, (2002).

[2] C. F. Barnett, et.al., "Atomic data for controlled fusion research", ORNL-5206, vol.**1**, (1977).

[3] N.D'angelo, S.V.Goeler, T.Ohe, Phys.Fluids, **9**, 1605, (1966).

[4] Y.Nakamura, T.Odagiri, I.Tsukabayashi, Plasma Phys. Control. Fusion, **39**, 105, (1997).

[5] A.Y.Wong, D.L.Mamas, D.Arnush, Phys.Fluids ,**18**, 1489, (1975).

[6] P.C.Stangby, Phys.Fluids, **27**, 2699 (1984).

[7] I.H.Hutchinson, Phys.Fluids, **30**, 3777, (1988).

[8] A.Y.Wong, R.W.Motley, N.D'angelo, Phys.Rev., **133**, A436, (1964).

[9] M.Shindo, S.Uchino, R.Ichiki, S.Yoshimura, Y. Kawai, Rev.Sci.Instrum., **72**, 2288, (2001).

[10] A.M.Hala, N.Hershkowitz, Rev.Sci.Instrum., **72**, 2279, (2001).

[11] O.Vollmer, B.Heinemann,W.Kraus, P.McNeely, R.Riedl, E.Speth, R.Trainham and R.Wilhelm, Fus.Eng. Des, **56-57**, 465 (2001).

[12] A.Tanga, M.Bandyopadhyay, P.McNeely, Appl. Phys.Lett. **84**, 182, (2004).

Chapter 8

Conclusions and Outlook

8.1 Main results

The main objective of the present work is to understand and optimize an inductively coupled H^-/D^- ion source which is being developed for ITER NBI system. The performance of BATMAN ion source is measured in terms of negative ion current density falling on to the calorimeter. The value of the current density improves from 2 mA/cm^2 (when Cs is not used) to 25mA/cm^2 (maximum obtained so far with Cs and with proper optimization). The current density depends upon various parameters like, the source pressure, the RF power, the extraction and acceleration voltage combination (perveance), the magnetic filter, the plasma confining field, the source depth, the cesium coverage on the plasma grid and its work function, the quantity of cesium present in the plasma, the grid temperature etc. Many of these parameters are interlinked to each other. For a given time frame and for a given effort, it is difficult to optimize all these parameters. Therefore the source modeling and simulation is required and its results can give a direction for optimization. There is no complete theory present, which can describe all the features of a negative ion source. Therefore different experiments are also required to find out the characteristics of the source. The present work produces a considerable amount of information to understand the source and these information are used to improve the source performance.

One of the 3-D Monte-Carlo simulations and the 0-D particle balance modeling of the negative ion source are carried out on the basis of volume production mechanism. Another 3-D Monte-Carlo simulation code calculates the transport of the surface produced H^- ions through the plasma grid. The obtained results from these studies are,

1. The results of the computer simulation clearly show that the pure volume production for H^- ions is not sufficient to reach the ITER target (28 mA/cm^2 H^- ion current, which roughly corresponds to ~10^{12} cm^{-3} H^- ion density in front of the plasma grid.

2. In pure H^- ion volume source, the H^- ion density, (n_-) near the grid system depends strongly on the local density of the vibrationally excited H_2 molecules, (n_v). The H^- ion density also depends on the local electron density, (n_e) until n_e becomes equal to the local n_v values. Near the grid n_- depends on the local electron temperature T_e but the dependency is not very significant. It is understood that magnetic filter is used mainly to reduce the electron flow towards the grid and therefore to reduce the co-extracted electron currents rather than to reduce T_e.

3. It is clearly visible from the n_v profile that the n_v distribution is a non-Boltzmann distribution due to E-V reaction. The vibrational molecular densities for upper vibrational quantum numbers are depleted as we move away from the *driver* mainly due to the wall-relaxation and DA reactions.

4. The volume produced n_- profile is nearly uniform (~ 10^{10} cm^{-3}) through out the source volume, but only those H^- ions, which are generated within 1-2 cm from the grid surface have a finite probability to reach grid holes. So surface produced H^- ions are expected to be extracted effectively.

5. The simulation and the simple 0D particle balance model give almost similar results. The discrepancies in absolute terms are due to the basic nature of the two approaches. Particle balance model is valid only in the local conditions, where as simulation takes into account the non-local phenomena by considering the transport. The transport depends upon the source geometry, plasma parameters profile, magnetic field topology etc.

6. In the case studying the transport of the H^- ions produced on the surface of the plasma grid (PG), ~ 35% of those surface produced H^- ions can be extracted through the PG holes. The initial direction of surface produced negative ions are towards the main plasma, which is in the opposite (wrong) direction with respect to (w.r.t.) the grid hole direction. The strong magnetic field due to the electron suppression magnets which are situated inside the extraction grid (EG) helps to change of direction of those negative ions. The direction change collisions, like elastic or charge-exchange collisions have less influence compare to that of the magnetic field.

7. If the extraction voltage ϕ_{EG} is increased, the fraction of extracted negative ions would increase following Child's law ($\propto \phi_{EG}^{3/2}$- space charge limited). When the supply of negative ions for the extraction is limited by the negative ion production rate, the fraction of extracted negative ions would never increase and become saturate.

8. Negative ions are confined inside the plasma volume due to the positive plasma potential (due to the plasma sheath). The life time of H^- ions is ~ 50μs due to mainly MN and ED collisions.

9. The intensity of the magnetic field is ~220 gauss near the plasma grid. The H^- ions try to gyrate around the magnetic lines of force near the plasma grid and follow a curved path. Due to this curved path, the effective collisional mean free path (in the laboratory frame) of an H^- ion is shortened considerably.

The plasma flow is an important aspect to design an ion source. This is the first time; the plasma flow is identified and measured in an ion source, which is developed for the fusion application. The results of the plasma flow measurements in BATMAN ion source are,

1. The observed plasma flow is a convective flow from the *driver* towards the *grid*.

2. The plasma flow is an important characteristic of an ion source where there is a large gradient of plasma potential exists due to the ambipolar diffusion. It has been shown that the plasma flow velocity can approach Mach number of 1 and it is strongly dependent on the transverse magnetic fields.

3. At steady state condition, the force on the plasma created by the ambipolar electric field is balanced by the frictional forces. In the case of ions, collisions with neutrals represent the dominant drag force term. The $u_z \times B$ force, due to the transverse filter field does not contribute because its direction is orthogonal to the axis. The effect of electron motion on the ions comes through the ambipolar electric field which is measured in this case and so included in the present analysis.

4. The electron dynamics can be changed by the presence of confining magnets. The presence of confining magnets does not allow the flow of hall current (in the x-direction) which makes a 20% correction term on the axial ion flow velocity with respect to the case when there are no confining magnets sitting on the source wall.

5. The collisions between the plasma ions and the background gas molecules create a pressure gradient along the flow direction. This pressure gradient along the axis is proportional to the radio frequency (RF) power and the filling gas pressure.

6. The plasma flow can change the sheath structure (make sheath thin) because ions can enter the pre-sheath with additional kinetic energy due to the flow.

7. The plasma flow could improve the negative ion production rate on the plasma grid surface.

It is observed that with proper positive biasing of the plasma grid (PG), the negative ion current density increases. The important results, obtained from the PG bias experiment are,

1. Positive plasma grid bias reduces the electron density in the vicinity of the plasma grid and decreases the co-extracted electron current. Due to the reduction of electrons near the grid, the density of H^- ions may increase near the grid to compensate the electron loss and therefore the negative ion current would increase as well.

2. A double layer forms near the PG due to the positive PG bias. This double layer may improve extraction probability of the surface produced H^- ions, because the negative ions which are generated inside the double layer are not confined by the plasma potential towards the PG side. Therefore those ions can be attracted towards the PG because of more positive potential.

The modulation technique is a phase sensitive diagnostic method. It is well known that the phase sensitive diagnostic method is always superior to other diagnostic techniques to detect a very low level signal in a very noisy environment. This is a new method used for negative ion density measurement, though few more experiments are needed to establish it

as a standard negative ion density measurement diagnostic. The preliminary results obtained from the ion source diagnostics by modulation technique are,

1. With the help of a Lock-in-amplifier modulation technique we can measure ~ 10nV signal level in the presence of ~ μV noise levels.

2. The H^- ion density is obtained as 1.8×10^{11} cm^{-3} in the negative ion source.

3. The electron temperature near the grid is ~ 2 eV.

8.2 Conclusions

In the case of high energy (> 100keV) neutral beam injection (NBI) system for fusion reactor like ITER, negative hydrogen ion (H^-/D^-) source based NBI system is desirable because of the higher neutralization efficiency (~ 60%) of the negative ions compare to positive ions (< 10%). But the production of H^-/D^- ions is difficult compare to that of positive ions. The H^-/D^- ions production can be done in many types of sources. Out of those, the filament based arc source and the RF source are the two suitable candidates for NBI systems. The filament based arc source has an inherent limitation due to its filament life time (few 100 hours) and needs regular maintenance. Therefore filament source is not useful for ITER type fusion reactor. The RF source has an advantage of having less maintenance requirement because it does not have any filament and it is simple to design and fabricate. The present work is done on a RF negative ion source, which is under a development project for ITER. The present thesis work is a study to understand the characteristics of BATMAN ion source 6-1 type with the help of simulations, modeling and experiments and helps to optimize the source.

The results of the computer simulation based on volume process clearly show that pure volume production for H^- ions are not sufficient to reach ITER target (28 mA/cm^2 H^- ion current, which roughly corresponds to ~10^{12} cm^{-3} H^- ion density in front of the plasma grid). It is observed from the 3-D Monte-Carlo simulation and a 0-D particle balance analytical model that the volume produced H^- ion density profile inside the source is nearly uniform although the electron density and temperature is not uniform. The H^- ions which are produced within few centimeters (~ 1-2 cm) from the plasma grid can reach the grid holes for the extraction. Therefore only those ions can be extracted effectively, which are generated very close to the grid surface. This indicates that surface produced H^- ions can be extracted more effectively. The amount of H^- ions can be produced by surface process depends upon the flux of energetic H atoms and positive ions, but their initial directions after their birth are towards the plasma and not towards the plasma grid holes. The strong magnetic field (~220 gauss) from the extraction grid magnets changes the direction of motion of those H^- ions, produced on the plasma grid surface. It is observed that a substantial fraction (~ 35%) of the surface produced H^- ions can reach the plasma grid hole for the extraction. This code and the model can be used as a predictive code to design a negative ion source with different geometries, magnetic field etc.

The presence of a strong plasma flow is an important observation in this thesis work. The plasma flow can influence the plasma dynamics and the transport of the molecules, atoms, ions and impurities. It also influences the production yield of the negative ions near the plasma grid. This physics was totally overlooked so far, particularly in those ion sources made for fusion application. The plasma flow is a characteristic of a bigger size ion source where there is a large gradient of plasma potential exists due to the ambipolar diffusion. It has been shown that the plasma flow velocity can approach Mach number of 1 and it is strongly dependent on the transverse magnetic fields. The measurements done in BATMAN ion source using a Mach probe along the axis comprehend the plasma density, plasma potential, electron temperature and the barometrically measured background gas pressure. This consistent set of experimental observations has been used to solve the one-dimensional force balance equation in its differential form. The collisions due to the charge exchange and with the neutrals have been considered as frictional terms. At steady state condition the force on the plasma created by the ambipolar electric field is balanced by the frictional forces. In the case of ions, collisions with neutrals represent the dominant drag force term. The effect of electron motion on the ions comes through the ambipolar electric field which is measured in this case and so included in the present analysis. The electron dynamics can be changed by the presence of confining magnets. The collisions between the plasma ions and the background gas molecules create a pressure gradient along the flow direction. This pressure gradient along the axis is proportional to the radio frequency (RF) power and the filling gas pressure. The one dimensional plasma dynamic analysis supports the consistency of the experimental observations. Presence of transverse magnetic filter reduces the plasma flow velocity, which could effect the negative ion production on the cesiated (covered with Cesium) grid surface, given that the surface production of negative ions also depends on the flux of the positive ions and energetic atoms impinging the surface. It is expected to improve the negative ion extraction up to a factor two due to the change in ion flux from isotropic nature to a directional one and an additional term in Bohm flux equation, because ions can enter the sheath with higher kinetic energy (kinetic energy due to plasma sheath potential and that of due to the plasma flow). The presence of plasma flow could also play an important role by influencing the extraction current by modifying the sheath structure (make sheath thinner) near the extraction grid. The flow will modify the effective distance from which the negative ions are able to reach the grid, before getting destroyed. Since transverse magnetic filter field reduces the plasma flow towards the extraction grid, it is therefore obvious that the optimization of the ion flux by changing the filter field strength could be an important parameter in the development of efficient negative ion sources.

Positive plasma grid bias reduces the electron density in the vicinity of the plasma grid and decreases the co-extracted electron current. Due to the reduction of electrons near the grid, the density of H^- ions may increase locally to make the plasma neutral there and correspondingly the negative ion current would increase. Positive grid bias produces a double layer near the plasma grid which is an important observation in this experiment. The double layer formation improves the surface produced H^- ions extraction probability. The positive grid bias effect is equivalent to the extraction field due to the positive extraction grid potential (~kV), penetrating into the plasma through the plasma grid hole.

The modulation technique is a phase sensitive diagnostic method. With the help of a Lock-in technique it can detect ~ 10 nV signal in the presence of ~ μV noise level. Its application

to negative ion density measurement is a new one. In the case electron temperature measurement for single ion species plasma, ion-acoustic wave modulation technique gives an alternative method of electron temperature T_e measurement. The standard Langmuir probe method needs noise rejection techniques (compensating circuit) in RF environment which normally are complex and even uncertain due to the presence of higher harmonics of the driving RF field. In the case of two-species plasma the dispersion relation analysis can lead to the determination of the ratio of the ion species.

8.3 Possible future developments

The work made in the framework of this thesis raises new questions which should be investigated for better understanding of the H^- ion production and transport processes and helps to make a computer model and correspondingly a predictive code to design a negative hydrogen ion source. This work ushers several paths in both simulation and experimental directions.

1. The surface production of H^- ions can be included in the code using wall surface interaction model. In the present work, only the transport of surface produced H^-ions towards the plasma grid hole is done without considering how H^- ions are generated on the surface.

2. The transport code of H^- ions along with the electrons inside the extraction and acceleration grid system can be done by solving 3-dimensional equation of motion. 3-D solution is must because of the magnetic field from the electron suppression magnets which are present in the extraction grid (2^{nd} grid). The solution must take into account space charge compensation due to the presence of different types of positive ions like Cs^+, H^+,H_2^+,H_3^+, impurity ions etc.

3. The grid system is an electrostatic lens system, so the individual shape of different grids has considerable effects on the ion trajectories. In the case of negative ions, an additional effect has to be considered. The surface production of H^- ions and corresponding initial direction of motion strongly depends on the shape of the plasma grid hole, on the side which is facing the plasma. The surface produced negative ion transport part of the present work can be extended by incorporating the geometry and shape of the plasma grid hole.

4. The present code can be used in the case of Deuterium by changing the cross-sectional and reaction rate data.

5. After the discovery of the plasma flow inside an ion source, a Monte-Carlo code like the present one (MOCASINIS code) with a combination of fluid code could be useful to design a bigger source (for ITER NBI system) which may have more than one drivers and different geometrical shape.

6. Plasma flow measurement near the plasma grid during the negative ion extraction would be a very interesting experiment. During the extraction how the plasma meniscus near the plasma grid hole looks like is unknown. These experimental results can be helpful to develop an efficient negative ion

extraction and acceleration code. In the present work all the measurements are carried out without extraction of H^- ions due to the hardware limitations.

7. The modulation technique diagnostic has a potential to open up a new branch of ion source diagnostic, particularly where noise is very big compared to the signal level, to be detected. To establish this technique as a standard diagnostic method few more experiments are required. The direct measurement of the cross-sections of the complete H^- ion absorption (photo detachment) spectra can be done. The existing databases are based on indirect method (combination of photo detachment and electrical method).

8. The modulation method diagnostic can also be applicable to quantify the gas composition or the impurity composition in a mixture of gases by selecting the wavelength of a laser which will be absorbed only by that particular gas or impurity whose quantity has to be measured but not absorbed by the remaining gas mixture. The modulation of the density of the gas mixture can be done with a piezo actuator.

Appendix 1

Energy levels of Hydrogen molecules

Hydrogen (H_2) is a diatomic molecule. Its energy levels are categorized into three states. These are (1) electronic state, (2) vibrational state and (3) rotational state. The last two states are as a result of additional vibrational and rotational degrees of freedom of their nuclei. For a diatomic molecule, the electronic states are specified first by the component (in units of $\hbar$) $\Lambda$of the total orbital angular momentum along the inter-nuclear axis, with the symbols Σ, Π, Δ and Φ corresponding to Λ= 0, ±1, ±2 and ±3 in analogy with the atomic nomenclature. All states except Σ states are doubly degenerate. For the Σ states, + and – superscripts are used to denote whether the wave function is symmetric or anti-symmetric with respect to the reflection at any plane through the inter-nuclear axis. The total electron spin angular momentum S (in units of $\hbar$) is also specified with the multiplicity 2S+1 written as a prefixed superscript, as for the atomic states. For S=0, the state is singlet and for S=1, the state corresponds to the triplet state. Since H_2 molecule is a homo-nuclear molecule the subscripts *g* or *u* are written to denote whether the wave function is symmetric or anti-symmetric with respect to the interchange of the nuclei. The potential energy level curves for H_2 molecules along with its different ionic family members are depicted in fig.A.1. In the fig A.1, a few horizontal line segments are drawn as an example in the ground electronic state $X^1\Sigma_g^+$, to show the vibrational energy levels for a stable electronic states. The length of each segment within an electronic state gives the range of classically allowed vibrational motions. The vibrational motion of a diatomic molecule can be model by a harmonic oscillator which leads to equally spaced quantized non-degenerate energy levels,

$$E_{v''} = \hbar\omega_{vib}\left(v'' + \frac{1}{2}\right) \tag{A.1.1}$$

where v"= 0, 1, 2, 3,….is the vibrational quantum number and ω_{vib} is the linearized vibration frequency, which depends on the spring constant and the reduced mass of the molecule [1]. With more vibrational energy, nonlinearity terms arises in equation A.1.1 and the vibrational motion becomes anharmonic. The level spacing tends to reduce [2]. At v"$\rightarrow\infty$ level spacing is zero, which corresponds to a continuum state, break up a molecule into its constituent atoms. Each vibrational level contains several rotational levels. A molecule can rotate around an axis, perpendicular to the inter-nuclear axis. Different energy levels of this rotational motion are denoted by rotational quantum numbers J. The simplest dumbbell model for the rotation of a diatomic molecule leads to the nonuniform quantized energy levels [1],

$$E_J = \frac{\hbar^2}{2I_{mol}}J(J+1) \tag{A.1.2}$$

where I_{mol} is the moment of inertia of the molecule.

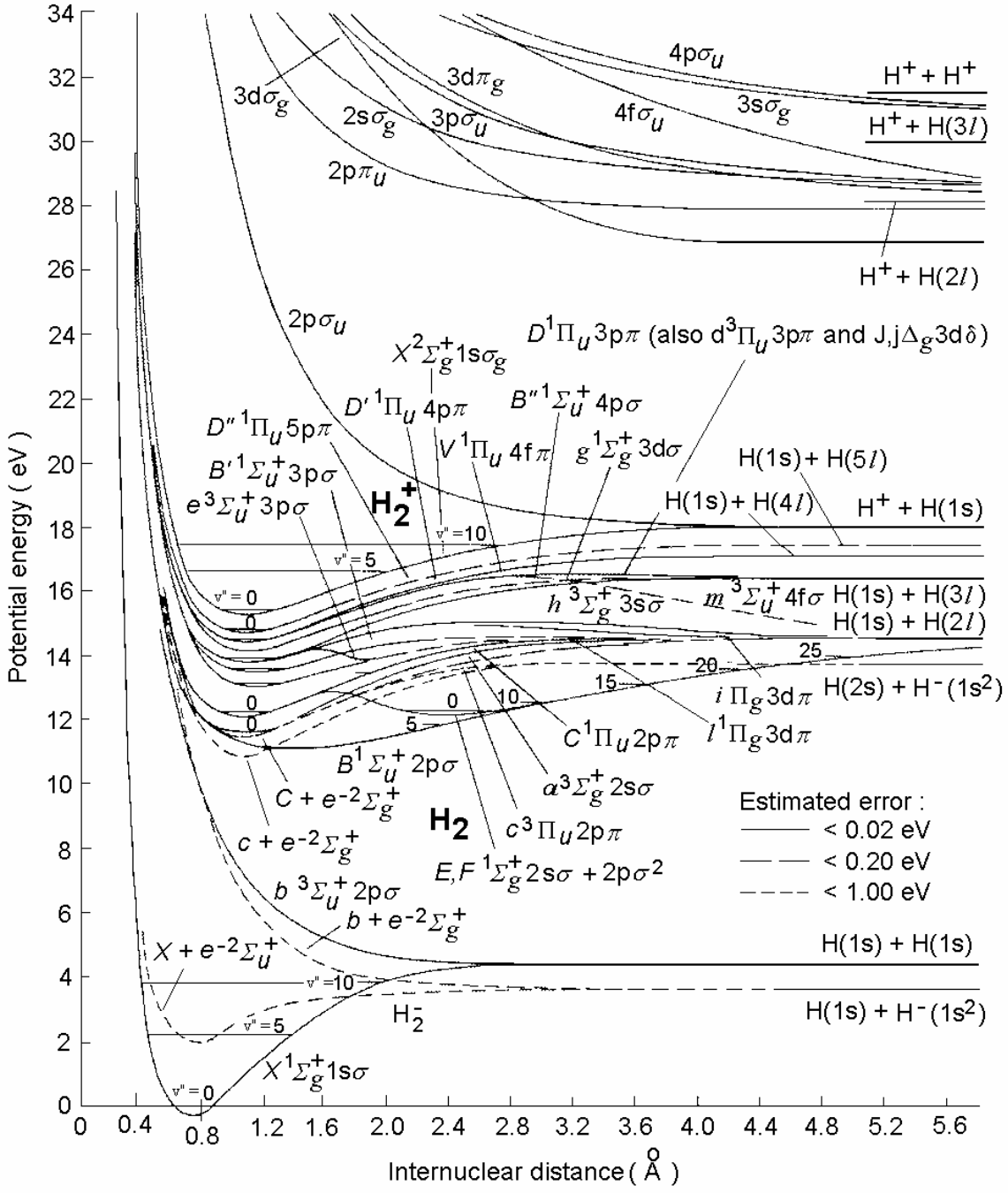

Fig. A.1. Potential energy curves for H_2, H_2^-, H_2^+. Few vibrational levels are also shown in the ground electronic state $X^1\Sigma_g^+$ of H_2 molecule and $X^2\Sigma_g^+$ of H_2^+ molecular ion [3].

[54] G. Herzberg, *Molecular Spectra & Molecular Structure*, VNR, (1966).

[55] P. M. Morse, Phys. Rev., 34, 57, (1929).

[56] T. E. Sharp, Atomic Data **2**, 119, (1971).

Appendix 2

Subsystems and diagnostic output of BATMAN ion source

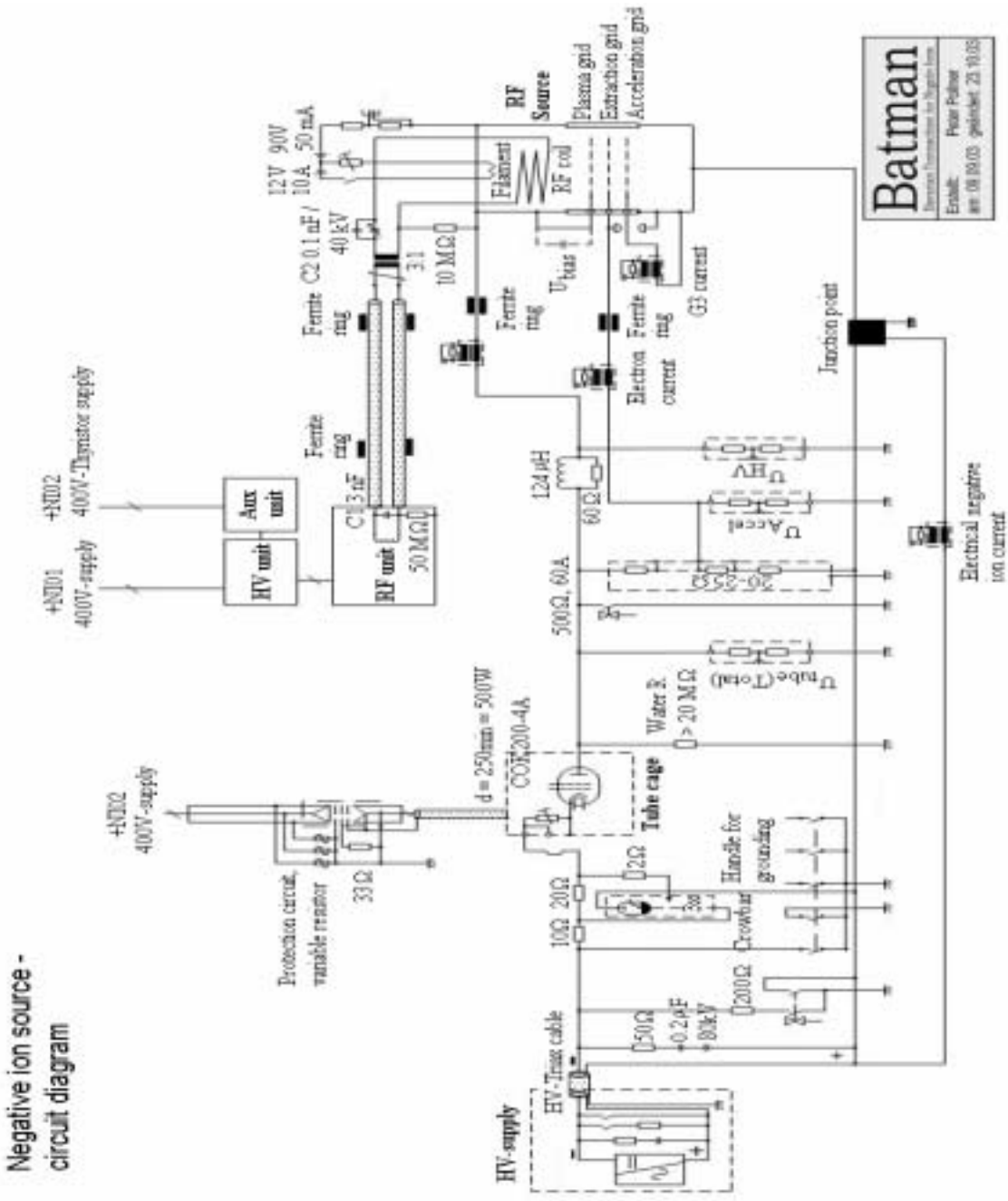

Fig.A.2.1. Complete electrical circuit diagram of BATMAN ion source.

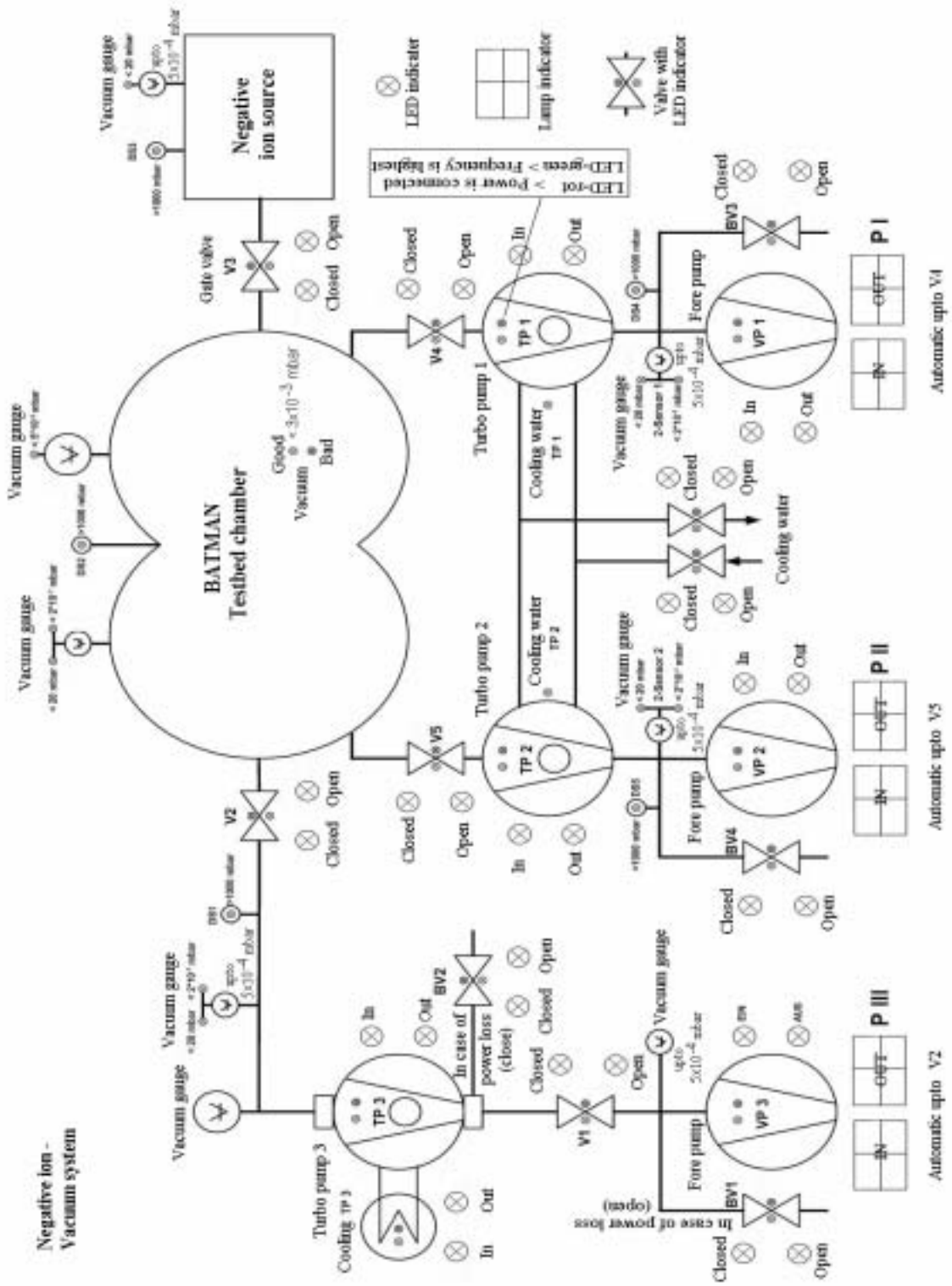

Fig.A.2.2. External vacuum system diagram of BATMAN ion source

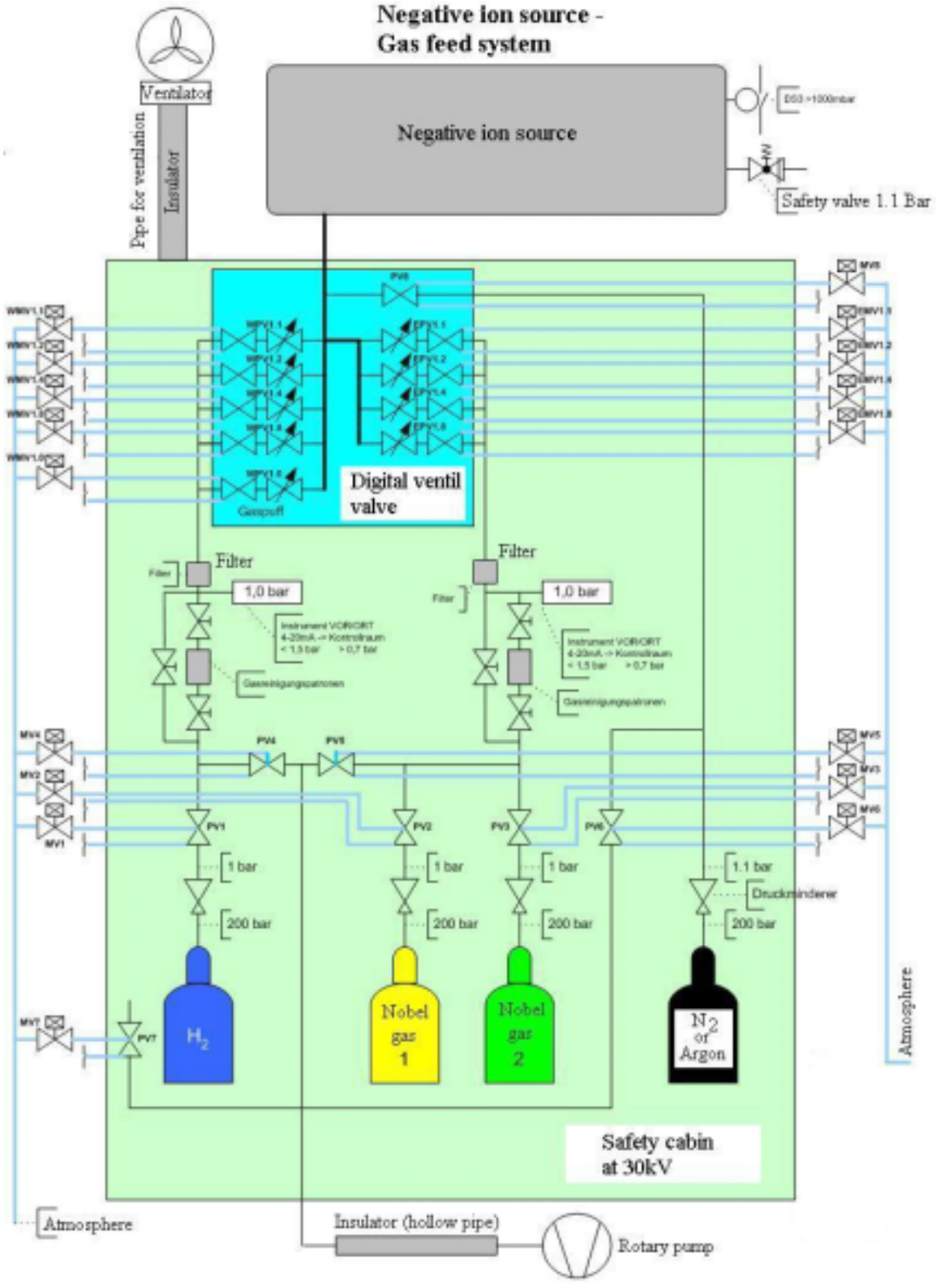

Fig.A.2.3. Gas feed system diagram of BATMAN ion source

Typical diagnostic output from DAC system

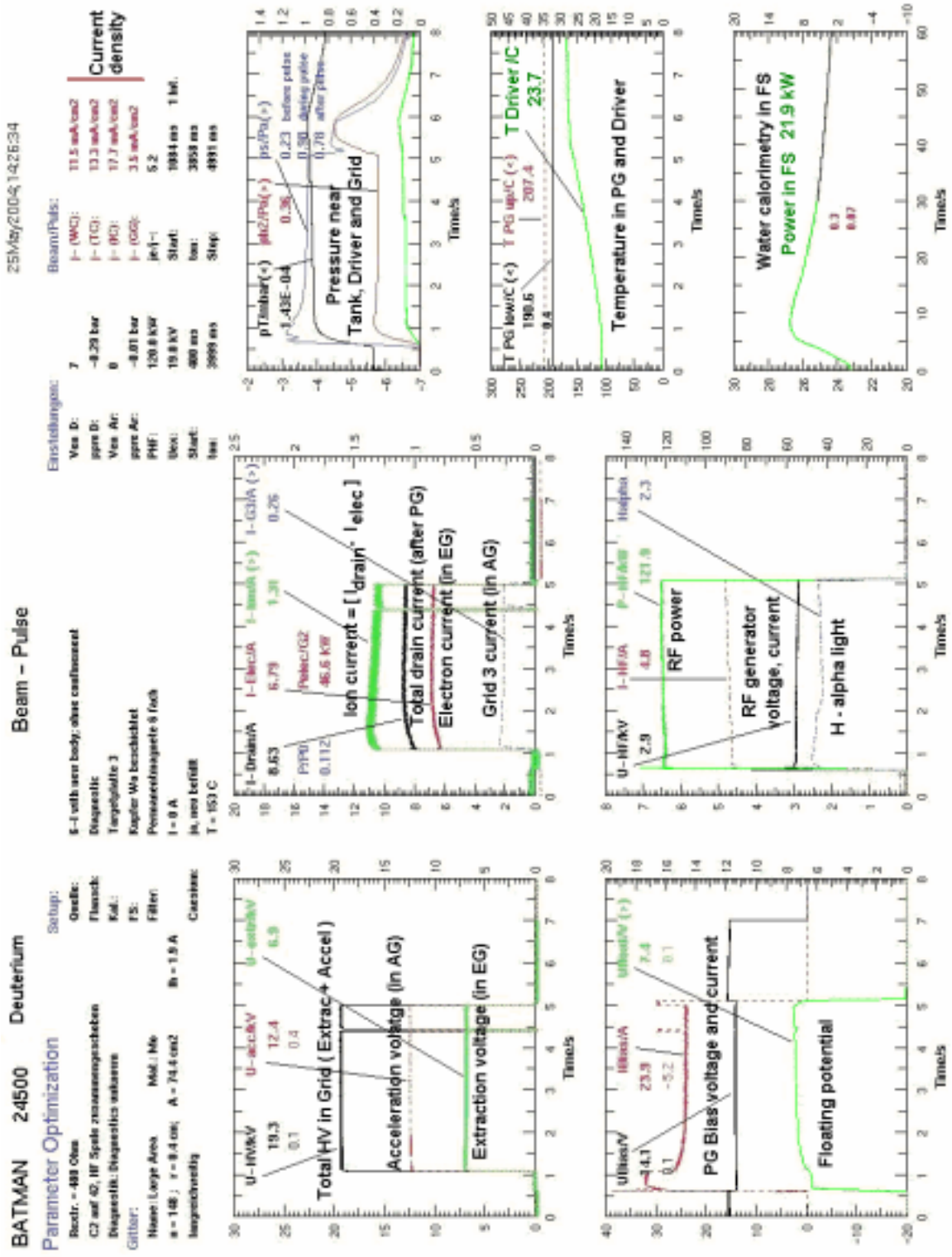

Fig. A.2.4. Data from electrical, pressure, H_α light measurements.

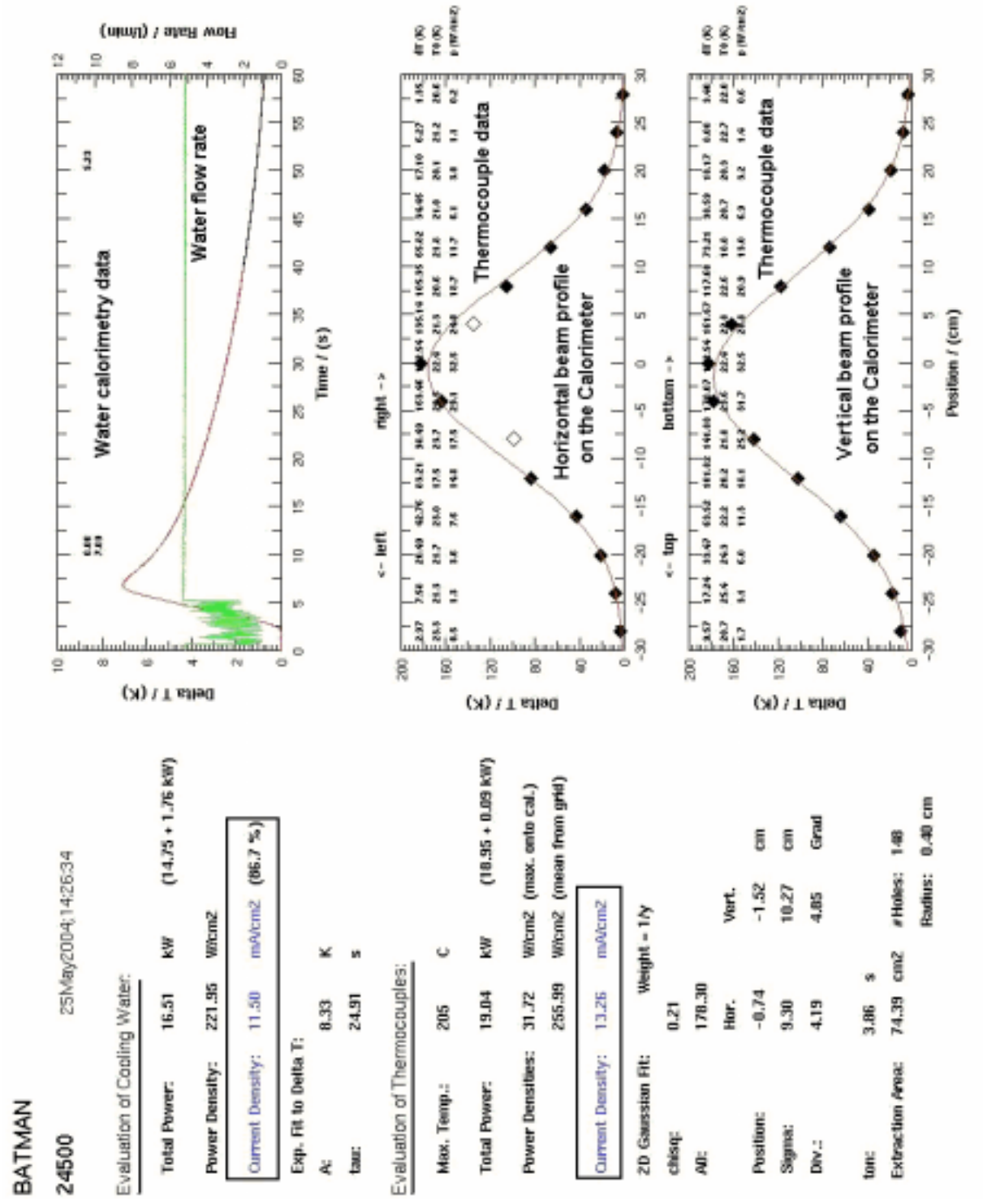

Fig.A.2.5. Calorimetric data. It contains beam profile, divergence and current density measurements

Appendix 3

Modeling of the source geometry

The expansion part of the BATMAN 6-1 type source is modeled as a rectangular box having volume (30×60×30) cm^3. The surface of each face of that box is denoted by a unique parametric form, $U_ix+V_iy+W_iz=T_i$ with the help of three orthogonal corner points of each rectangular surface plane.The co-ordinates of the orthogonal corners of i^{th} surface are $(x1_i, y1_i, z1_i)$, $(x2_i, y2_i, z2_i)$ and $(x3_i, y3_i, z3_i)$ in right handed rectangular co-ordinate system. The coefficients U_i, V_i, W_i and T_i are calculated as,

$$\begin{aligned} x21_i &= x2_i - x1_i \\ y21_i &= y2_i - y1_i \\ z21_i &= z2_i - z1_i \\ x31_i &= x3_i - x1_i \\ y31_i &= y3_i - y1_i \\ z31_i &= z3_i - z1_i \end{aligned} \tag{A.3.1}$$

$$\begin{aligned} U_i &= (y21_i \cdot z31_i - z21_i \cdot y31_i) \\ V_i &= -(x21_i \cdot z31_i - z21_i \cdot x31_i) \\ W_i &= (x21_i \cdot y31_i - y21_i \cdot x31_i) \\ T_i &= U_i \cdot x1_i + V_i \cdot y1_i + W_i \cdot z1_i \end{aligned} \tag{A.3.2}$$

The direction cosines of the i^{th} surface in x,y and z directions are denoted as,

$$Dx = \frac{U_i^2}{L};\ Dy = \frac{V_i^2}{L} \text{ and } Dz = \frac{W_i^2}{L} \text{ where } L = \sqrt{\left(U_i^2 + V_i^2 + W_i^2\right)}. \tag{A.3.3}$$

Appendix 4

Magnetic field calculation

The geometry used for a permanent magnet is shown in fig. A.4.1.

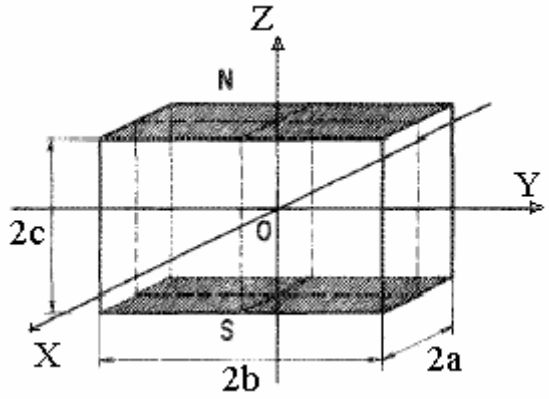

Fig. A.4.1. Schematic model diagram of a permanent magnet, showing north (N) and south (S) pole in the co-ordinate system.

The individual components of the magnetic field for a single permanent magnet are calculated as,

$$B_x = \frac{B_{res}}{8\pi}\left[sig(y-b)\log\frac{F(-a,-b,-c)F(a,-b,c)}{F(a,-b,-c)F(-a,-b,c)} - sig(y+b)\log\frac{F(-a,b,-c)F(a,b,c)}{F(a,b,-c)F(-a,b,c)}\right],$$

$$B_y = \frac{B_{res}}{8\pi}\left[sig(x-a)\log\frac{G(-a,-b,-c)G(-a,b,c)}{G(-a,b,-c)F(-a,-b,c)} - sig(x+a)\log\frac{G(a,-b,-c)G(a,b,c)}{G(a,b,-c)G(a,-b,c)}\right],$$

$$B_z = \frac{B_{res}}{4\pi}\left[\begin{matrix} -sig(z-c)sig(x-a)H(-a,-b,-c) + sig(z-c)sig(x+a)H(a,-b,-c) + \\ sig(z+c)sig(x-a)H(-a,-b,c) - sig(z+c)sig(x+a)H(a,-b,c) \end{matrix}\right],$$

where (A.4.1)

$$F(a,b,c) = \frac{\sqrt{(x+a)^2+(y+b)^2+(z+c)^2} - \sqrt{(y+b)^2}}{\sqrt{(x+a)^2+(y+b)^2+(z+c)^2} + \sqrt{(y+b)^2}},$$

$$G(a,b,c) = \frac{\sqrt{(x+a)^2+(y+b)^2+(z+c)^2} - \sqrt{(x+a)^2}}{\sqrt{(x+a)^2+(y+b)^2+(z+c)^2} + \sqrt{(x+a)^2}},$$

$$H(a,b,c) = \arctan\frac{(y+b)}{|z+c|}\sqrt{\frac{(x+a)^2}{(x+a)^2+(y+b)^2+(z+c)^2}} - \arctan\frac{(y-b)}{|z+c|}\sqrt{\frac{(x+a)^2}{(x+a)^2+(y-b)^2+(z+c)^2}}$$

$$sig(x) = \begin{cases} 1; & \text{for} \quad x > 0 \\ 0; & \text{for} \quad x = 0 \\ -1; & \text{for} \quad x < 0 \end{cases}$$

In equation (A.4.1) B_{res} is the residual magnetic flux density of the magnet (reminence), which is a characteristic parameter of a magnet, whose value can be obtained from the magnet supplier.

Appendix 5

Detailed flow chart diagrams.

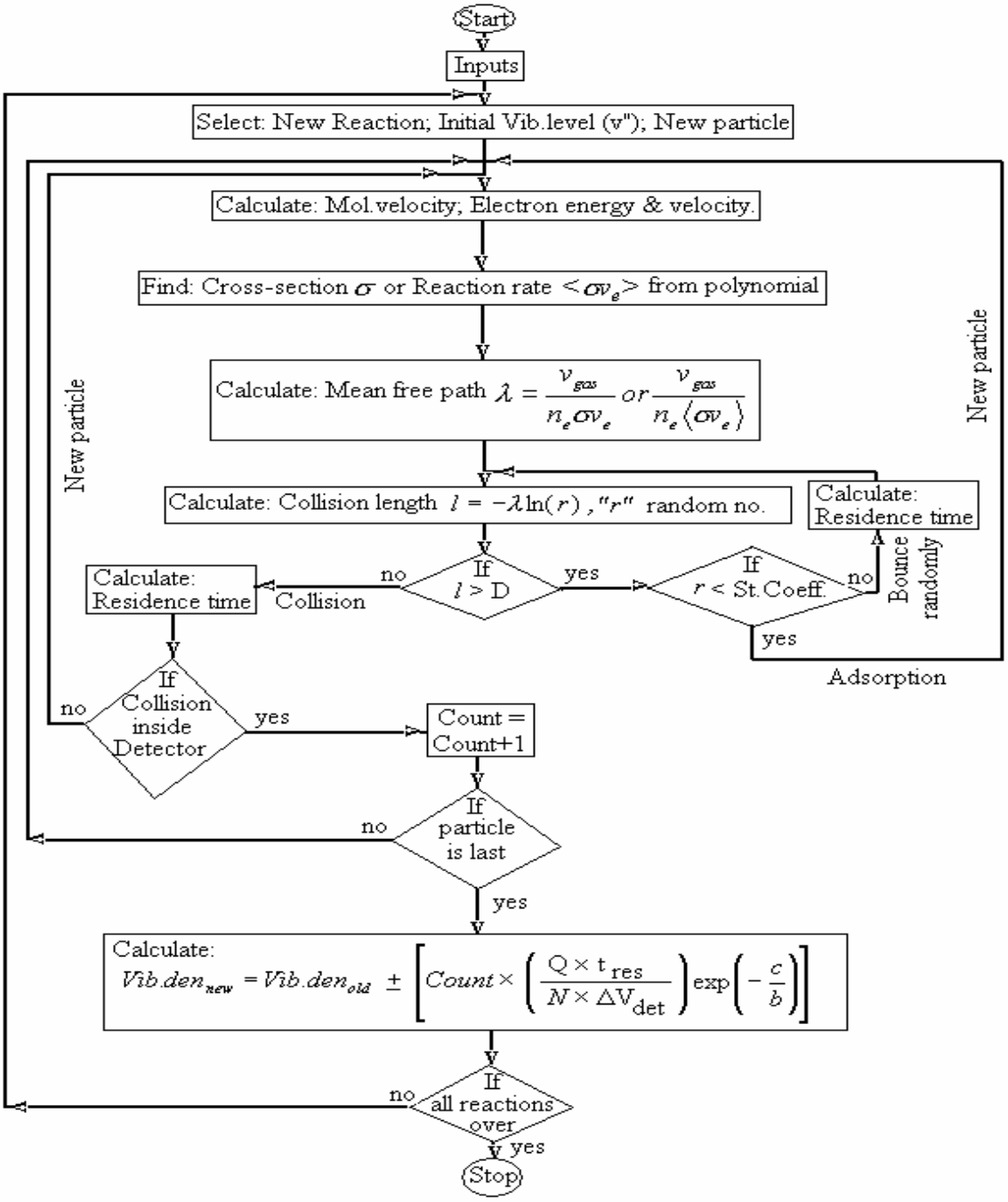

Fig.A.5.1. Flow chart diagram of neutral transport code. "D" is the dimension of the chamber, "Q" is the gas throughput, "N" is the total number of simulated particles, "Count" is the number of a particular reaction incident occurs a detector of volume ΔV_{det}.

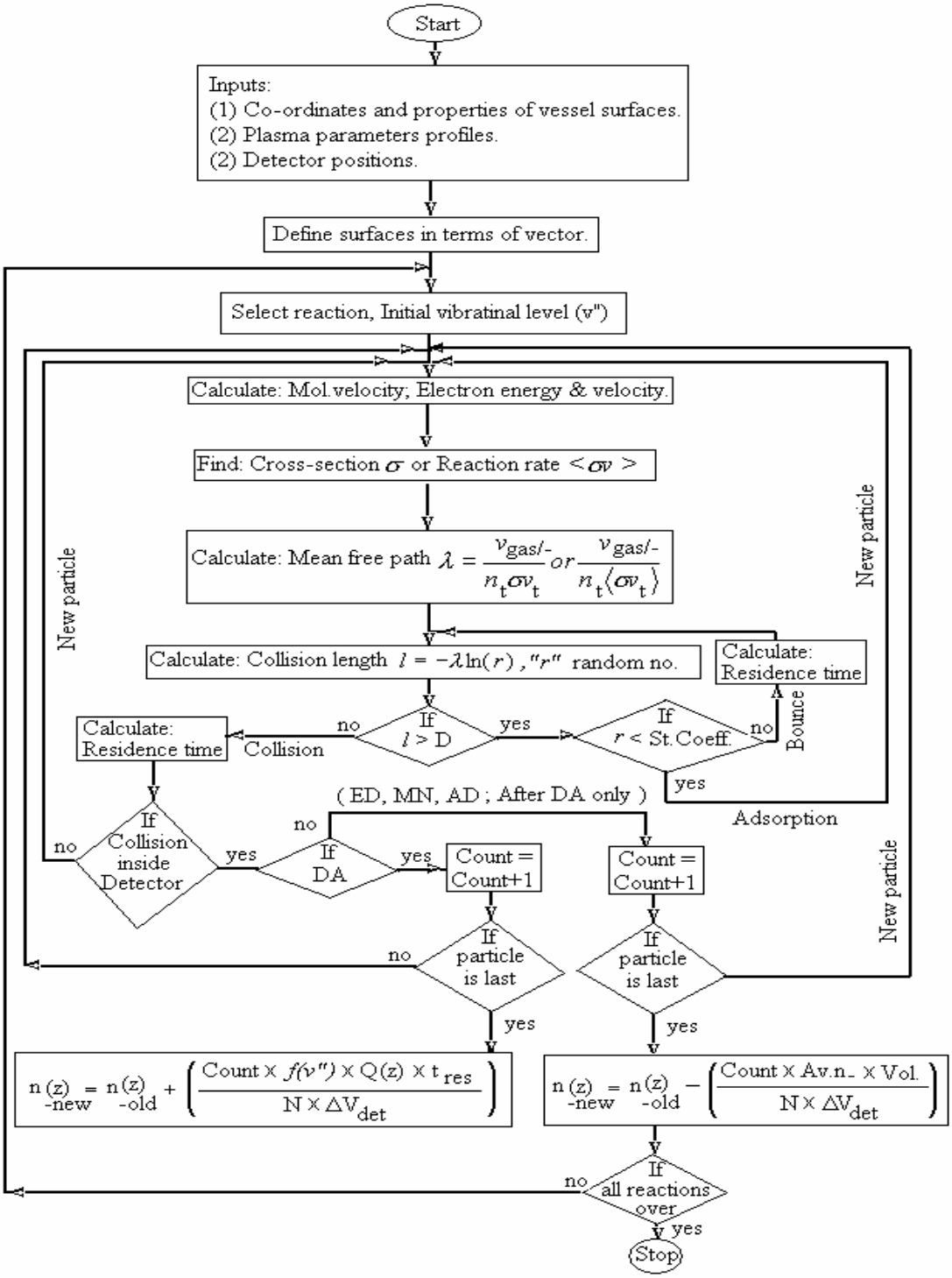

Fig.A.5.2. Flow chart diagram of negative ion production code. Fraction of molecules of having vibrational quantum number v" is denoted as *f*(v").

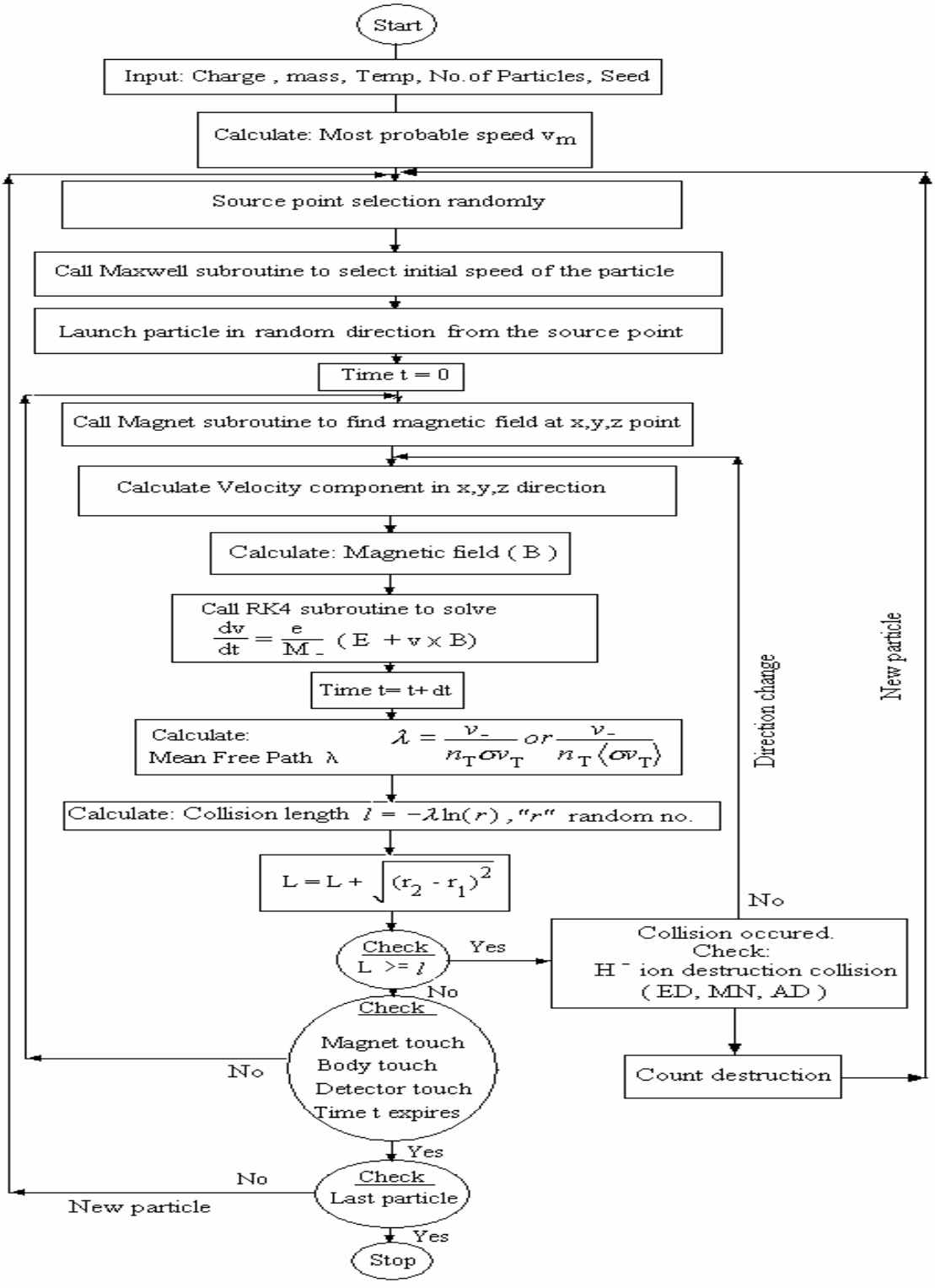

Fig.A.5.3. Flow chart diagram of volume produced negative ion transport code.

Appendix 6

Lock-in-Amplifier

1. Introduction

A lock-in-amplifier (LIA) is used to capture very small (μV – nV range) AC signal embedded in a much larger (mV) noise. The output of a LIA is always in DC, whose magnitude is proportional to the AC signal under investigation. The special rectifier, called a phase-sensitive detector (PSD) which performs this AC to DC conversion is the heart of a LIA. It works on Fourier's theorem.

2. Principle of Lock-in amplifier application

A LIA is always feed with a reference signal (V_{ref}) separately along with the signal to be investigated (V_{in}). Any input signal (V_{in}), including the noise accompanying it, can be represented as the sum of many sine-waves of different amplitudes, phases and frequencies. The PSD in a LIA multiplies all these components by the reference signal (V_{ref}), having fixed reference frequency. In the case of a sine-wave V_{in} the output is a DC signal proportional to that component of V_{in} , which is exactly in phase and frequency locked with the V_{ref}. If V_{in} is not sinusoidal, LIA gives a DC output which is proportional to the amplitudes of other harmonic components, which are phase locked with the V_{ref} and the relative response at the nth harmonic is given by $1/n$. The principle of operation is given below in mathematical framework.

Let consider a noise free sinusoidal reference signal voltage V_{ref},

$$V_{ref} = A \cdot \cos(\omega t) \tag{A.6.1}$$

The input signal is,

$$V_{in} = B \cdot \cos(\omega t + \theta) \tag{A.6.2}$$

where ω is the angular frequency of the reference signal and θ is the phase difference between V_{ref} and V_{in}. The phase θ is a user-adjustable parameter. Now multiplying these two signals, the PSD output is given by,

$$V_{psd} = A\cos(\omega t) \cdot B\cos(\omega t + \theta)$$

After multiplying and rearranging V_{psd} become,

$$V_{psd} = \frac{1}{2} AB\cos\theta + \frac{1}{2} AB\cos(2\omega t + \theta) \tag{A.6.3}$$

If the magnitude A (amplitude of reference signal) is kept constant, then the output from the PSD is a DC signal – $(ABcos\theta)/2$ with a ripple on the top $[ABcos(\omega t+\theta)]/2$. This ripple can be removed by introducing a low-pass filter at the output of PSD and a pure DC signal can be obtained. The DC signal from the PSD is,

- proportional to the amplitude of input signal B.
- proportional to the cosine of the phase angle θ between V_{in} and $V_{ref.}$ and the phase angle θ is user adjustable.

So it is very clear that if the noise, accompanied with V_{in} does not have a consistent phase relationship with the signal, the output of the PSD due to the noise will not be steady and can therefore be removed by the output low-pass filter. The schematic diagram of a simple LIA is shown in fig. A.6.1.

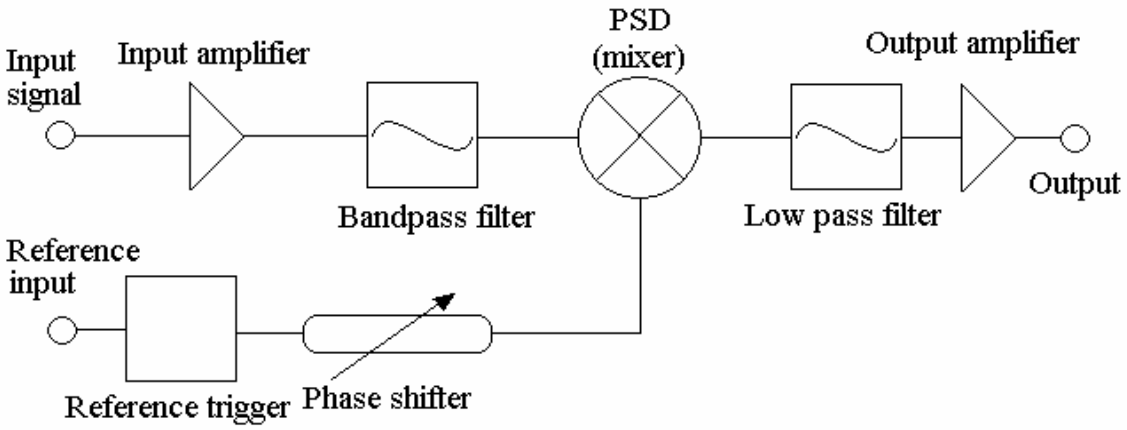

Fig. A.6.1. Schematic diagram of a single phase Lock-in-amplifier.

Acknowledgments

My PhD work would not have been possible without the help, the encouragement and the nice hospitality from my colleagues in Max-Planck-Institut für Plasmaphysik (IPP), particularly the NBI group. I would like to thank everybody who have helped and encouraged me during my PhD work.

I am deeply grateful to Prof. Dr. Rolf Wilhelm and Dr. Eckehart Speth who gave me the opportunity to carry out my PhD and supervised me during my tenure. I still remember that I had started communication with Dr. Eckehart Speth through email about the possibility of a PhD position in his highly regarded laboratory since May 2000. Their doors are always open for me for the scientific discussion in spite of been very busy. I would like to acknowledge their help in my work, particularly in the modeling and simulation part. Prof. Wilhelm has spent considerable amount of time to read my thesis and suggested to me many ways to improve it. He also shared his many bright ideas with me in different fields of plasma physics, particularly in the diagnostics.

I am fortunate that I got "friend, philosopher and guide", Dr. Arturo Tanga during my PhD work. I am very much influenced by his simpler ways of thinking about the implementations of different experiments, when time is short. I shall remember also his sense of humor and I have enjoyed his company during the experiments and the writing of our publications.

I am grateful to Frau Waltraud Sinz and Frau Hedi Martin for helping me to solve many problems related to organizational and personal matters. Particularly Frau W. Sinz took care all the responsibility for my visa and for the registration in the Technical University of München (TUM). Frau Martin helped me to get an Institute apartment. I am also grateful to Frau Knebel who help me to renew my work and residence permits in Deutschland. Frau Gabriela Daube helped me to fulfill an essential criterion to get my PhD degree from TUM by giving me the opportunity to assist the diploma students when they were doing the Plasma interferometer experiment.

I would like to thank Dr. Hans Falter, Dr. Peter Franzen, Frau Dr. Ursel Fantz, Dr. Werner Kraus, Dr. Paul McNeely for their continuous help and support during my experiments. I would also like to thank Mr. Bernd Heinemann, Mr. Rudolf Riedl and Ms. Anna Entschewa who helped me to design my probes. They have provided me with some drawings of the ion source which I have used in my publications and thesis.

I would like to thank Mr. Peter Pollner, Mr. Peter Turba, Mr. Frank Fackert, Mr. Jürgen Steinberger, Mr. Erich Kühn, Mr. Stefan Obermayer. Without their help I could not do my experiments even for a single day. I am also grateful to Mr. Karl-Heinz Wagner, who used to fix my computer related problems. Mr. Karl-Heinz Wagner helped me to install a web-cam in my computer which makes the geographical distance between me and my relatives and friends who are living in India, very short. I also acknowledge the help I have received from the TE workshop to fabricate some parts of my diagnostic setup and I am deeply grateful for that.
I got deeper insight in the plasma and the probe theories from Prof. Dr. Karl Lackner and from Dr. Beatrice Annaratone. I have enjoyed fruitful discussions with them. I would like to acknowledge their contributions in the analysis of my experimental data. Beatrice also

helped me in my experiment with her frequency spectrum analyzer, many optical filters and an optical fiber. I also get some optical filters from Dr. Murmann and Dr. R. Narayanan (Mani), which I have used in my modulation diagnostic experiments.

Before coming to Germany for my PhD, I have worked as a Scientist in NBI group in the Institute for Plasma Research (IPR), India. I have spent 3 years extra-ordinary leave from my Institute (IPR) to get ion source operational experience and at the same time to complete my PhD. I am grateful to my Institute. I am also deeply grateful and would like to thank to Prof. Dr. Predhiman Kaw (Director), Prof. Dr. Abhijit Sen (Dean), Prof. Dr. Shiban Mattoo (Project Leader of NBI), Mr. Arun Chakraborty (Group Leader of NBI Physics) and Mr. Ujjwal Baruah (Group Leader of NBI Engineering) for their support. I would also like to thank all of my other lab mates in India for their friendship specially Partha Sarkar, Rajendra Bhattacharya, Mrityunjay Kundu, Malay, Mukti Ranjan Jana, Gourab Bansal and Rajesh Kumar.

Since my childhood my parents, Mrs. Bela Bandyopadhyay and (Late) Mr. Arindam Bandyopadhyay; my Chotomama, Mr. Gopal Mukherjee; my Maashi, Mrs. Maatu Mukherjee; my grandparents, (Late) Mrs. Manju Mukherjee and (Late) Mr. Paresh Nath Mukherjee; my Jethu, (Late) Mr. Anupam Bandyopadhyay and all other family members always encouraged me in every ways, particularly in my study. I am fortunate to have their blessings always and I remember all of them. I could not come to Germany and finish my PhD unless I got moral support from my father-in-law, Mr. Pranab Kr. Ganguly; my mother-in-law, Mrs. Sikha Ganguly and my sister-in-law Ms. Prachi Ganguly.

I will remember my friends who are mostly Post Doctoral fellows and PhD students in MPI and TUM and are living in Garching. I would like to acknowledge their moral support and their different cuisine which we used to enjoy in our get-together party, held in almost at every weekend. Because of them we have never felt home sick. They are: Mani and Sudha, Souradip and Paramita, Neena and Vikas, Neethu and Shah, Suresh and Aparna, Kiran, Abhishek, Subhasis and Dr. Amitava Gupta. I acknowledge also that my daughter Maiolica has got a nice company from Bhavanarayeni (Kutty), a very intelligent girl (daughter of Mani and Sudha) and she has learnt a lot from Kutty. Recently Kutty has been blessed with a sister, Sugayaalini (Sugi). We all love them.

Overall, I must acknowledge that my beloved wife Mrs. Pieu Bandyopadhyay and my sweet daughter Ms Maiolica Bandyopadhyay have sacrificed a lot in the last three years and helped me everyday to complete my PhD in time. Maiolica used to wait until late at night daily to play with me after I come back home from the Institute. I have never bothered about my food because of Pieu. She take care everything which is necessary for our daily life without getting any help from me. She also keeps our communications and correspondences up to date with our friends and relatives. It is only Pieu who inspired me to do my PhD at that time when I had almost given up this idea. She used to ask me everyday about my progress in work and suggests me the way if I have some problems. **I dedicate my complete PhD work to Pieu and Maiolica for their unconditional love, support and inspiration.**